APPLYING CONTROL OF HETEROGENEITY WITHIN ATOM TRANSFER RADICAL POLYMERIZATION

Andrea M. Elsen

Carnegie Mellon University

Department of Chemistry

Spring 2014

in partial fulfillment of the requirements for a Ph.D. in Chemistry

ACKNOWLEDGEMENTS

There are several people without whom this Ph.D. would not have been possible. First, I would like to thank Prof. Matyjaszewski for not only accepting me into his group and passing on his knowledge of polymer chemistry but also giving me the position of lab manager; an invaluable experience that likely changed the course of my career. My time in the Matyjaszewski group provided me with incredible opportunities, allowing me to grow as a writer and presenter, to meet the top scientists and to find my most valued friendships.

To that end, I would have never applied to Carnegie Mellon without Prof. Eric Fossum. I first encountered Dr. Fossum as my freshman chemistry professor at Wright State University and continued to enroll in his classes throughout my degree. Despite the fact I nearly ran him over with my car that freshman year, he accepted me into his group for the M.S. program at WSU. He was the first to believe in me and most importantly, got me to believe in myself, which allowed me to enter this Ph.D. with confidence. He is an incredible advisor, mentor and friend and someone that I will always look up to.

I must also mention the two post-docs Dr. Steve Diamanti and Dr. Robert MacCuspie who were key factors in my development from student to researcher at Wright-Patterson Air Force Base. Striking the perfect balance between direction and freedom, treating me as an equal, Steve and Rob's mentorship allowed me to

directly contribute to our science. Additionally, both played an instrumental role in my decision to attend graduate school as well as the choice of Carnegie Mellon University specifically.

All of the Matyjaszewski group members, past and present, have played a significant role in my Ph.D. for which I would like to thank them. In particular, I would like to thank Dr. Chi-How Peng for always having the right advice to give; Dr. Nick Tsarevsky not only for great advice but even better stories; Dr. Wenwen Li for setting the bar on organization and efficiency as well as being a pleasure to work with; Saadyah Averick for reminding me that first impressions aren't always right and to always wait for the owner of a car to arrive before getting in...just in case it isn't the right car; Hong Cho and Sangwoo Park for making me laugh and Dr. Jim Spanswick for being the voice of reason.

Of course without the amazing women on the staff of Mellon Institute, there would be no department or graduate program. Brenda Chamber, Valerie Bridge, Rea Freeland, and Sara Wainer are have all contributed to the success of my Ph.D. In particular, I would like to thank Brenda Chambers as she and I spent countless hours together renovating the labs during which time we became good friends. She always had a moment to spare for a quick chat; something which made the renovations meeting a little better and my day a little brighter.

A Ph.D. is meaningless without my friends and family, all of whom have been supportive throughout this process. Countless evenings were spent with what

Wojtek aptly named “The Base” and without them and all of the PHI Friday nights, dinner parties and grill outs I wouldn’t have survived. I must thank Paweł and Paulina Kryś for the great memories, especially, game nights and Game of Thrones parties; Maciek Kopec for bringing laughter to everyone around you and being the absolute, hands-down, best dancer I’ve ever known! A very special thanks to Drs. Laura and Wojtek Jakubowski for reasons too numerous to list here but they have been the truest of friends and made these past five years a time in my life that I will never forget. I don’t even know where to being with Asia Burdyńska, my very best friend. Only a true friend can laugh and cry and be crazy as we did. She made this Ph.D. worth it because without it, I wouldn’t have her.

My parents instilled a belief that I could do anything and go anywhere, which gave me the confidence to take on this Ph.D. and my sister has always been a strong believer in my abilities. Of course I would be remiss to not mention Don Wahrer, although as an engineer he wasn’t a fan of chemistry, he was always supportive of my quest for science and this degree. Finally, but certainly not least, I have to thank my wonderful husband, Nick. These five years were not easy and yet he was gracious, kind and generous enough to allow me to do what I needed for this Ph.D. Without his unending support, I wouldn’t be where I am today.

ABSTRACT

This work explores the application and control of heterogeneity within ATRP. The term "heterogeneity" can be applied to polymers in many ways however, this dissertation focuses on molecular weight distribution (MWD) and copolymer composition. The first chapter reviews not only controlled radical polymerizations (CRPs) but also current research on heterogeneity within CRPS, including methods to reduce or purposefully incorporate MWD into polymers as well as advances made to intricate copolymer compositions such as sequence controlled or gradient copolymers. Chapters II and III discuss avenues to reduce MWD values in homogeneous and heterogeneous media, respectively. Dual initiating systems are utilized to provide well controlled polymerizations of methyl acrylate in Chapter II while Chapter III details the synthesis of new active yet hydrophobic ligands for use in ARGET ATRP miniemulsion polymerizations. On the other hand, work in Chapter IV focuses on synthesizing block copolymers with broad MWD through the manipulation of catalyst concentration in ARGET ATRP. Chapter V utilizes the concepts and procedures of Chapter IV to generate gradient copolymers with broad MWD whose quality of gradient architecture is with MWD values. ABA triblock copolymers with disperse center blocks were generated in Chapter VI, however this was not accomplished with ATRP but with polycondensation. From the disperse telechelic macroinitiator synthesized via polycondensation, outer blocks were polymerized under ATRP conditions. The final chapter studies the effects of composition (random, block, and gradient) and topology (linear and star) copolymers utilized as polymeric surfactants in emulsions.

TABLE OF CONTENTS

LIST OF ABBREVIATIONS

AA	L-ascorbic acid
AFM	atomic force microscopy
AGET ATRP	activators generated by electron transfer
AIBN	azobisisobutyronitrile
ARGET ATRP	activators regenerated by electron transfer ATRP
ATRA	atom transfer radical addition
ATRC	atom transfer radical coupling
ATRP	atom transfer radical polymerization
BA	butyl acrylate
BiB	2-bromoisobutyryl bromide
BiBEM	2-bromoisobutyryloxyethyl methacrylate
BMA	butyl methacrylate
BPA	bisphenol-A
BPMODA	bis(2-pyridylmethyl)octadecylamine
BPMODA*	(bis[2-(4-methoxy-3,5-dimethyl)pyridylmethyl]octadecylamine)
Brij 98	polyoxyethylene(20) oleyl ether
$Bu_3P^+Br^-$	tributylhexadecyl phosphonium bromide
CC	Cumulative composition
CDB	cumyl dithiobenzoate
$CHCl_3$	chloroform

conv.	conversion
CRP	controlled radical polymerization
CTA	chain transfer agent
CTA	chain transfer agent
Cu^0	copper wire
CuBr	copper (I) bromide
$CuBr_2$	copper (II) bromide
CuCl	copper (I) chloride
$CuCl_2$	copper (II) chloride
$Cu^{II}(OTf)_2$	copper(II) trifluoromethanesulfonate
CV	cyclic voltammetry
DFS	bis(4-fluorophenyl)sulfone
DMF	*N*,*N*-dimethylformamide
dNbpy	4,4′-dinonyl-2,2′-dipyridyl
DOD-BPED	*N*′,*N*″-dioctadecyl-*N*′,*N*″-bis(2-pyridylmethyl)ethane-1,2-diamine
DOD-BPED*	*N*′,*N*″-dioctadecyl-*N*′,*N*″-bis[2-(4-methoxy-3,5-dimethyl)pyridylmethyl]ethane-1,2-diamine
DP	degree of polymerization
DSC	differential scanning calorimetry
***e*ATRP**	electrochemically mediated ATRP
EBiB	ethyl α-bromoisobutyrate
EBPA	ethyl-α-bromophenylacetate
EDG	electron donating groups

EGDA	ethylene glycol diacrylate
FRP	free radical polymerization
GC	gas chromatography
GPC	gel permeation chromatography
HEA	hydroxyethyl acrylate
HEMA-TMS	2-(trimethylsilyl-oxy)ethyl methacrylate
HMTETA	1,1,4,7,10,10-hexamethyltriethylenetetramine
HPL	hexagonally perforated lamellar
ICAR ATRP	initiators for continuous activator regeneration
KF	potassium fluoride
KF	potassium fluoride
LCCC	liquid chromatography under critical conditions
$LiAlH_4$	lithium aluminum hydride
MA	methyl acrylate
Me_6TREN	tris(2-(dimethylamino)ethyl)amine
MEA	methylene glycol ether methacrylate
MeCN	acetonitrile
MeOH	methanol
$MgSO_4$	magnesium sulfate
MMA	methyl methacrylate
M_n	number average molecular weights
M_w/M_n	molecular weight distribution

MWD	molecular weight distribution
NaOH	sodium hydroxide pellets
nBA	*n*-butyl acrylate
NMP	nitroxide mediated polymerization
NMR	nuclear magnetic resonance
PAES or PS	poly(arylene ether sulfone)
PBA	poly(butyl acrylate)
PEEK or PK	poly(ether ether ketone)
PEM	proton exchange membrane
PFS	2,3,4,5,6-pentafluorostyrene
PHEMA-TMS	poly(2-(trimethylsilyl-oxy)ethyl methacrylate)
PMA	poly(methylacrylate)
PMDETA	*N,N,N',N'',N*''-pentamethyldiethylenetriamine
PMMA	poly(methyl methacrylate)
PSt	polystyrene
Py-HCl*	chloromethyl-4-methoxy-3,5-dimethylpyridine hydrochloride
r_1 **or** r_2	reactivity ratio of monomer 1 or 2
RAFT	reversible addition-fragmentation chain transfer
RI	refractive index
ROMP-CT	chain-transfer ring opening metathesis polymerizaiton
ROP	ring opening polymerization
R_p	rate of polymerization

SARA ATRP	supplemental activators and reducing agent ATRP
$Sn^{II}(EH)_2$	tin(II) 2-ethylhexanoate
$Sn^{II}(EH)_2$	tin (II) ethylhexanoate
St	styrene
TBABr	tetraethylammonium bromide
$TBAClO_4$	tetrabutylammonium perchlorate
TBAF	tetrabutylammonium fluoride in THF (1M)
TBAF	tetrabutylammonium fluoride in THF
$TBAPF_6$	tetrabutylammonium hexafluorophosphate
T_g	glass transition temperature
THF	tetrahydrofuran
TPMA	tris(2-pyridylmethyl)amine
$\chi_{AB}N$	segregation strength

LIST OF SCHEMES

LIST OF TABLES

LIST OF FIGURES

CHAPTER I

HETEROGENEITY WITHIN ATOM TRANSFER RADICAL POLYMERIZATION

I.1. General Introduction

I. 1. 1 The advantages and potential of controlled radical polymerization

Commodity polymers synthesized by free radical polymerization (FRP)[1,2] account for a significant portion of all polymers industrially synthesized. A wide variety of monomers, including vinyl chloride, styrene, acrylates, acrylamides, vinyl acetate, and vinyl alcohol are polymerized with this technique and are used for a range of applications. However, this method does not allow for significant control over the molecular weight and molecular weight distribution, nor the composition, topology or functionality present. In other words, due to the extremely quick lifetime of a radical and growing polymer chain, typically ~1 second, FRP is an inefficient method to generate well defined macromolecules.[3]

In 1956, Michael Szwarc permanently changed the field of polymer science with the introduction of the first "living" polymerization method: anionic polymerization.[4,5] The key feature to this living polymerization, in comparison to FRP, is the active chain end. Once all monomer has been consumed, the chain ends remain active and upon

addition of more monomer, polymerization will continue. Chain end activity is attributed to inherent stability of carbanions in the absence of electrophiles. Polymer chains terminate only when CO_2 or moisture is introduced to the polymerization, therefore, as long as the reaction system remains air and moisture free, the chain ends will remain active.

The introduction of anionic polymerization was noteworthy not only for the livingness of the system, but also for the control of molecular weight and molecular weight distributions. Unlike FRP, initiation of anionic polymerization is quite fast while propagation is relatively slow, thus providing control and well defined materials. Utilizing this method, the synthesis of the first block copolymer was reported followed by many reports of complex and novel macromolecules.[6-9]

While the tremendous advances made by Szwarc are important to the field of polymer science and were adopted on an industrial scale, it also suffers from drawbacks. As discussed, a key feature to anionic polymerization is the "livingness" of the chain ends, which stems from a lack of electrophiles and moisture present. Consequently, the anionic process demands a time consuming and complex, high-vacuum set up to ensure the stringent requirements are met. In comparison to FRP, the monomers which are polymerizable via anionic polymerization are limited. Therefore, the advent of controlled radical polymerizations was a welcome compromise to achieve well defined materials with a variety of monomers, without the strict procedures necessary for anionic polymerization.[10]

Three main methods of controlled radical polymerization (CRP) exist: nitroxide mediated polymerization (NMP)[11-14], reversible addition-fragmentation chain transfer

(RAFT)[15-18], and atom transfer radical polymerization (ATRP)[3,7,19-21]. In each case, the four main steps of radical polymerization still exist: (1) initiation: the process to generate a radical, (2) propagation: the incorporation of monomer units into the growing polymer chain, (3) termination: reaction of two radicals to produce an inactive polymer chain either through coupling or disproportionation, and (4) transfer: termination of one polymer chain to initiate another. A differentiating factor between CRP systems and FRP is the lifetime of the radical. Through various mechanisms, the radical is reversibly deactivated into a dormant state where neither polymerization nor termination is possible.[22] In turn, this increases the lifetime of the radical from ~1 second to ≥1 hour. This dynamic equilibrium between active and dormant states also effects the molecular weight distributions; the faster the exchange between states, the more narrow molecular weight distribution that can be achieved.[7]

NMP employs an alkoxyamine to both initiate and mediate polymerization (Scheme I.1a). Initiation occurs at elevated temperatures through the thermolytically unstable C-O bond while the remaining nitroxide radical participates in reversible termination. The nitroxide radical is considered stable and therefore controls the dynamic equilibrium between active and dormant states. Early systems of NMP had an extremely limited assortment of polymerizable monomers; however advances have been made which have broadened this range to include methacrylates, acrylates, acrylamides and styrene. While it is advantageous that NMP is purely organic, requiring no catalytic species, the range of molecular weights achievable with narrow molecular weight distributions is limited.

On the other hand, RAFT is a degenerative chain transfer process. Similar to FRP, a constant radical source is needed, thus a thermal initiator such as azobisisobutyronitrile (AIBN) is used. Chain transfer agents (CTAs), for example xanthates, dithioesters, and thiocarbamates, are used to mediate the polymerization *via* a reversible chain-transfer process (Scheme I.1b). RAFT is a useful polymerization method as it is successful with a wide variety of monomers in a variety of solvents and is capable of synthesizing complex architectures. However, there is limited commercial availability of CTAs, potentially requiring multistep synthesis. Additionally, the CTAs produce a strong color and odor in the final product if purification is not complete.

Control in ATRP relies on the dynamic equilibrium between propagating ($P_n^{\bullet}$) and dormant species (P_n-X, X = Cl or Br) as in Scheme I.1c. The alkyl halide is reversibly activated by lower oxidation state catalyst complexes ($Cu^{I}X/L$, L = Ligand) to form the macroradical species, $P_n^{\cdot}$, and deactivated by the high oxidation state catalyst complex ($Cu^{II}X_2/L$). The equilibrium constant of ATRP, K_{ATRP}, is defined as the ratio of activation (k_a) and deactivation (k_{da}) rate constants, which determines concentration of radicals present in the polymerization. As the equilibrium of ATRP favors the deactivated state, the number of active radials ($P_n^{\bullet}$) available for propagation (k_p) and termination (k_t) is well controlled. While copper is the most common choice for use in catalyst complexes, several other transition metals have proven to be successful including manganese, cobalt, nickel, ruthenium, rhodium and iron among others. ATRP provides excellent control over a wide variety of monomers; however, it is necessary to remove the catalyst during post polymerization purification.

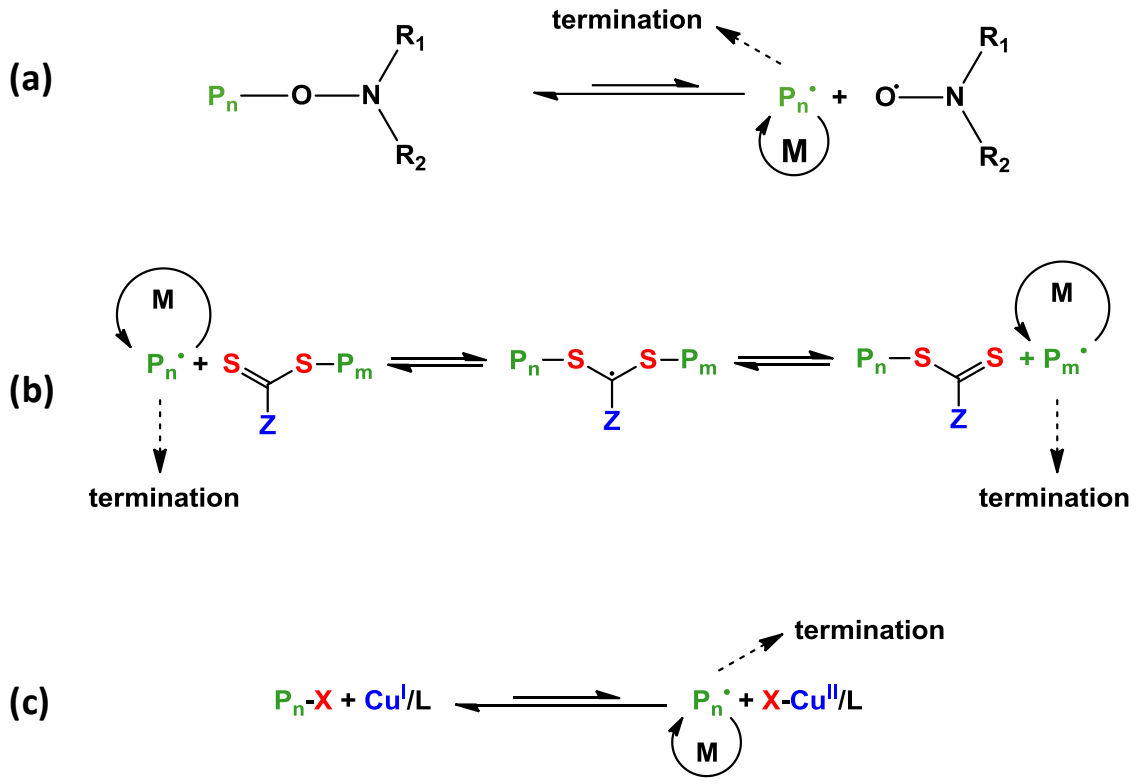

Scheme I.1. Mechanisms of (a) NMP, (b) RAFT, and (c) ATRP.

I.1.2 The contribution of ATRP to precise polymer synthesis

ATRP is a robust and powerful method of polymerization. Several advances have been made to the homogenous ATRP mechanism described in section I.1.1, making it more environmentally friendly and industrially viable.[23,24] The addition of an appropriate reducing agent, such as tin(II) 2-ethylhexanoate, glucose, ascorbic acid or hydrazine in activators regenerated by electron transfer (ARGET) ATRP,[25,26] application of a potential as in electrochemically mediated ATRP (*e*ATRP),[27] addition of copper wire as in supplemental activators and reducing agent (SARA) ATRP,[28] or addition of thermal initiators as in initiators for continuous activator regeneration (ICAR) ATRP[25] are all

proven methods of well-controlled ATRP with ppm levels of catalyst. In each case, reduction of Cu^{II}/L species, accumulated during irreversible termination, restores the activator, Cu^{I}/L (Scheme I.2).

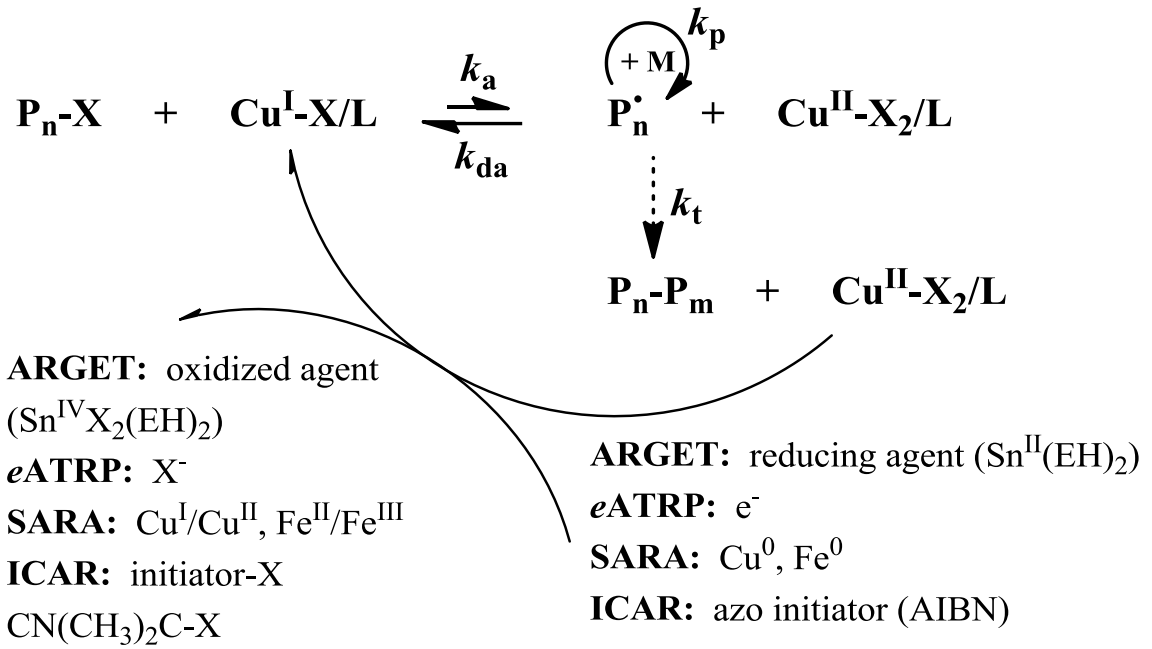

Scheme I.2. Low ppm catalyst ATRP mechanisms.

Utilizing such systems decreases the catalyst concentrations up to one thousand times in comparison to normal ATRP. As the rate of polymerization decreases with decreasing catalyst concentrations, the rate of activation (k_a) must be significantly enhanced to maintain a rate of polymerization comparable to normal ATRP. Enhancing k_a can be achieved by using the complex of $Cu^{I}X$ with branched multidentate ligands. The most common branched tetradentate ligands are tris[2-(dimethylamino)ethyl]amine (Me_6TREN)[29] and tris(2-pyridylmethyl)amine (TPMA).[30] Copper catalyst complexes with these ligands in normal ATRP display 10^3-10^5 times higher activity than the originally used $Cu^{I}X$/2,2'-bipyridine complex.[19,31]

In addition to the aforementioned advances, ATRP has been successfully extended to aqueous dispersed media (e.g., microemulsion,[32,33] miniemulsion,[34-37] and emulsions[38-42]), all of which resulted in well-defined polymer latexes. Polymerizations utilizing aqueous conditions are also under consideration for industrial processes as they are recognized to be a mild, environmentally benign technique. Water as a polymerization medium not only eliminates the necessity of using volatile organic solvents but also ensures greater heat dissipation during polymerization. Moreover, low viscosity of the dispersed aqueous solutions allows for obtaining high weight fractions of the polymer, which is not accessible in bulk or organic solvent polymerizations.[43]

The plethora of monomers, initiators, ligands, solvents and/or reaction media as well as catalyst concentrations available with ATRP allows for tailor made conditions for every polymerization, be it basic or complex. As shown in Figure I.1, ATRP is able to control not only the composition (e.g., statistical, block, and gradient), and topology (e.g., stars and brushes), but can polymerize monomers with a range of functionalities (e.g., (meth)acrylates, styrenics, and acrylamides) with predetermined molecular weights and narrow molecular weight distributions (M_w/M_n).[44-48] Furthermore, ATRP has proven to be successful in homogenous (i.e., organic and aqueous) and heterogenous[49-52] (e.g., microemulsion,[32,33] miniemulsion,[34-37] and emulsions[38-42]) media. Materials synthesized *via* ATRP are being studied for a wide variety of applications including thermoplastic elastomers, porous membranes, particle dispersants, surfactants, components of cosmetic products, and biomedical applications.

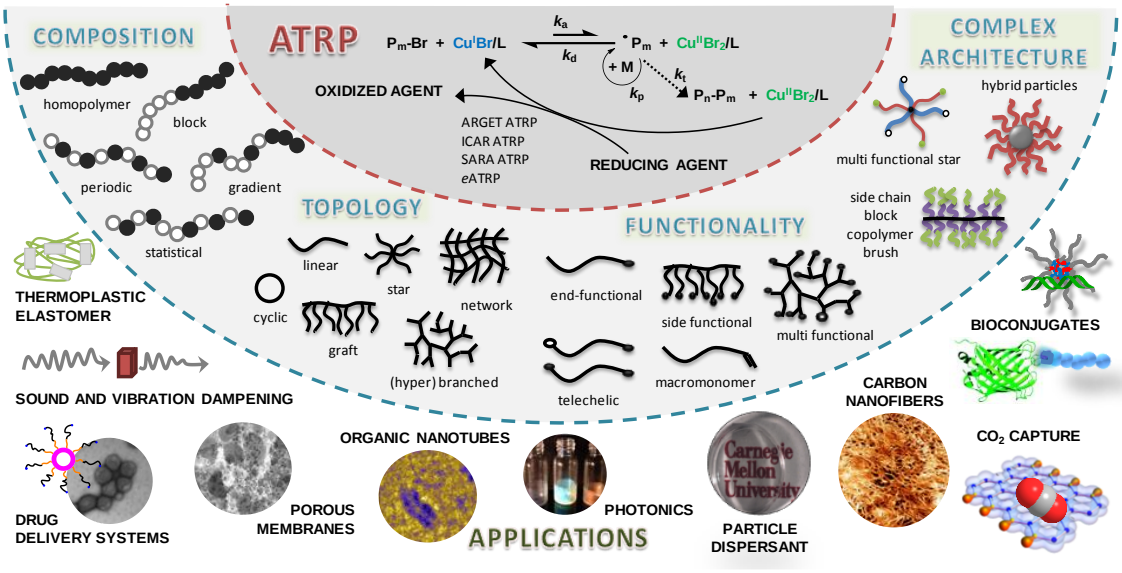

Figure I.1. Overview of polymers synthesized by ATRP and their applications.[3,20,23,45,53]

I.2. Introduction to research topics

I.2.1. Exploring heterogeneity of copolymers

The term "heterogeneity" has one definition: different in kind; incongruous. However, it can be applied to polymer science in many ways. Most commonly, heterogeneity brings to mind molecular weight distribution (MWD), specifically broad MWD. Nearly all research in polymer science prides itself on improving control to remove heterogeneity, thereby producing polymers with narrow MWD. This is certainly a vital element of research as properties are intimately linked with structure, therefore, the structure-property relations will be best understood with well defined structures. For high-end applications, such as biomedical applications, precise synthesis is essential as exact knowledge of the structure is required. Chapters II and III of this thesis will focus on

reducing heterogeneity. Each chapter demonstrates a new avenue to generate precise materials while utilizing lower catalyst concentrations.

Interestingly, there is another side to this coin: purposefully introducing heterogeneity into polymers. Theoretical predictions in the 1980s sparked a new branch of polymer science which studied the effects of introducing a controlled amount of dispersity into block copolymers. Since these initial predictions, a growing number of reports have been published which demonstrate experimental results corroborating the computational studies. Chapters IV and V of this thesis explores the effects of dispersity on the quality of block and gradient copolymers, respectively. Chapter VI utilizes two polymerization mechanisms to generate triblock copolymers with a disperse center block.

Furthermore, "heterogeneity" may be applied to polymer science other terms, such as composition. For example, random, block, gradient and periodic copolymers may all be considered heterogeneous polymers as they consist of two or more monomers different in kind. Chapter VII details the synthesis of random, block, and gradient copolymers for use as polymeric surfactants. The following sections in this chapter will outline the state of the art research on heterogeneous polymers, both in relation to broad molecular weight distribution and polymeric composition.

I.2.1.1 Block copolymers with narrow molecular weight distribution

Block copolymers are defined as two or more homopolymers which are covalently linked and may be argued as one of the largest areas of study within polymer science. Formation of a block copolymer is achieved by many methods, including sequential

addition and coupling, both of which utilize one polymerization mechanism. It is also possible to employ two or more polymerization mechanisms with a heterofunctional initiator or chain end transformation procedures.[9,48,54,55] As discussed in section I.1.2, ATRP is an excellent method to synthesize block copolymers in a controlled manner.[44]

Perhaps the most common procedure to synthesize block copolymers is sequential addition. ATRP retains chain end functionality and is therefore capable of this procedure to generate AB or ABC block copolymers among others.[56] Likewise, utilizing a difunctional initiator allows for the formation of ABCBA type copolymers. A consideration of this procedure is the activity of the monomers to be polymerized; to successfully generate a block copolymer, monomers must be polymerized in decreasing order of activity. For example, utilizing poly(methyl methacrylate), PMMA, as a macroinitiator for the polymerization of butyl acrylate (BA) will result in a well defined block copolymer. On the other hand, if the copolymer is synthesized in the reverse order, the diblock will not be well defined. (Figure I.2a). It is possible to circumvent this issue in ATRP through the process of halogen exchange.[57]

Halogen exchange with ATRP takes advantage of the differences in halogen reactivity to counteract the effects of monomer reactivity. Using the previous example, if it was necessary to first polymerize BA before MMA, a well defined block copolymer can be generated by polymerizing BA with the more active catalyst, CuBr/L. The sequential polymerization of MMA from the PBA macroinitiator with a bromine chain end, should be done with the less active catalyst, CuCl/L. Therefore, once a MMA monomer unit is added to the chain end, it remains inactive as the chlorine chain end is less active than the

bromine chain ends. The exchange of halogen results in well defined block copolymer, regardless of the monomer activity (Figure I.2.b).

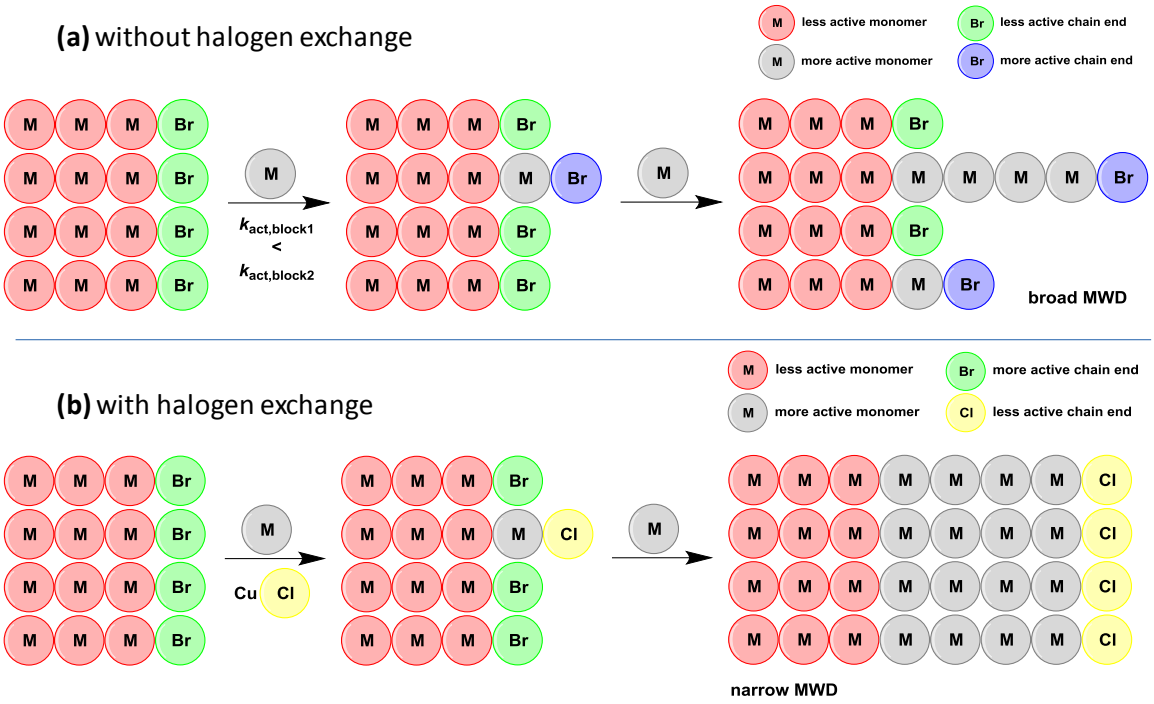

Figure I.2. Synthesis of block copolymer from a less active macroinitiator using a more active monomer (a) without and (b) with halogen exchange.

Coupling is another method to generate block copolymers. Click chemistry has been extremely successful in forming block copolymers from controlled radical polymerizations, as ATRP is tolerant to azide or alkine functionalities.[58] For example, initiators with either group may be utilized to generate functional homopolymers for click reactions. Coupling of telechelic polymers with hydroxyl, thiol, halogen, caryboxyl and amine end groups have been used to synthesize multiblock copolymers. While there are many advantages to coupling, a major drawback is the limited molecular weight of the blocks as well as potential for homopolymer contamination.

Additionally, it is possible to form block copolymers from two polymerization mechanisms.[48,54,59,60] The advantage of using two or more mechanisms is the possibility joining two homopolymers containing mechanistically incompatible monomers. Using multiple mechanisms may be done in two ways: a heterofunctional initiator or chain end transformation. A heterofunctional initiator is a small molecule which contains functionality for initiating two different types of polymerization, which may be conducted concurrently or independently, though each initiating site must be inactive for the opposing polymerization method. Heterofunctional initiators have been very successful as they are a direct procedure which requires no transformation or purification steps.

Mechanistic transformation is a process which takes advantage of functionalities present within polymers formed by one mechanism to be used for a second polymerization mechanism. The most common procedure to switch between one polymerization method and another is through chain end functionalization. Both AB diblocks and ABA triblocks are possible through this method if a semitelechelic or telechelic macroinitiator is used, respectively. A significant consideration to this method is the yield of functionalization; if less than 100% functionalization occurs, contamination by homopolymer or AB diblocks is possible.

Bulk properties of block copolymers with narrow MWD have also been widely studied. If the blocks are sufficiently incompatible, the polymers can self assemble into various phase domains including spheres, cylinders, gyroid and lamellae. Microphase separation relies on the segregation strength ($\chi_{AB}N$) which is a result of the interaction parameter (χ_{AB}) of the blocks in addition to the overall degree of polymerization (N).[61] For most polymers, segregation strength $\geq$10.5 is required for phase separation to occur. The

type of phase domain which arises is based on the volume fraction monomers, while the domain spacing (D) is in relation to the molecular weight of the block polymer ($D \propto M^{2/3}$).

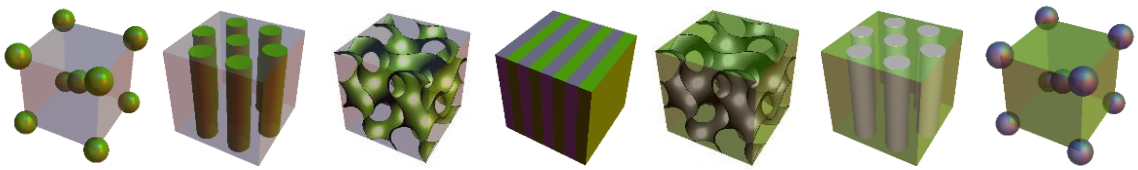

Figure I.3. Phase domains of diblock copolymers with narrow MWD.

I.2.1.2 Block copolymers with broad molecular weight distribution

It has been a long held opinion that the formation of well-ordered and long-range morpohologies requires block copolymers with narrow MWD. The concept of introducing a controlled amount of polydispersity into block copolymers was first theorized by Leibler *et al*.[62] in 1980. It was predicted that chain length disparity results in an increased amount of compositional fluctuations. This manuscript was promptly followed by Noolandi *et al.*[63] and Semenov *et al*.[64] who predicted that increased domain spacing will occur as well as a decrease in critical degree of segregation, respectively. In 2007, Matsen[65] predicted a coexsistance of lamellae and cylinders. While their findings were conceptually very exciting, experimental confirmation of the theoretical predictions was difficult due to a series of stumbling blocks, namely the synthesis of polymers with symmetrically broad molecular weight distributions.

Early forays into experimentally confirming the theoretical predictions of heterogeneity within polymers utilized blends of homogenous polymers. A library of

poly(styrene-*b*-vinylpyridine), PS-PVP, block copolymers were synthesized *via* anionic polymerization. The overall molecular weight of the block copolymers was held constant in the series while the chain composition was varied from 0.1 – 0.9 volume fraction PSt.[66] Using a blend of these well-defined polymers, a sample with broad distribution could be imitated. As predicted, the authors found that the domain spacing was larger for the disperse sample in comparison to monodisperse sample. The increase in domain size has been attributed to the wide range of molecular weights present in the disperse sample. An identical study was conducted with PVP-PS-PVP triblock copolymers;[67] a library of polymers with identical molecular weights but a range of compositions blended to simulate a disperse sample. Once again, the domain spacing was dilated in comparison to traditional samples without heterogeneity.

A second set of studies was conducted once again based on PS-PVP diblocks and PVP-PS-PVP triblocks. Unlike the previous studies where molecular weight was held constant throughout the samples, in this series composition was held constant while molecular weight was varied.[68] Interestingly, the increase in domain size was nearly identical for the blends of molecular weight as those for the blends of composition.

While synthetic blends were an admirable start, polymers whose broad molecular weight distributions are created during synthesis are more suitable candidates to experimentally confirm the theoretical predictions. Methods such as slow initiation and adding initiators or terminators to an ongoing polymerization can generate polymers with broad MWD.[69] However, these approaches lead to tailing in the GPC traces, which is not desired. Therefore, other synthetic paths were required and recent work has demonstrated

that manipulating the mechanism of a CRP itself is an excellent route to provide samples symmetrically broad and unimodal GPC traces.

Mahanthappa *et al*. took advantage of weaknesses in NMP to generate block copolymers with one disperse block.[70] For example, it has been well documented that NMP can successfully polymerize styrene while on the other hand PMMA is a notoriously difficult polymer to synthesize with this technique. In turn, uniform homopolymer of polystyrene (PSt) was synthesized by NMP, which was chain extended with MMA to result in a diblock copolymer with broad MWD (c.a. $M_w/M_n > 1.33$) as displayed in Figure I.4. Targeting a range of volume fractions of PMMA (f_M), the authors were able to confirm several of the theoretical predictions. Specifically, the phase diagram is shifted toward the disperse fraction as the cylinder/lamellae phase boundary occurred at $f_M = 0.5$, while the monodisperse analogue exhibits the same boundary at $f_M = 0.4$. The phase domains themselves were found to be dilated, which corroborated the work by Hillmyer *et al*.[71]; a phenemonon attributed to small chains not at the interface but acting as homopolymers in one domain. Finally, microphase separation occurred at lower χN values in comparison to the theoretical values for monodisperse analogues.

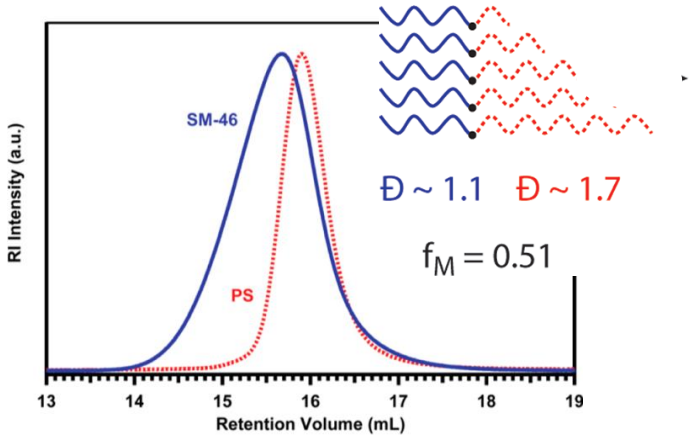

Figure I.4. Graphical representation of disperse PS-PMA diblock copolymers and the respective gel permeation chromatograph traces for PS homopolymer and PS-PMA diblock copolymer. Reprinted with permission from ref 69. Copyright © 2013 American Chemical Society.

ARGET ATRP was also utilized to generate diblock copolymers containing one disperse block.[72] As expressed in equation (I.1), the dispersity of molecular weights, defined as M_w/M_n, is determined by the deactivator concentration and lowering said concentration should increase the M_w/M_n of the final polymers.

$$\frac{M_w}{M_n} = 1 + \frac{1}{DP_n} + \frac{k_p[\text{R-X}]_0}{k_{da}[\text{X-Mt}^{n+1}/\text{L}]}\left(\frac{2}{p} - 1\right) \qquad \text{(I.1)}$$

Utilizing 50 ppm of Cu/L catalyst under ARGET ATRP conditions, a precise homopolymer of PSt was synthesized with M_w/M_n = 1.11. From this macroinitiator, two chain extensions of methyl acrylate (MA) were performed; the first a well controlled polymerization with 50 ppm of catalyst and the second with only 5 ppm of catalyst, resulting in a disperse second block. Hexagonally packed cylinders were observed for the well defined block

copolymer while the dispserse PSt-PMA sample exhibited hexagonally perforated lamellar (HPL) morphology for short- and long-term solvent-casting conditions. The stabilization of HPL morphology, typically considered to be metastable in well defined diblock copolymers, suggests that the distribution of the molecular weight in one segment of the block copolymer is an important parameter for morphology development during the microphase separation process.

Changes in microphase separation behavior due to heterogeneity within block copolymers is not limited to diblock copolymers, but has also been shown to equally affect triblock copolymers.[73,74] Perhaps one of the most thorough and exhaustive studies of heterogeneity within triblock copolymers was conducted by Mahanthappa *et al*.[75,76] Chain transfer ring-opening metathesis polymerization (ROMP-CT) was used to generate a disperse telechelic poly(butadiene) macroinitiator from which PSt was polymerized under ATRP conditions. Initial research on this triblock copolymer indicated stable morphologies with χN values as low as ~ 6.5, while monodiserse analogues require $\chi N \geq 17.9$ for microphase separation. Later studies included a library of 17 ABA triblock copolymer samples with a range of B-block volume fractions ($0.27 \geq f_B \leq 0.82$) from which a new phase diagram was created (Figure I.5). Most notable is the asymmetry of the phase diagram for ABA triblock copolymers with disperse B block, unlike that of precise copolymers. Overall, the diagram is shifted towards the disperse segment, meaning higher f_B values are required to achieve the same morphology as a monodisperse sample. Another significant alteration to the phase diagram is the bicontinuous domain; typically this morphology is limited to a very small volume fraction window. However, in the case of disperse ABA triblock copolymers, the bicontinuous window spans from $f_B = 0.45 - 0.53$.

The authors attribute the stable bicontinuous domain to the packing frustration that occurs for lamaellar morphology caused by the B block dispersity. Therefore, the interface buckles toward the B block forming the bicontinuous domain.

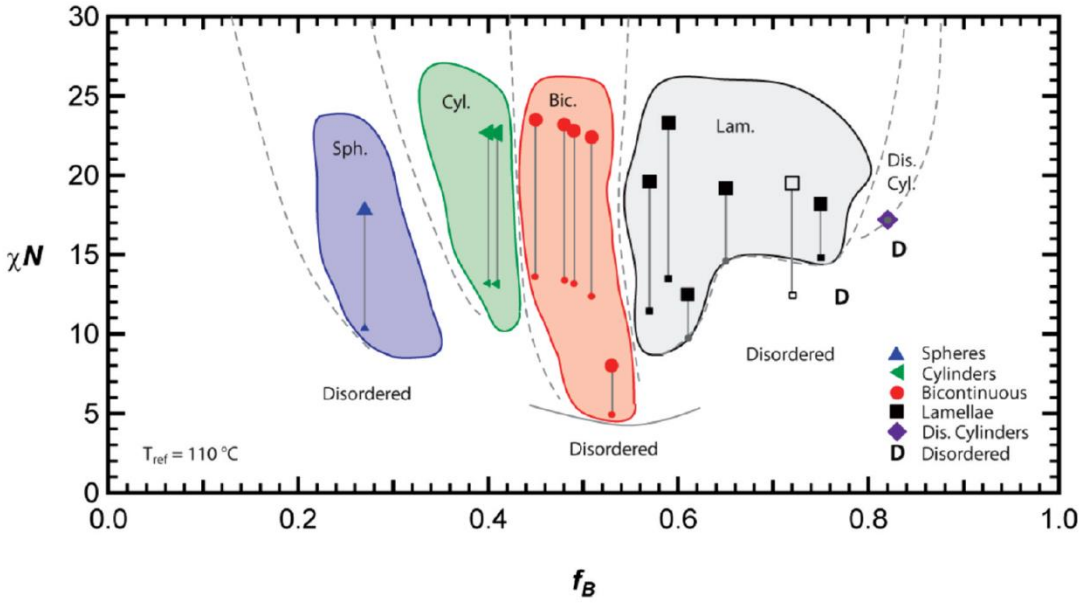

Figure I.5. Phase diagram created from 17 poly(styrene-*b*-butadiene-*b*-styrene) ABA triblock copolymers with disperse B block. Reprinted with permission from ref 75. Copyright © 2012 American Chemical Society.

Solution properties of similar ABA triblock copolymers with disperse B block were also studied.[77] Once again ROMP-CT was used to generate a disperse telechelic poly(butadiene) macroinitiator from which poly(ethylene oxide) was polymerized under anionic ring opening polymerization (ROP) conditions. As with the lamaller morphology, the B block dispersity within the ABA triblock copolymer caused frustration during micelle arrangement. The smaller chains formed areas of higher curvature than that of larger chains, resulting in football-like micelles. Typically, high aspect ratio micelles are created

through complex macromolecular architectures requiring tedious synthetic procedures or use of crystallizable segements,[78-81] while this work demonstrates similar micelles have been formed based solely on introducing a controlled amount of heterogeneity into the ABA triblock structure.

It is interesting to note that the previous examples of disperse block copolymers were asymmetrically disperse; meaning only one segment of the di- or triblock copolymer had broad molecular weight distribution. This is not to say that the molecular weight distribution was asymmetrically disperse as all samples exhibited symmetrically broad and unimodal GPC traces. However, the placement of the dispersity within the block copolymer segments was asymmetric. Studies were conducted on symmetrically disperse AB diblock and $(AB)_n$ copolymers; contrary to the previous examples, the copolymers with dispersity in all blocks were found to behave similarly to their monodisperse analogues.[82-85] On the other hand, Milner[86] found that distorted phase diagrams may be achieved by mikto star copolymers in which each arm is either of type A or B. It was predicted that the number of kind of arm as well as the length ratio between A and B have a profound effect on the morphology realized.

I.2.1.3 Heterogeneous compositions: periodic and gradient copolymers

Composition is an extremely important aspect to polymer chemistry as the properties of polymers are closely linked with their structure.[9,87] The simple act of including a second type of monomer unit into a polymer chain can drastically alter the final properties and applications of a material. Furthermore, the placement, or order, of monomer units also has a major impact on how the polymer behaves. For example, the

same two monomers may be utilized to generate block, periodic and gradient copolymers, however each material will be relevant for a unique set of applications resulting from distinct properties. The syntheses, properties and applications of block, periodic and gradient copolymers are summarized in Figure I.6. Section I.2.1.1 focused on block copolymers therefore this section will center on periodic and gradient copolymers, compositions which are more difficult to synthesize but result in equally complex properties and applications.

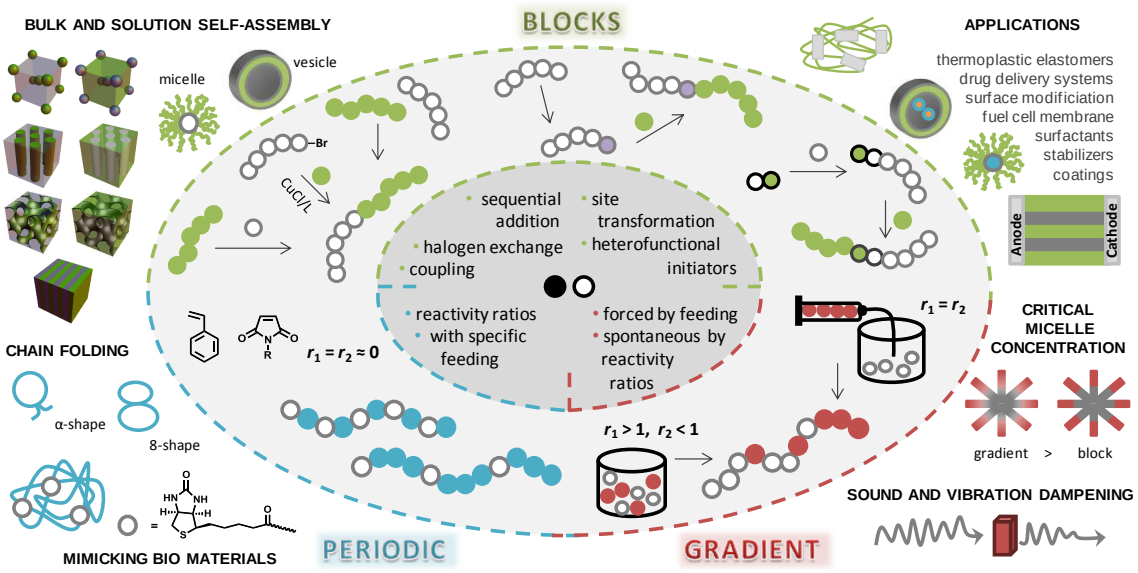

Figure I.6. Synthetic methods and properties of block, periodic and gradient copolymers.[53]

When more than one type of monomer is incorporated during polymerization, the reactivity ratios of monomers play a central role in polymer composition as they are a measure of the likelihood of an active center to propagate with its own monomer over the second monomer (Scheme I.3). Specifically, the ratio of homopropagation (k_{11}) to cross-propagation (k_{12}) rate constants defines the reactivity ratio for monomer one (r_1). The same is then true for monomer two; r_2 is defined by the homopropagation (k_{22}) to cross-

propagation (k_{21}) rate constant ratio. In turn, reactivity ratios determine the rate at which the monomers are incorporated into the polymer chain and may give insight to the type of composition formed. For example, if the reactivity ratios are very similar ($r_1 = r_2$) as with two acrylate based monomers, a statistical copolymer will be formed as they are equally likely to homopropagate as cross-propagate. A gradient copolymer is formed when $r_1 > 1$ and $r_2 < 1$ as with a methacrylate/acrylate monomer pair. In this case, the methacrylate is more likely to homopropagate and will therefore be incorporated into the polymer at a faster rate than the acrylate based monomer, which prefers to cross-propagate. Perhaps one of the most rare examples is $r_1 = r_2 \approx 0$ in which case both monomers almost exclusively prefer to cross-propagate than homopropagate, thereby resulting in an alternating copolymer.[88] The most classic example describes the copolymerization of styrene with other vinyl monomers in the presence of a Lewis acid to form an alternating composition.[89-91]

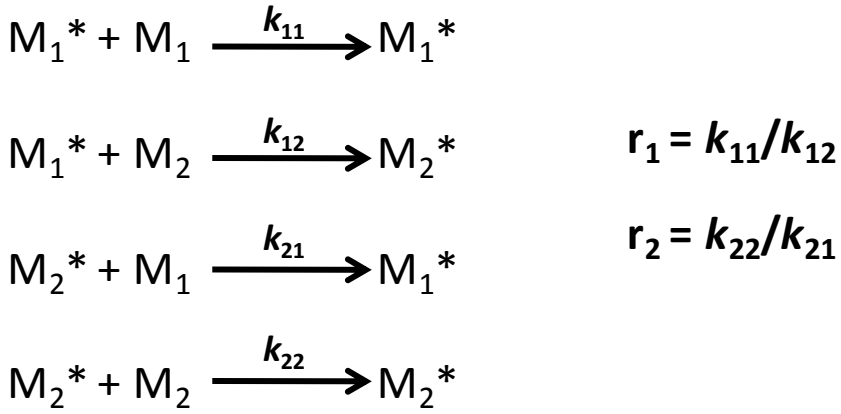

Scheme I.3. Rate constants of homo- and cross propagation and the resulting reactivity ratios for M_1 and M_2.

Alternating copolymers are the simplest model of a periodic copolymer, a style of composition which contains a repeat component, in this case AB, recurring throughout the polymer chain. However, recent work has focused on expanding periodic copolymers to include repeat components such as ABB, ABC, ABA as well as other more intricate systems (Figure I.7).

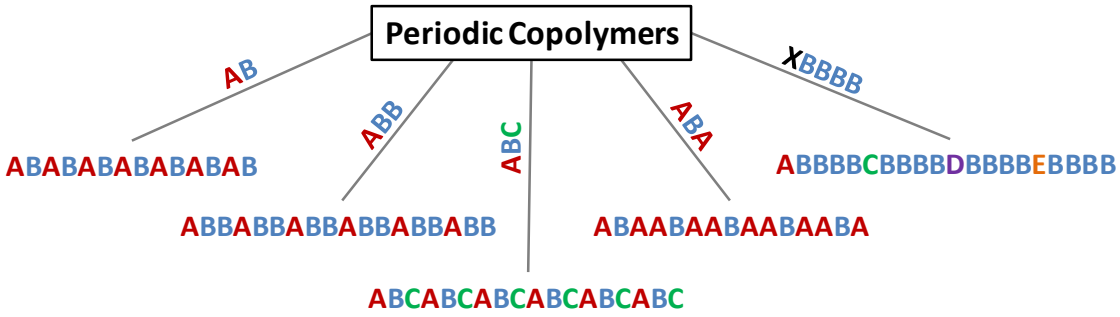

Figure I.7. Representations of potential periodic copolymers.

An alternating copolymer based on a templated monomer was reported by Sawamoto *et al.* in 2011.[92] Acrylic and methacrylic monomer units were tethered to naphthalene, which was cleaved post-polymerization resulting, in an AB alternating copolymer. While the functionality of the (meth)acrylic acid polymer was not particularly exciting, this work paved the way for the next templated monomer and consequential ABA periodic copolymer.[93] Utilizing a palladium template, a 4-vinylpiridine unit was encased by styrene on either side. The π -π stacking of the aromatic side groups in combination with a bulky fluoroalcohol solvent aligned the three vinyl groups to prevent gelation and afford 95% cyclization efficiency. Post polymerization removal of the template then gave the ABA periodic copolymer.

Templated initiators were also proven to be effective for sequence controlled polymerization by Sawamoto *et al.*[94-96] Preliminary studies indicated that template initiators with functional groups for monomer recognition could selectively add monomers *via* radical addition. In particular, an initiator with a crown ether moiety could select ionic monomers based on the size of their cation while amine functionality selected acidic monomers over other non-recognizable monomers present. The authors extended this work to include template polymerization by first generating a polymer with pendant amine functionalities which selectively recognized and polymerized methacrylic acid over benzyl methacrylate (Figure I.8). It is interesting to note that upon polymerization of these monomers without the template resulted in a polymer consisting mainly of benzyl methacrylate as it is the more reactive monomer.

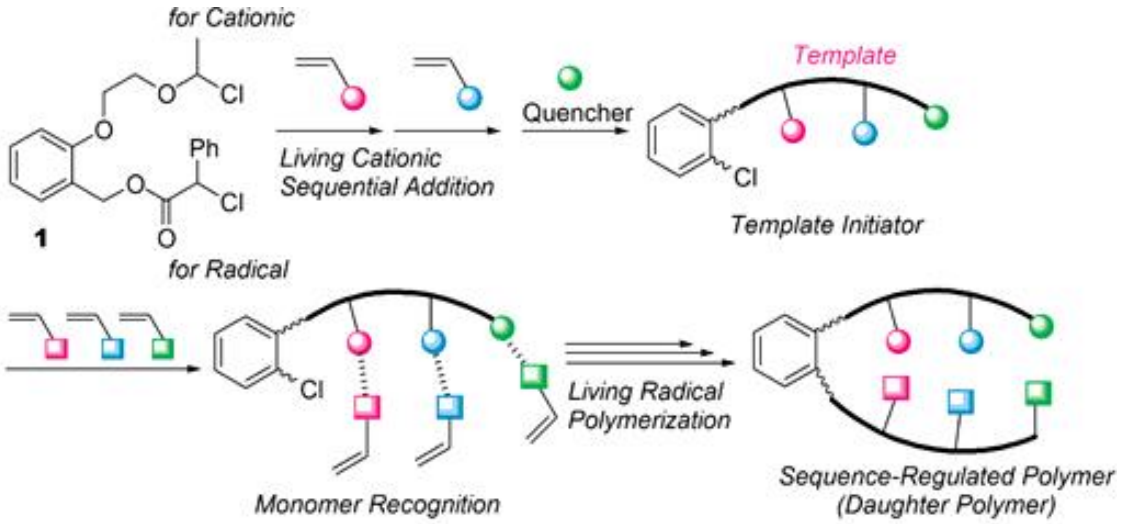

Figure I.8. Template initiators for sequence regulated polymerization. Reprinted with permission from ref 92. Copyright © 2010 American Chemical Society.

Lutz and coworkers have also contributed significantly to the field of periodic copolymers.[97-99] Their approach manipulates monomers with typically alternating characteristics in a very clever way to direct placement of functional monomers along the polymer chain. The majority of the work by Lutz *et al.* follows the initial 2007 report in which styrene and maleimide based monomers were polymerized (Figure I.9).[100] By the sequential addition of one equivalent of functional maleimide relative to initiator into the polymerization of styrene, a polymer with pre-programmed functional side groups was achieved. This technique was accomplished with both ATRP and NMP[101] and was applied to a variety of functional monomers resulting in polymers with pendant hydrophilic groups[102] as well as dendrons[103]. Post polymerization modification techniques were also used to afford biotin functionality at dictated points in the polymer chains.[104]

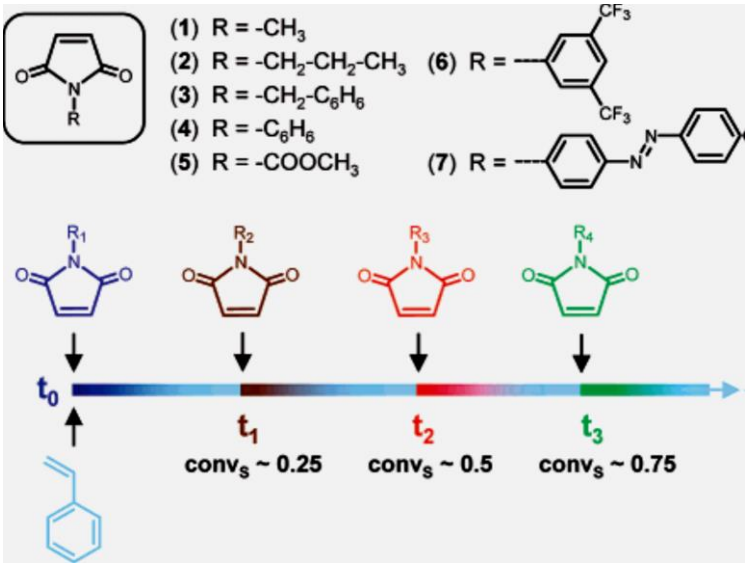

Figure I.9. Sequence controlled polymerizations of styrene and maleimide based monomers. Reprinted with permission from ref 98. Copyright © 2007 American Chemical Society.

Perhaps the most exciting use of the directed pendant functionality afforded with Lutz's technique was the opportunity for chain folding. Unlike telechelic or heterotelechelic polymers, this method was not limited to chain end functionality. Therefore, placement of alkyne groups within the polymer chain in conjunction with chain end azide functionality resulted in P-, Q-, and 8-shaped polymers. Utilizing two alkyne groups within one chain in addition to an azide functional small molecule afforded α-shaped materials. [105] Furthermore, incorporating two cysteine groups into the polymer chains also allowed for intramolecular cyclization with the formation of twin difsulide cyclic bridge. [106]

The previous examples of periodic copolymers were focused on sequence controlled polymerization. However, it is possible to generate periodic composition not through polymerization, but by smaller synthetic steps.[107] Atom transfer radical addition was utilized with di-functional initiators, containing AA functionality, to add individual single monomer units thereby creating BAAB repeat components. After purification, the periodic copolymer was synthesized *via* atom transfer radical coupling. While some side reactions did occur, high molecular weight copolymers were obtained.[108]

Lutz utilized the Merrifield synthesis as inspiration to generate coded oligomers based on an "AB+CD" approach.[109] Two types of chemoselective reactions, azide-alkyne cycloaddition and amidification, were alternated in an iterative process to synthesize monodisperse coded oligomers without any deprotection steps. While the "coding" was simply an additional methyl group, the proof of concept was clear: polymer science is capable of coding information within monodisperse synthetic oligomers.

Periodic copolymers, including those discussed above, are of particular interest owing to their well defined sequenced microstructure; a crucial feature to mimicking nature. Natural proteins have an extremely specific sequence of amino acids allowing them to perform incredible tasks such as organocatalysis, selective transport and signal transduction.[98] While Nature has perfected sequence controlled polymerizations,[97] to date there is only one synthetic method which controls the microstructure on such a detailed level: the Merrifield synthesis of proteins.[110] Unfortunately, this is an extremely tedious and time consuming process but has since been successfully automated. Therefore, it is up to polymer scientists to find alternative paths to sequence controlled polymerizations so that non-natural polymers may reach the complexity and functionality of their natural analogues. The recent surge within this field has certainly narrowed the gap between biology and polymer science though there is still much work to be done.[111,112]

Gradient copolymers have also received increasing attention due to their ability to achieve properties which are unavailable by homopolymers and traditional copolymers.[113,114] Unlike block copolymers, which comprise an instantaneous switch between monomer units, gradient copolymers have a continuous compositional drift from one chain end to the other.[115] Resulting from this unique composition, gradient copolymers may exhibit special interfacial phase behaviors, increased critical micelle concentrations, reeling-in micelle effects, and broadened glass transition temperatures (T_g).[116-125] The degree to which these properties occur may be tuned by the specific composition of monomers and gradient quality. These rare properties suggested the use of gradient copolymers as polymer blend compatibilizers, additives for sound and vibration dampening, and stabilizers for emulsions.[118,126]

Two main methods exist to synthesize gradient copolymers via controlled/living polymerization: spontaneous and forced methods (Figure I.10).[113] The spontaneous gradient, or batch method, takes advantage of differences in reactivity ratios (r_1 *and* r_2) between monomers to spontaneously generate a smooth change in monomer composition along the polymer chain. Therefore, all monomers are present in the reaction flask throughout the polymerization. The reactivity ratios can be used to estimate the severity/quality of the gradient or the composition of the polymer chains. On the other hand, forced gradient may utilize monomers with similar reactivity ratios but requires a continuous feeding of one monomer into a solution of a second monomer throughout the polymerization. The severity of the gradient is controlled by the feed time of the second monomer as well as the overall ratio of monomers.

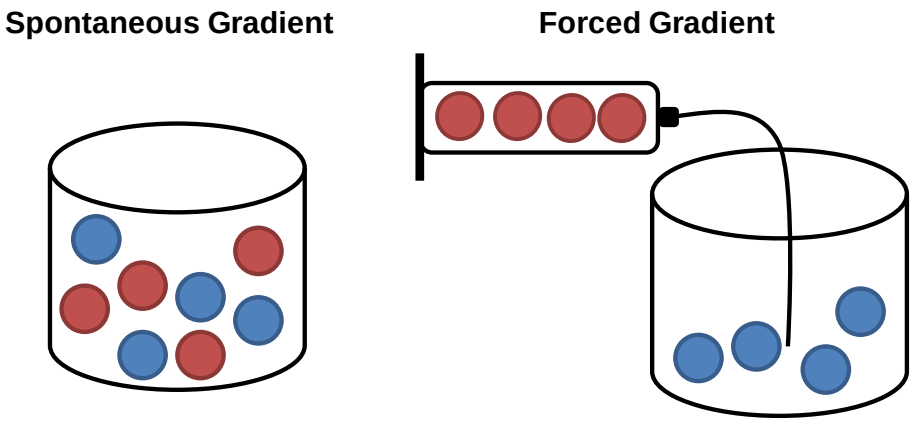

Figure I.10. Spontaneous and forced methods for gradient copolymer synthesis.

Requirements for the synthesis of precise gradient copolymers include fast initiation, uniform chain growth and facile cross-propagation. Such requirements allow all polymer chains to initiate at once while propagating at the same pace, allowing a consistent gradient composition among all chains. Atom transfer radical polymerization (ATRP) is

an excellent candidate for synthesizing gradient copolymers due to its controlled/living nature and has proven to successfully synthesize a variety of such copolymers.[113,127-130] Furthermore, ATRP has allowed for the synthesis of gradient copolymers in aqueous dispersed media and, as discussed in Section I.1.2, conducting polymerizations in dispersed media has a plethora of benefits. Both the spontaneous[130] and forced[127] gradient methods were applied to aqueous dispersed media, specifically the miniemulsion system; in each case, the copolymers formed in miniemulsion were similar to those formed in bulk.

A recent study has taken a unique perspective on the forced gradient method to generate gradient copolymers.[131] Unlike the traditional method, where one monomer is continuously fed into a polymerization of another, this work fed both monomers in "shots" throughout the polymerization. By allowing each addition to reach high monomer conversion as well as varying the ratio of monomers within each, a gradient copolymer was formed. In essence, one polymer chain was treated as a decablock copolymer, gradually altering the composition within each block. Nevertheless, the copolymers were found to have the expected properties of gradient copolymers including broad glass transition temperature and tenuous microphase separation.

In 2009 Sawamoto and coworkers took an alternative route to synthesize gradient copolymers by producing the second monomer in situ (Figure I.11).[132] MMA was polymerized by ruthenium-mediated living radical polymerization in the presence of a metal alkoxide [$Al(O\textit{i}\text{-}Pr)_3$ or $Ti(O\textit{i}\text{-}Pr)_3$] and various alcohols as the solvent. The metal alkoxide together with the alcohol resulted in transesterification of the pendent ester groups on MMA monomers. As the reaction only proceeded with monomers, as proven by the lack of transesterification on a pure PMMA polymer, the monomer composition gradually

changed as propagation occurred, thereby resulting in a gradient copolymer. This technique was applicable toward a variety of alcohols for the transesterification including dodecanol, which resulted in a gradient copolymer with an extremely broad glass transition temperature, spreading over 170 °C.[133] The versatility of this technique was further established by the synthesis of other composition styles including random, block and gradient-block copolymers.[134]

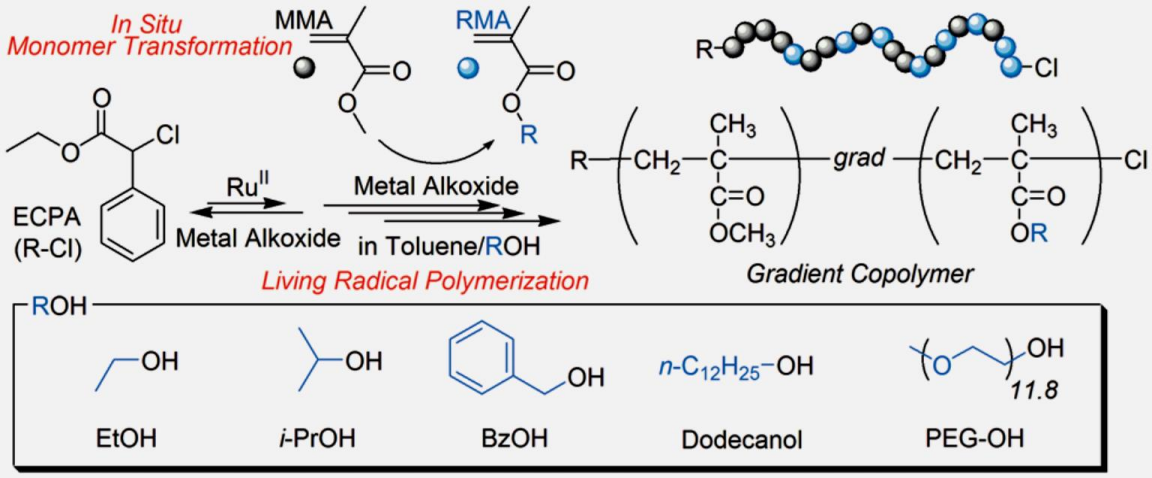

Figure I.11. Gradient copolymers via in situ monomer transformation. Reprinted with permission from Ref 129. Copyright © 2009 American Chemical Society.

Characterization of gradient profile is most often accomplished through changes in monomer conversion measured by ^{1}H NMR. Knowing the conversion of each monomer (%*conv*) as well as the initial concentrations for monomers 1 and 2 ($[M_1]_0$ and $[M_2]_0$) the cumulative composition can be calculated using equation (I.2). The cumulative composition may then be translated into the instantaneous composition with equation (I.3).

$$F_{cum,1} = \frac{(\%conv)_1[M_1]_0}{(\%conv)_1[M_1]_0+(\%conv)_2[M_2]_0} \quad \text{(I.2)}$$

$$F_{inst,1} = F_{cum,1} + (\%conv)\frac{\Delta F_{cum,1}}{\Delta(\%conv)} \quad \text{(I.3)}$$

While these two equations are regularly used and accepted as methods to characterize gradient profile, they may not necessarily be an accurate portrayal of the architecture. ^{1}H NMR measures the overall change in monomer conversion and therefore the equations result in the average composition among all chains. However, when utilizing a monomer such as HEMA-TMS during gradient copolymer synthesis, the material may be transformed into molecular bottlebrushes which allows for single molecule visualization with atomic force microscopy (AFM).[129] As the gradient composition is directly tied to grafting density of the side chains, the gradient may be visualized through the height profile as measured by AFM.[128] It was further shown that the height profile of the molecular bottlebrushes corresponds to the instantaneous composition measured by ^{1}H NMR indicating this is indeed a sufficient method to illustrate gradient profile for well controlled polymerizations.

I.3. Conclusions

Since the emergence of controlled radical polymerizations such as ATRP, there has been a tremendous increase in the control over molecular weight and molecular weight distributions for a wide range of synthetic polymers. While these well defined materials have very interesting properties including bulk and solution self-assembly, recent work has shown that introducing a controlled amount of distribution may produce even more fascinating results. Likewise, generating complex compositions such as gradient or periodic copolymers also afford unique properties which provide avenues for single-chain folding or stabilizers for emulsions. However, there is much work to be done fully

exploring their use within the proposed applications. In summary, including some degree of heterogeneity into materials does not detract from their performance, but may enhance their qualities and ATRP is an excellent method to provide such tailored materials.

I.4. References

1. Moad, G.; Solomon, D. H. *The chemistry of free radical polymerization* Elsevier Science Bath, 1995.
2. Odian, G. *Principles of Polymerization, 4th Edition* 2004.
3. Matyjaszewski, K. *Macromolecules* **2012,** *45*, 4015-4039.
4. Szwarc, M. *Nature* **1956,** *178*, 1168-1169.
5. Szwarc, M.; Levy, M.; Mikovich, R. *J. Am. Chem. Soc.* **1956,** *78*, 2656-2657.
6. Webster, O. W. *Science* **1991,** *251*, 887-893.
7. Braunecker, W. A.; Matyjaszewski, K. *Prog. Polym. Sci.* **2007,** *32*, 93-146.
8. Hadjichristidis, N.; Iatrou, H.; Pitsikalis, M.; Mays, J. *Progress in Polymer Science* **2006,** *31*, 1068-1132.
9. Matyjaszewski, K.; Gnanou, Y.; Leibler, L., Eds. *Macromolecular Engineering: From Precise Macromolecular Synthesis to Macroscopic Materials Properties and Applications*; Wiley-VCH Weinheim, 2007.
10. Matyjaszewski, K. *Prog. Polym. Sci.* **2005,** *30*, 858-875.
11. Georges, M. K.; Veregin, R. P. N.; Kazmaier, P. M.; Hamer, G. K. *Macromolecules* **1993,** *26*, 2987-2988.
12. Hawker, C. J.; Bosman, A. W.; Harth, e. *Chem. Rev.* **2001,** *101*, 3661-3688.
13. Grubbs, R. B. *Polym. Rev.* **2011,** *51*, 104-137.

14. Nicolas, J.; Guillaneuf, Y.; Lefay, C.; Bertin, D.; Gigmes, D.; Charleux, B. *Prog. Polym. Sci.* **2013,** *38*, 63-235.

15. Chiefari, J.; Chong, Y. K.; Ercole, F.; Krstina, J.; Jeffery, J.; Le, T. P. T.; Mayadunne, R. T. A.; Meijs, G. F.; Moad, C. L.; Moad, G.; Rizzardo, E.; Thang, S. H. *Macromolecules* **1998,** *31*, 5559-5562.

16. Moad, G.; Rizzardo, E.; Thang, S. H. *Polymer* **2008,** *49*, 1079-1131.

17. Moad, G.; Rizzardo, E.; Thang, S. H. *Aust. J. Chem.* **2006,** *59*, 669-692.

18. Moad, G.; Chiefari, J.; Chong, Y. K.; Krstina, J.; Mayadunne, R. T. A.; Postma, A.; Rizzardo, E.; Thang, S. H. *Polym. Int.* **2000,** *49*, 993-1001.

19. Wang, J. S.; Matyjaszewski, K. *J. Am. Chem. Soc.* **1995,** *117*, 5614-5615.

20. Matyjaszewski, K.; Xia, J. *Chem. Rev.* **2001,** *101*, 2921-2990.

21. Kato, M.; Kamigaito, M.; Sawamoto, M.; Higashimura, T. *Macromolecules* **1995,** *28*, 1721-1723.

22. Goto, A.; Fukuda, T. *Prog. Polym. Sci.* **2004,** *29*, 329-385.

23. Tsarevsky, N.; Matyjaszewski, K. *Chem. Rev.* **2007,** *107*, 2270-2299.

24. Pintauer, T.; Matyjaszewski, K. *Chem. Soc. Rev.* **2008,** *37*, 1087-1097.

25. Matyjaszewski, K.; Jakubowski, W.; Min, K.; Tang, W.; Huang, J.; Braunecker, W. A.; Tsarevsky, N. V. *Proc. Natl. Acad. Sci. U.S.A.* **2006,** *103*, 15309-14.

26. Jakubowski, W.; Matyjaszewski, K. *Angew. Chem., Int. Ed.* **2006,** *45*, 4482-4486.

27. Magenau, A. J. D.; Strandwitz, N. C.; Gennaro, A.; Matyjaszewski, K. *Science* **2011,** *332*, 81-84.

28. Magenau, A. J. D.; Kwak, Y.; Matyjaszewski, K. *Macromolecules* **2010,** *43*, 9682-9689.

29. Xia, J. H.; Gaynor, S. G.; Matyjaszewski, K. *Macromolecules* **1998,** *31*, 5958-5959.

30. Xia, J. H.; Matyjaszewski, K. *Macromolecules* **1999,** *32*, 2434-2437.

31. Wang, J. S.; Matyjaszewski, K. *Macromolecules* **1995,** *28*, 7901-7910.

32. Min, K.; Matyjaszewski, K. *Macromolecules* **2005,** *38*, 8131-8134.

33. Kagawa, Y.; Kawasaki, M.; Zetterlund, P. B.; Minami, H.; Okubo, M. *Macromol. Rapid Commun.* **2007,** *28*, 2354-2360.

34. Min, K.; Gao, H. F.; Matyjaszewski, K. *J. Am. Chem. Soc.* **2005,** *127*, 3825-3830.

35. Min, K.; Jakubowski, W.; Matyjaszewski, K. *Macromol. Rapid Commun.* **2006,** *27*, 594-598.

36. Bombalski, L.; Min, K.; Dong, H. C.; Tang, C. B.; Matyjaszewski, K. *Macromolecules* **2007,** *40*, 7429-7432.

37. Min, K.; Yu, S.; Lee, H. I.; Mueller, L.; Sheiko, S. S.; Matyjaszewski, K. *Macromolecules* **2007,** *40*, 6557-6563.

38. Qiu, J.; Gaynor, S. G.; Matyjaszewski, K. *Macromolecules* **1999,** *32*, 2872-2875.

39. Jousset, S.; Qiu, J.; Matyjaszewski, K. *Macromolecules* **2001,** *34*, 6641-6648.

40. Eslami, H.; Zhu, S. P. *Polymer* **2005,** *46*, 5484-5493.

41. Eslami, H.; Zhu, S. P. *J. Polym. Sci., Part A: Polym. Chem.* **2006,** *44*, 1914-1925.

42. Min, K.; Gao, H.; Yoon, J. A.; Wu, W.; Kowalewski, T.; Matyjaszewski, K. *Macromolecules* **2009,** *42*, 1597-1603.

43. Cunningham, M. F. *Prog. Polym. Sci.* **2008,** *33*, 365-398.

44. Davis, K. A.; Matyjaszewski, K. In *Advances in Polymer Science*; Springer Berlin / Heidelberg, 2002.

45. Matyjaszewski, K.; Tsarevsky, N. V. *Nat. Chem.* **2009,** *1*, 276-288.

46. Matyjaszewski, K. *Science* **2011,** *333*, 1104-1105.

47. Gao, H.; Matyjaszewski, K. *Prog. Polym. Sci.* **2009,** *34*, 317-350.

48. Coessens, V.; Pintauer, T.; Matyjaszewski, K. *Progress in Polymer Science* **2001,** *26*, 337-377.

49. Cunningham, M. F. *Progress in Polymer Science* **2002,** *27*, 1039-1067.

50. Qiu, J.; Charleux, B.; Matyjaszewski, K. *Progress in Polymer Science* **2001,** *26*, 2083-2134.

51. Min, K.; Gao, H. F.; Matyjaszewski, K. *J. Am. Chem. Soc.* **2006,** *128*, 10521-10526.

52. Min, K.; Matyjaszewski, K. *Cent. Eur. J. Chem.* **2009,** *7*, 657-674.

53. Matyjaszewski, K.; Tsarevsky, N. *J. Am. Chem. Soc.* **2014,** *ASAP*, DOI: 10.1021/ja408069v.

54. Atilla Tasdelen, M.; Kahveci, M. U.; Yagci, Y. *Prog. Polym. Sci.* **2011,** *26*, 455-567.

55. Hadjichristidis, N.; Pitsikalis, M.; Iatrou, H. *Advances in Polymer Science* **2005,** *189*, 1-124.

56. Davis, K. A.; Matyjaszewski, K. *Macromolecules* **2001,** *34*, 2101-2107.

57. Peng, C.-H.; Kong, J.; Seeliger, F.; Matyjaszewski, K. *Macromolecules* **2011,** *44*, 7546-7557.

58. Golas, P. L.; Matyjaszewski, K. *Chem. Soc. Rev.* **2010,** *39*, 1338-1354.

59. Bernaerts, K.; Du Prez, F. E. *Prog. Polym. Sci.* **2006,** *31*, 671-722.

60. Yagci, Y.; Tasdelen, M. A. *Prog. Polym. Sci.* **2006,** *31*, 1133-1170.

61. Bates, F. S. *Annu. Rev. Phys. Chem.* **1990,** *41*, 525-527.

62. Leibler, L.; Benoit, H. *Polymer* **1981,** *22*, 195-201.

63. Hong, K. M.; Noolandi, J. *Polym. Commun.* **1984,** *25*, 265-268.

64. Burger, C.; Ruland, W.; Semenov, A. N. *Macromolecules* **1990,** *23*, 3339-3346.

65. Matsen, M. W. *Phys. Rev. Lett.* **2007,** *99* 1-4.

66. Matsushita, Y.; Noro, A.; Suzuki, J.; Ohtani, H.; Takano, A. *Macromolecules* **2003,** *36*, 8074-8077.

67. Noro, A.; Iinuma, M.; Suzuki, J.; Takano, A.; Matsushita, Y. *Macromolecules* **2004,** *37*, 3804-3808.

68. Noro, A.; Cho, D.; Suzuki, J.; Takano, A.; Matsushita, Y. *Macromolecules* **2005,** *38*, 4371-4376.

69. Lynd, N. A.; Hillmyer, M. A. *Macromolecules* **2007,** *40*, 8050-8055.

70. Widen, J. M.; Kim, M.; Schmitt, A. K.; Han, E.; Gopalan, P.; Mahanthappa, M. K. *Macromolecules* **2013** *46*, 4472-4480.

71. Lynd, N. A.; Hillmyer, M. A. *Macromolecules* **2005,** *38*, 8803-8810.

72. Listak, J.; Jakubowski, W.; Mueller, L.; Plichta, A.; Matyjaszewski, K.; Bockstaller, M. R. *Macromolecules* **2008,** *41*, 5919-5927.

73. Ruzette, A.-V.; Tence-Girault, S.; Leibler, L. *Macromolecules* **2006,** *39*, 5804-5814.

74. Schmitt, A. L.; Mahanthappa, M. K. *Soft Matter* **2012,** *8*, 2294-2303.

75. Widin, J. M.; Schmitt, A. K.; Im, K.; Schmitt, A. L.; Mahanthappa, M. K. *Macromolecules* **2010,** *43*, 7913-7915.

76. Widin, J. M.; Schmitt, A. K.; Im, K.; Mahanthappa, M. K. *J. Am. Chem. Soc.* **2012,** *134*, 3834-3844.

77. Schmitt, A. K.; Repollet Pedrosa, M. H.; Mahanthappa, M. K. *ACS Macro Lett.* **2012,** *1,* 300-304.

78. Percec, V.; Wilson, D. A.; Leowanawat, P.; Wilson, C. J.; Hughes, A. D.; Kaucher, M. S.; Hammer, D. A.; Levine, D. H.; Kim, A. J.; Bates, F. S.; Davis, K. P.; Lodge, T. P.; Klein, M. L.; DeVane, R. H.; Aqad, E.; Rosen, B. M.; Argintaru, A. O.; Sienkowska, M. J.; Rissanen, K.; Nummelin, S.; Ropponen, J. *Science* **2010,** *328,* 1009-1014.

79. Cho, B. K.; Jian, A.; Gruner, S. M.; Wiesner, U. *Chem. Commun.* **2005**, 2143−2145.

80. Gadt, T.; Ieong, N. S.; Cambridge, G.; Winnik, M. A.; Manners, I. *Nat. Mater.* **2009,** *8,* 144-150.

81. Yin, L.; Hillmyer, M. A. *Macromolecules* **2011,** *44,* 3021-3028.

82. Bendejacq, D.; Ponsinet, V.; Joanicot, M.; Loo, Y. L.; Register, R. A. *Macromolecules* **2002,** *35,* 6645-6649.

83. Hustad, P. D.; Marchand, G. R.; Garcia-Meitin, E. I.; Roberts, P. L.; Weinhold, J. D. *Macromolecules* **2009,** *42,* 3788-3794.

84. Li, S.; Register, R. A.; Landes, B. G.; Hustad, P. D.; Weinhold, J. D. *Macromolecules* **2010,** *43,* 4761-4770.

85. Matsen, M. W. *Macromolecules* **2012,** *45,* 2161-2165.

86. Milner, S. T. *Macromolecules* **1994,** *27,* 2333-2335.

87. Badi, N.; Chan-Seng, D.; Lutz, J. F. *Macromol. Chem. Phys.* **2013,** *214*, 135-142.

88. Cowie, J. M. G. *Alternating Copolymers*; Plenum Press: New York, 1985.

89. Rzaev, Z. M. O. *Prog. Polym. Sci.* **2000,** *25*, 163-217.

90. Hirooka, M.; Yabuuchi, H.; Iseki, J.; Nakai, Y. *J. Polym. Sci., Part A: Polym. Chem.* **1968,** *6*, 1381-1396.

91. Lutz, J. F.; Kirci, B.; Matyjaszewski, K. *Macromolecules* **2003,** *36*, 3136-3145.

92. Hibi, Y.; Tokuoka, S.; Terashima, T.; Ouchi, M.; Sawamoto, M. *Polym. Chem.* **2011,** *2*, 341-347.

93. Hibi, Y.; Ouchi, M.; Sawamoto, M. *Angew. Chem. Int. Ed.* **2011,** *50*, 7434-7437.

94. Ida, S.; Terashima, T.; Ouchi, M.; Sawamoto, M. *J. Am. Chem. Soc.* **2009,** *131*, 10808-10809.

95. Ida, S.; Ouchi, M.; Sawamoto, M. *J. Am. Chem. Soc.* **2010,** *132*, 14748-14750.

96. Ida, S.; Ouchi, M.; Sawamoto, M. *Macromol. Rapid Commun.* **2011,** *32*, 209-214.

97. Badi, N.; Lutz, J. F. *Chem. Soc. Rev.* **2009,** *38*, 3383-3390.

98. Lutz, J. F. *Polym. Chem.* **2010,** *1*, 55-62.

99. Lutz, J. F.; Schmidt, B. V. K. J.; Pfeifer, S. *Macromol. Rapid Commun.* **2011,** *32*, 127-135.

100. Pfeifer, S.; Lutz, J. F. *J. Am. Chem. Soc.* **2007,** *129*, 9542-9543.

101. Zamfir, M.; Lutz, J. F. *Nat. Commun.* **2012,** *3*, 1138.

102. Srichan, S.; Chan-Seng, D.; Lutz, J. F. *Macro Lett.* **2012,** *1*, 589-592.

103. Baradel, N.; Gok, O.; Zamfir, M.; Sanyal, A.; Lutz, J. F. *Chem. Commun.* **2013,** *49*, 7280-7282.

104. Kakuchi, R.; Zamfir, M.; Lutz, J. F.; Theato, P. *Macromol. Rapid Commun.* **2012,** *33*, 54-60.

105. Schmidt, B.; Fechler, N.; Falkenhagen, J.; Lutz, J. F. *Nature Chemistry* **2011,** *3*, 234-238.

106. Shishkan, O.; Zamfir, M.; Gauthier, M. A.; Borner, H. G.; Lutz, J. F. *Chem. Commun.* **2014,** *50*, 1570-1572.

107. Satoh, K.; Ozawa, S.; Mizutani, M.; Nagai, K.; Kamigaito, M. *Nat. Commun.* **2010,** *1*, 6.

108. Wang, C.-H.; Song, Z.-Y.; Deng, X.-X.; Zhang, L.-J.; Du, F.-S.; Li, Z.-C. *Macromol. Rapid Commun.* **2014,** *35*, 474-478.

109. Trinh, T. T.; Oswald, L.; Chan-Seng, D.; Lutz, J. F. *Macromol. Rapid Commun.* **2014,** *35*, 141-145.

110. Merrifield, R. B. *J. Am. Chem. Soc.* **1963,** *85*, 2149-2154.

111. Ouchi, M.; Badi, N.; Lutz, J. F.; Sawamoto, M. *Nat. Chem.* **2011,** *3*, 917-924.

112. Lutz, J. F.; Ouchi, M.; Liu, D. R.; Sawamoto, M. *Science* **2013,** *341*, 1238149.

113. Matyjaszewski, K.; Ziegler, M. J.; Arehard, S. V.; Greszta, D.; Pakula, T. *Journal of Physical Organic Chemistry* **2000,** *13*, 775-786.

114. Zaremski, M. Y.; Kalugin, D. I.; Golubev, V. B. *Polymer Science* **2009,** *51*, 103-122.

115. Pakula, T.; Matyjaszewski, K. *Macromolecular Theory and Simulations* **1996,** *5*, 987-1006.

116. Shull, K. R. *Macromolecules* **2002,** *35*, 8631-8639.

117. Okabe, S.; Seno, K.; Kanaoka, S.; Aoshima, S.; Shibayama, M. *Macromolecules* **2006,** *39*, 1592-1597.

118. Mok, M. M.; Pujari, S.; Burghardt, W. R.; Dettmer, C. M.; Nguyen, S. T.; Ellison, C. J.; Torkelson, J. M. *Macromolecules* **2008,** *41*, 5818-5829.

119. Kim, J.; Mok, M. M.; Sandoval, R. W.; Woo, D. J.; Torkelson, J. M. *Macromolecules* **2006,** *39*, 6152-6160.

120. Jakubowski, W.; Juhari, A.; Best, A.; Koynov, K.; Pakula, T.; Matyjaszewski, K. *Polymer* **2008,** *49*, 1567-1578.

121. Sandoval, R. W.; Williams, D. E.; Kim, J.; Roth, C. B.; Torkelson, J. M. *Journal of Polymer Science: Part B: Polymer Physics* **2008,** *46*, 2672-2682.

122. Mok, M. M.; Kim, J.; Wong, C. L. H.; Marrou, S. R.; Woo, D. J.; Dettmer, C. M.; Nguyen, S. T.; Ellison, C. J.; Shull, K. R.; Torkelson, J. M. *Macromolecules* **2009,** *42*, 7863-7876.

123. Qin, S.; Saget, J.; Pyun, J.; Jia, S.; Kowalewski, T.; Matyjaszewski, K. *Macromolecules* **2003,** *36*, 8969-8977.

124. Lee, S. B.; Russell, A. J.; Matyjaszewski, K. *Biomacromolecules* **2003,** *4*, 1386-1393.

125. Buzin, A. I.; Pyda, M.; Costanzo, P.; Matyjaszewski, K.; Wunderlich, B. *Polymer* **2002,** *43*, 5563-5569.

126. Beginn, U. *Colloid Polymer Science* **2008,** *286*, 1465-1474.

127. Min, K.; Oh, J. K.; Matyjaszewski, K. *J. Polym. Sci., Part A: Polym. Chem.* **2007,** *45*, 1413-1423.

128. Lee, H.-i.; Matyjaszewski, K.; Yu, S.; Sheiko, S. S. *Macromolecules* **2005,** *38*, 8264-8271.

129. Boerner, H. G.; Duran, D.; Matyjaszewski, K.; da Silva, M.; Sheiko, S. S. *Macromolecules* **2002,** *35*, 3387-3394.

130. Min, K.; Li, M.; Matyjaszewski, K. *J. Polym. Sci., Part A: Polym. Chem.* **2005,** *43*, 3616-3522.

131. Guo, Y.; Zhang, J. Y.; Xie, P.; Gao, X.; Luo, Y. *Polym. Chem.* **2014,** *Advance Article*, DOI: 10.1039/C4PY00003J.

132. Nakatani, K.; Terashim, T.; Sawamoto, M. *J. Am. Chem. Soc.* **2009,** *131*, 136000-13601.

133. Ogura, Y.; Terashima, T.; Sawamoto, M. *Macro Lett.* **2013,** *2*, 985-989.

134. Nakatani, K.; Ogura, Y.; Koda, Y.; Terashima, T.; Sawamoto, M. *J. Am. Chem. Soc.* **2012,** *134*, 4373-4383.

CHAPTER II

DUAL CONCURRENT ATRP/RAFT OF METHYL ACRYLATE CO-INITIATED BY ALKYL HALIDES*

II.1. Preface

As discussed in Chapter I, a significant amount of research has been conducted specifically on lowering the amount of catalyst required for ATRP while maintaining a well controlled polymerization. There are several examples of methods which accomplish this goal including ICAR ATRP, ARGET ATRP, and SARA ATRP, all of which introduce (re)generation of the active catalyst system throughout the polymerization. However, it is known that if the catalyst concentration is decreased enough, the molecular weight distribution will broaden. Is it possible to maintain narrow molecular weight distribution even at low catalyst concentrations? Work by Dr. Renaud Nicolaÿ and Dr. Yungwan Kwak introduced degenerative chain transfer, a key concept of Reversible Addition-Fragmentation chain Transfer (RAFT) polymerization, to classic activation/deactivation

*Work in this chapter has been published in the following manuscript: 1) Elsen, A. M.; Nicolaÿ, R.; Matyjaszewski, K. "Dual Concurrent ATRP/RAFT of Methyl Acrylate Co-initiated by Alkyl Halides" *Macromolecules* **2011**, *44*, 1752-1754. Copyright ©2012 American Chemical Society

cycles of ATRP. This new method of polymerization was aptly named concurrent ATRP/RAFT.

Concurrent ATRP/RAFT includes a chain transfer agent which may be activated by classical ATRP catalysts such as CuBr/N,N,N′,N′′,N′′-pentamethyldiethylenetriamine (PMDETA), CuBr/2,2'-bipyridine (bpy), CuBr/tris[2-(dimethylamino)ethyl]amine (Me_6TREN), or CuBr/*tris*-[(2-pyridyl)methyl) amine] (TPMA) allowing them to behave as alkyl pseudo halides. When a reducing agent is included, such as Cu^0 wire as in SARA ATRP, concurrent ATRP/RAFT has been successful at both low catalyst concentrations as well as synthesis of ultra-high molecular weight polymers. However, these procedures encountered difficulty in the polymerization of acrylates, due to the inability of the available catalysts to activate the less active polyacrylate pseudohalide chain-ends.

This chapter reports the continuation of prvious work through the use of alkyl halides as co-initiators in the new dual concurrent ATRP/RAFT of acrylates. In these systems, alkyl halides (first low molar mass initiators and then macromolecular dormant species) were used to continuously generate propagating radicals while alkyl pseudohalides retained control over molecular weight and molecular weight distribution even at low concentration of metal complexes.

II.2. Introduction

Reversible Addition-Fragmentation chain Transfer (RAFT) polymerization is another versatile and robust controlled radical polymerization technique which proceeds through a degenerative transfer process.[1-3,4]. Control in RAFT polymerization relies on fast

and reversible transfer reactions between dormant species, dithiocarbonyl compounds, i.e., chain transfer agents (CTA), and radicals propagating with rate constant k_p (Scheme II.1a). This system, however, requires a constant supply of radicals through decomposing radical initiators such as AIBN (with the rate constant k_i), to compensate for radical termination (with the rate constant k_t).[5]

Recently, it was shown that the presence of appropriate ATRP catalysts, including CuBr/N,N,N′,N′′,N′′-pentamethyldiethylenetriamine (PMDETA), CuBr/2,2'-bipyridine (bpy), CuBr/tris[2-(dimethylamino)ethyl]amine (Me_6TREN), or CuBr/*tris*-[(2-pyridyl)methyl) amine] (TPMA), can directly activate RAFT chain transfer agents, including dithioesters, so that they act as alkyl pseudohalides.[6-14] When the CTA is activated by an ATRP catalyst, the need for a constant supply of external radicals is eliminated and purer block copolymers can be prepared. The mechanism of ATRP with alkyl pseudohalides (i.e., concurrent ATRP/RAFT or a copper-catalyzed RAFT) is shown in Scheme II.1b.

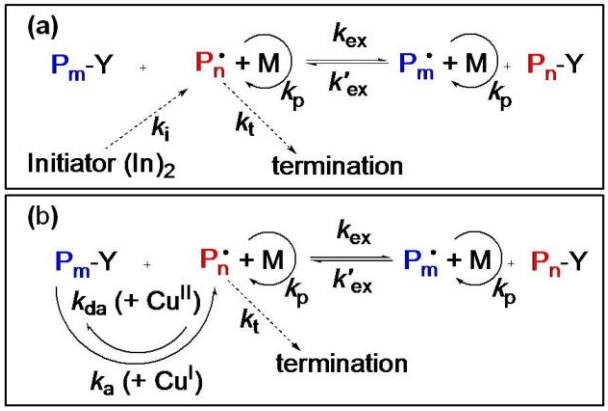

Scheme II.1. Mechanism for RAFT (a) and concurrent ATRP/RAFT with alkyl pseudohalides (b).

The concept of concurrent ATRP/RAFT with alkyl pseudohalides was then extended to ARGET systems with diminished amount of catalyst and Cu^0 as the reducing agent. Both concurrent ATRP/RAFT and ARGET with alkyl pseudohalides successfully polymerized styrene (St) and methacrylates in a controlled manner.[15] However, these procedures encountered difficulty in the polymerization of acrylates, due to the inability of the available catalysts to activate the less active polyacrylate pseudohalide chain-ends.

This work reports the use of alkyl halides as co-initiators in the new dual concurrent ATRP/RAFT of acrylates (Scheme II.2). In these systems, alkyl halides (first low molar mass initiators and then macromolecular dormant species) were used to continuously generate propagating radicals while alkyl pseudohalides retained control over molecular weight and molecular weight distribution even at low concentration of metal complexes.

Scheme II.2. Mechanism for dual concurrent ATRP/RAFT co-initiated by alkyl halides

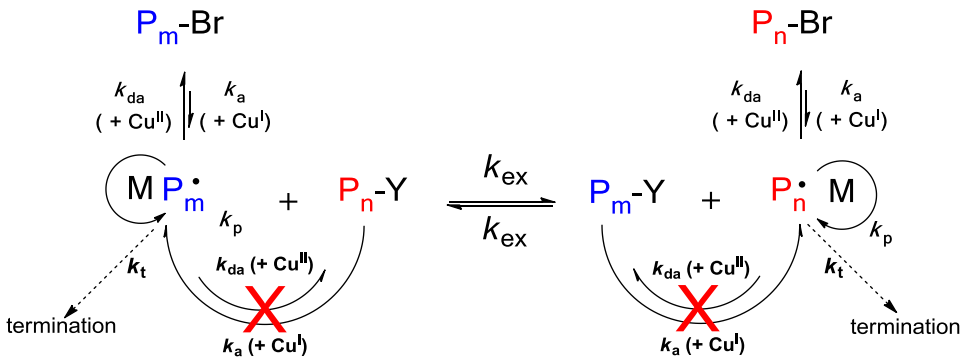

II.3. Experimental

II.3.1. Materials

Methyl acrylate (MA, 99%, Aldrich), was passed through a basic alumina column filled with prior to use. Cumyl dithiobenzoate (CDB) was synthesized *via* literature procedures.[28] Copper(II) bromide ($CuBr_2$, 99.999%, Aldrich), *tris*-(2-pyridylmethyl)amine (TPMA, 98%, ATRP Solutions), ethyl bromoisobutyrate (EBiB, 98%, Aldrich), copper wire (d = 1 mm, Alfa Aesar) and anisole (99%, Aldrich) were all used as received.

II.3.2. Polymerization of MA via dual initiation concurrent ATRP/RAFT

An example dual initiation concurrent ATRP/RAFT formulated with equimolar amounts of alkyl halides and alkyl pseudo haldies is given as follows; see Table II.1 for specific reaction conditions. A 10 mL Schlenk flask equipped with a stir bar was charged with 20 cm Cu^0 wire after which the flask was evacuated and backfilled with N_2 six times. A solution of $CuBr_2$ (1.2 mg, 0.55 µmol), TPMA (4.6mg, 1.6 µmol), and anisole (5 mL, 50% (v/v)) was bubbled under N_2 for 20 min. A second solution of MA (5 mL, 55.5 mmol), CDB (15.1 mg, 55.5 µmol), and EBiB (10.8 mg, 55.5 µmol) was bubbled under N_2 for 20 min. Each solution was transferred *via* an airtight syringe to the Schlenk flask from which a small aliquot was taken for time-zero NMR analysis. Finally, the flask was lowered into an oil bath at 50 °C and was allowed to polymerize for 7 h. Samples were taken periodically to measure conversion *via* ^{1}H NMR and number average molecular weights *via* GPC.

II.3.3. Analyses

Molecular weight and molecular weight distributions of the formed polymers were measured by gel permeation chromatography (GPC) using Polymer Standards Services (PSS) columns (guard, 10^5, 10^3, and 10^2 Å), with THF eluent at 35 °C, flow rate 1.00 mL/min, and differential refractive index (RI) detector (Waters, 2410). Toluene was used as the internal standard to correct for any fluctuation of the THF flow rate. The number-average molecular weights (M_n) and molecular weight distribution (M_w/M_n) were determined with a calibration based on linear poly(methyl methacrylate) standards using WinGPC 6.0 software from PSS. ^{1}H NMR spectra were recorded in $CDCl_3$ as a solvent using Bruker 300 MHz spectrometer.

II.4. Results and discussion

Previous concurrent ARGET ATRP/RAFT polymerizations of methyl methacrylate (MMA) and St were carried out with 5 ppm of initially added copper halide and a similar concentration of catalyst was selected for this study. However, in the previous systems no alkyl halide (R-Br) as traditional ATRP co-initiator was needed. The new dual concurrent ATRP/RAFT system developed for acrylates is comprised of seven components: monomer methyl acrylate (MA); the ATRP co-initiator, ethyl 2-bromoisobutyrate (EBiB); alkyl pseudohalide, i.e., CTA, cumyl dithiobenzoate (CDB); transition metal salt, copper (II) bromide ($CuBr_2$); TPMA ligand; solvent, anisole; and reducing agent, copper wire.

Table II.1. Conditions and results of dual concurrent ATRP/RAFT of MA[a]

Entry	% R-Br	EBiB	CDB	t (h)	*Conv.*[b]	$M_{n,GPC}$	M_w/M_n[c]	M_w/M_n[d]
1	0	0	1	48	0	N/A	N/A	N/A
2	50	1	1	7	0.41	20,000	1.14	1.15
3[e]	50	1	1	4	0.42	169,400	1.14	1.14
4	70	1.4	0.6	8	0.41	23,000	1.11	1.3
5	85	1.7	0.3	8	0.42	22,500	1.11	1.33
6	100	2	0	3	0.39	17,200	1.19	1.6

[a] All polymerizations were conducted in 50% (v/v) anisole at 50 °C with Cu^0 wire (L = 20 cm and d = 1 mm), while targeting a DP = 500 with [TPMA]/[$CuBr_2$] = 3. [b] Determined by ^{1}H NMR. [c] At 40% monomer conversion. [d] At 10% monomer conversion. [e] This reaction was targeting DP = 5,000.

Concurrent ATRP/RAFT without alkyl halide ATRP co-initiator was unable to polymerize MA (Table II.1, entry 1). After 48 h no polymer was detected via GPC and ^{1}H NMR showed no conversion of monomer. Table II.1. entry 2, shows the results of the initial study starting with a targeted degree of polymerization DP = 500. The ratio of [MA]/[EBiB]/[CDB] was set to 1,000/1/1, giving a (50%) alkyl halide (R-Br) co-initiated system. As seen in Figure II.1, the addition of the alkyl halide ATRP initiator to the concurrent ATRP/RAFT system allowed for the controlled polymerization of MA, utilizing low catalyst concentrations. Figure II.1 also shows that this system can be applied to higher degrees of polymerization (Table II.1, entry 3). When DP = 5,000 was targeted, the addition of alkyl halide again allowed for a controlled polymerization of MA. Both polymerizations showed linear first-order kinetics. The values of number-average molecular weights (M_n) follow the theoretical molecular weights values, ($M_{n,th}$) and have a

molecular weight distribution (M_w/M_n) near 1.1 at 40% conversion of monomer (Figure II.1b).

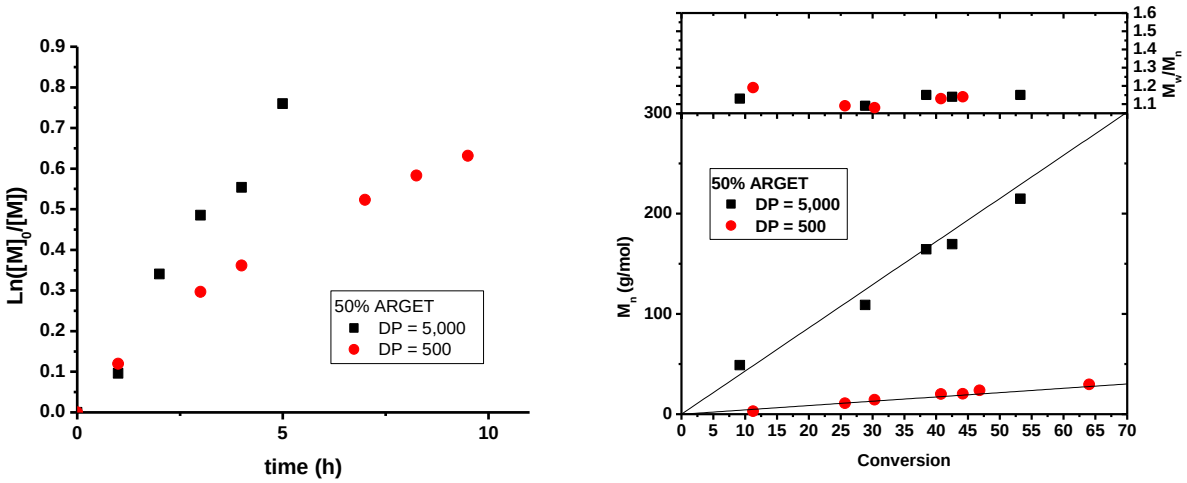

Figure II.1. (a) First-order kinetic plots of 50% R-Br co-initiated dual concurrent ATRP/RAFT at targeted DP = 5,000 (black) and DP = 500 (red) and (b) molecular weight evolution and MWD versus conversion as a function of degree of polymerization. All polymerizations were conducted in 50 % (v/v) anisole at 50 °C with $[EBiB]_0/[CDB]_0$ = 1, $[TPMA]/[CuBr_2]$ = 3, and Cu^0 wire (L = 20 cm and d = 1 mm). (Table II.1, entries 2 and 3)

The effect of changing the relative proportion of ATRP initiator was then examined by keeping the same targeted DP (the same total initiator concentration), while varying the amount of EBiB relative to CDB. Table II.1 (entries 2, 4-6) shows the reaction conditions for DP = 500 at 1:1 (50% R-Br), 1.4:0.6 (70% R-Br), 1.7:0.3 (85% R-Br), and 2:0 (100 % R-Br). While targeting DP = 500 for increasing [R-Br] (50 – 100 %) two trends can be observed. The first is related to the M_w/M_n values for each polymerization. The data in Table II.1 shows that all polymerizations resulted in low values of M_w/M_n after 40%

monomer conversion. However, it is interesting to analyze the M_w/M_n values at lower monomer conversion. For 100% ARGET ATRP (no CDB, Table II.1, entry 6) at *ca.* 10% conversion the M_w/M_n value was significantly higher than for systems which included alkyl pseudohalides. As the overall amount of alkyl halide was decreased and alkyl pseudohalide (CTA) was increased, the M_w/M_n early in the conversion of monomer decreases. This indicates that RAFT agent as alkyl pseudohalide allows for more uniform chain growth throughout the polymerization at very low catalyst concentration, especially at low conversion. This is agreement with the equation II.1 that correlates M_w/M_n with conversion and concentrations of initiators (R-Br and R-Y) and deactivators (R-Y and Cu^{II} species that should be essentially constant, as defined by the ligand concentration) where p defines monomer conversion.

$$\frac{M_w}{M_n} = 1 + \left(\frac{k_p([R-Br]+[R-Y])}{k_d[Cu^{II}]+k_{ex}[R-Y]} \right) \left(\frac{2}{p} - 1 \right) \qquad \text{(II.1)}$$

The second trend seen by varying the relative amount of alkyl halide relates to polymerization rate. Without alkyl halide present, no polymerization occurred because the alkyl pseudohalides alone are not active enough to initiate polymerization. However, with alkyl halide present to generate radicals, polymerization occurred. Therefore, as the relative concentration of alkyl halide to alkyl pseudohalide increased, the time required to reach 40% monomer conversion decreased, indicating an increased polymerization rate.

II.4. Conclusions

It was shown that addition of an alkyl halide as a co-initiator to concurrent ATRP/RAFT (i.e. ATRP with alkyl pseudohalides or a copper-catalyzed RAFT) allows for the polymerization of MA at low concentrations of copper catalyst over a range of degrees of polymerization. The presence and relative concentrations of alkyl pseudohalide and alkyl halide affected the molecular weight distribution at early monomer conversion and rate of polymerization; an increase in the concentration of alkyl pseudohalide resulted in lower M_w/M_n values but decreased rates of polymerization. In summary, it is possible to achieve a well-controlled polymerization of methyl acrylate at various DP in new dual concurrent ATRP/RAFT, at ARGET levels of copper catalyst concentration. Increasing the relative amount of alkyl pseudohalide afford polymers with narrow molecular weight distribution, even at early stages of monomer conversion.

II. 5. Acknowledgements

Sincere thanks to Dr. Renaud Nicolaÿ and Dr. Yungwan Kwak for many helpful discussions throughout the duration of this project, my first in the Matyjaszewski group. They were kind enough to pass on their knowledge of the Concurrent ATRP/RAFT system as well as fundamentals to polymer chemistry.

I.I. 6. References

1. Chiefari, J.; Chong, Y. K.; Ercole, F.; Krstina, J.; Jeffery, J.; Le, T. P. T.; Mayadunne, R. T. A.; Meijs, G. F.; Moad, C. L.; Moad, G.; Rizzardo, E.; Thang, S. H. *Macromolecules* **1998,** *31*, 5559-5562.
2. Moad, G.; Rizzardo, E.; Thang, S. H. *Polymer* **2008,** *49*, 1079-1131.
3. Moad, G.; Rizzardo, E.; Thang, S. H. *Aust. J. Chem.* **2006,** *59*, 669-692.
4. Perrier, S.; Takolpuckdee, P. *Journal of Polymer Science, Part A: Polymer Chemistry* **2005,** *43*, 5347-5393.
5. Moad, G.; Chiefari, J.; Chong, Y. K.; Krstina, J.; Mayadunne, R. T. A.; Postma, A.; Rizzardo, E.; Thang, S. H. *Polym. Int.* **2000,** *49*, 993-1001.
6. Kwak, Y.; Nicolay, R.; Matyjaszewski, K. *Macromolecules* **2008,** *41*, 6602-6604.
7. Nicolay, R.; Kwak, Y.; Matyjaszewski, K. *Macromolecules* **2008,** *41*, 4585-4596.
8. Kwak, Y.; Matyjaszewski, K. *Macromolecules* **2008,** *41*, 6627-6635.
9. Nicolay, R.; Kwak, Y.; Matyjaszewski, K. *Macromolecules (Washington, DC, U. S.)* **2008,** *41*, 4585-4596.
10. Nicolay, R.; Kwak, Y.; Matyjaszewski, K. *Chem. Commun. (Cambridge, U. K.)* **2008**, 5336-5338.
11. Kwak, Y.; Nicolay, R.; Matyjaszewski, K. *Macromolecules (Washington, DC, U. S.)* **2009,** *42*, 3738-3742.
12. Kwak, Y.; Nicolay, R.; Matyjaszewski, K. *Australian Journal Of Chemistry* **2009,** *62*, 1384-1401.
13. Kwak, Y.; Matyjaszewski, K. *Macromolecules (Washington, DC, U. S.)* **2010,** *43*, 5180-5183.

14. Kwak, Y.; Yamamura, Y.; Matyjaszewski, K. *Macromol. Chem. Phys.* **2010,** *211*, 493-500.

15. Nicolay, R.; Kwak, Y.; Matyjaszewski, K. *Angew. Chem. Int. Ed.* **2010,** *49*, 541-544.

CHAPTER III

ACTIVE LIGANDS FOR LOW PPM MINIEMULSION ATRP*

III.1. Preface

As discussed in Chapter I, polymerizations conducted with low catalyst concentrations have been successful in homogenous polymerizations through the development of systems such as ARGET, ICAR, *e*ATRP as well as concurrent ATRP/RAFT. However, these low catalyst systems have not been successfully applied to aqueous dispersed media. Ligands traditionally used in heterogeneous systems do not possess a large enough K_{ATRP} value, or activity, to maintain control in a low catalyst polymerization. On the other hand, the active catalysts for low catalyst homogeneous

*Work in this chapter has been published in the following manuscripts: 1) Elsen, A. M.; Burdyńska, J.; Park, S.; Matyjaszewski, K. "Active Ligand for Low PPM Miniemuslion Atom Transfer Radical Polymerization" *Macromolecules* **2012**, *45*, 7356-7363. Copyright ©2012 American Chemical Society and 2) Elsen, A. M.; Burdyńska, J.; Park, S.; Matyjaszewski, K. "Activators Regenerated by Electron Transfer Atom Transfer Radical Polymerization in Miniemulsion with 50 ppm of Copper Catalyst" *ACS Macro Letters* **2013**, *2*, 822-825. Copyright ©2013 American Chemical Society

polymerizations, which contain ligands with large K_{ATRP} values, are too hydrophilic to be useful in aqueous dispersed media.

The goal of this work was to synthesize new ligands for use in low catalyst heterogeneous ATRPs. Modification of typical ligands for ATRP was accomplished through the incorporation of electron donating substituents and/or hydrophobic octadecyl chains, resulting in more powerful ligands for aqueous dispersed media polymerizations with low catalyst concentrations. The new ligands, bis[2-(4-methoxy-3,5-dimethyl)pyridylmethyl]octadecylamine (BPMODA*) and *N′*,*N″*-dioctadecyl-*N′*,*N″*-bis(2-(4-methoxy-3,5-dimethyl)pyridylmethyl)ethane-1,2-diamine (DOD-BPED*) were synthesized and compared with bis(2-pyridylmethyl)octadecylamine (BPMODA), a traditional ligand for heterogeneous polymerizations.

There are many environmental benefits to conducting polymerizations in aqueous dispersed media and the technique is currently an industrially utilized method, albeit with free radical polymerizations. ATRP has yet to truly enter the industrial field with aqueous dispersed media polymerizations due to the large amounts of catalyst required. Therefore, the application of low catalyst systems to aqueous dispersed media allows us to take one step closer to the industrial use of ATRP.

This project was initiated by Joanna Burdyńska with the synthesis of each of the new ligands. Sangwoo Park was kind enough to run all cyclic voltamograms to aid in the characterization of the ligand activity. My role in this project was to test the ligand's activity and hydrophobicity through homogeneous polymerizations, partition experiments and finally, miniemulsion polymerizations.

III.2. Introduction

In addition to the advances of homogenous ATRP systems mentions in Chapter 1, ATRP has been successfully extended to aqueous dispersed media (e.g., microemulsion,[1,2] miniemulsion,[3-6] and emulsions[7-11]), all of which resulted in well-defined polymer latexes. Polymerizations utilizing aqueous conditions are also under consideration for industrial processes as they are recognized to be a mild, environmentally benign technique. Water as a polymerization medium not only eliminates the necessity of using volatile organic solvents but also ensures greater heat dissipation during polymerization. Moreover, low viscosity of the dispersed aqueous solutions allows for obtaining high weight fractions of the polymer, which is not accessible in bulk or organic solvent polymerizations.[12]

However, such heterogeneous polymerizations require careful design, as there are multiple components involved. A surfactant which generates a stable dispersion but does not interfere with the polymerization, a reducing agent which quickly and efficiently reduces $Cu^{I}X_2$/L, and a hydrophobic catalyst which remains in the oil phase are all necessary ingredients for a successful ATRP in aqueous dispersed media.[13] The most commonly utilized ligand in emulsion based ATRP is bis(2-pyridylmethyl)octadecylamine (BPMODA).[14] While this ligand is successful under normal ATRP conditions in dispersed media, it is unable to perform well at low catalyst concentrations due to a relatively low K_{ATRP} value. Conversely, highly active ligands such as $CuBr_2$/TPMA and $CuBr_2$/Me_6TREN complexes, which have thrived in low catalyst homogenous ATRP, show much higher affinity towards water than the organic phase and, therefore, are less useful in aqueous dispersed media.

While remarkable headway has been made within homogenous ATRP polymerizations, including low ppm catalyst systems,[15,16] the synthesis of highly active ligands,[17] and development of new metal complexes[18] etc., less progress has been made for low catalyst heterogeneous ATRPs. To date, there are very few reports of successful ARGET ATRP in aqueous dispersed media;[19-21] the majority of these systems utilize activators generated by electron transfer (AGET) ATRP as the higher oxidation state catalyst may be used for the polymerization set up, but requires >1000 ppm of total catalyst.

Herein, this chapter outlines the design, synthesis, and characterization of new ligands, (bis[2-(4-methoxy-3,5-dimethyl)pyridylmethyl]octadecylamine) (BPMODA*) and *N*′,*N*″-dioctadecyl-*N*′,*N*″-bis[2-(4-methoxy-3,5-dimethyl)pyridylmethyl]ethane-1,2-diamine (DOD-BPED*), as shown in Figure III.1, for ARGET ATRP in aqueous dispersed media. Each ligand included six electron donating groups (EDG)[17,22] to increase the K_{ATRP} values for high ligand activity, while octadecyl chains were incorporated into the ligand structures to promote hydrophobicity.

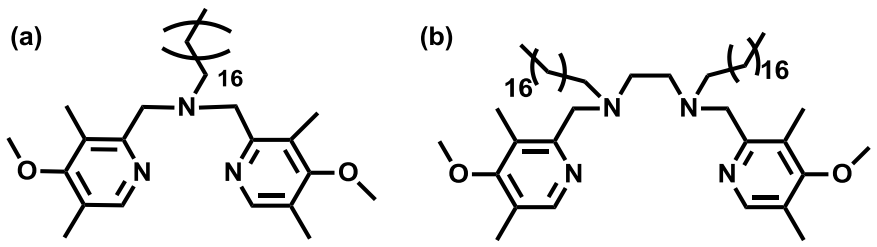

Figure III.1. Structures of (a) BPMODA* and (b) DOD-BPED*.

III.3. Experimental

III.3.1. Materials

n-Butyl acrylate (*n*-BA, 99%, Aldrich) and butyl methacrylate (BMA, 99%, Aldrich) were passed through a column filled with basic alumina prior to use. 2-Chloromethyl-4-methoxy-3,5-dimethylpyridine hydrochloride (Py-HCl*, 98%, Aldrich), copper(I) bromide ($Cu^{I}Br$, 99.999%, Aldrich), copper(III) bromide ($Cu^{III}Br_2$, 99.999%, Aldrich), copper(III) chloride ($Cu^{III}Cl_2$, 99.999%, Aldrich), copper(III) trifluoromethanesulfonate ($Cu^{III}(OTf)_2$, 98%, Aldrich) copper wire (*dia.* = 0.5 mm, 99.9%, Alfa Aesar), *N*,*N*-dimethylformamide, **(**DMF, Fisher Scientific, >99%), ethyl α-bromoisobutyrate (EBiB, 98%, Aldrich), ethyl-α-bromophenylacetate (EBPA, 97%, Aldrich), *N*,*N*'-ethylenebis(stearamide) (beads, < 840 μm, Aldrich), hexadecane (99%, Aldrich), L-ascorbic acid (AA, >99%, Aldrich), lithium aluminum hydride ($LiAlH_4$, powder, 95%, Aldrich), magnesium sulfate ($MgSO_4$, Fisher Scientific), octadecyl amine (95%, Fluka), polyoxyethylene(20) oleyl ether (Brij 98, Aldrich), sodium hydroxide pellets (NaOH, 99.2%, Fisher Scientific), tetrabutylammonium hexafluorophosphate ($TBAPF_6$, >98%, Aldrich),tetrabutylammonium perchlorate ($TBAClO_4$, 98%, Aldrich), tetraethylammonium bromide (TBABr, 99% Aldrich), tin(III) 2-ethylhexanoate ($Sn^{III}(EH)_2$, 95%, Aldrich), tributylhexadecyl phosphonium bromide ($Bu_3P^+Br^-$, 97%, Fluka), and solvents were purchased from Aldrich and used as received. BPMODA,[23] tris(2-pyridylmethyl)amine (TMPA)[23] and tris(2-(dimethylamino)ethyl)amine (Me_6TREN)[24] were synthesized according to previously published procedures.

III.3.2. Synthetic procedures

III.3.2.1. Synthesis of BPMODA*

Octadecyl amine (17 g, 64 mmol), Py-HCl* (30 g, 135 mmol, 2.1 eq) $Bu_3P^+Br^-$ (1.6 g, 3.2 mmol, 0.05 eq), and a stir bar were added to a 500 mL round bottom flask. The solids were dissolved in THF (200 mL), followed by 5N $NaOH_{aq}$ (110 mL). The biphasic mixture was refluxed at 60 °C for 5 d. After separation of the organic phase from the aqueous, it was washed with brine until the pH ~ 9. The organic layer was dried with $MgSO_4$ and the solvent was removed *via* rotary evaporator. The resulting solid was characterized via ^{1}H NMR (300 MHz, $CDCl_3$). δ: 0.85 (*t*, 3H, CH_2*Me*), 1.00-1.22 (*m*, 30H, $(CH_2)_{15}$Me), 1.40 (*m*, 2H, $CH_2CH_2(CH_2)_{15}$Me), 2.04 (*s*, 6H, 5-Py-CH_3), 2.18 (*s*, 6H, 3-Py-CH_3), 2.42 (*m*, 2H, $CH_2CH_2(CH_2)_{15}$Me), 3.63 (*s*, 4H, 2-Py-CH_2), 3.67 (*s*, 6H, 4-Py-OCH_3), 8.11 (*s*, 2H, 5-Py*H*).

III.3.2.2. Synthesis of *N*,*N*'-dioctadecylethylenediamine

A dry 500 mL three-neck round bottom flask was charged with *N*,*N*'-ethylenebis(stearamide) (3.00 g, 5.1 mmol), lithium aluminum hydride (0.577 g, 15.2 mmol) and then dry THF (150 mL) was added under nitrogen atmosphere. The flask was equipped with a condenser, sealed and placed in an oil bath. The reaction mixture was refluxed under nitrogen atmosphere for 48 hrs. The process was terminated by the slow addition of 1M $HCl_{aq.}$ until the evolution of bubbles ceased. After the quenching, the mixture was extracted with hexanes (4 x 50 mL), and then combined organic phases were washed with 1 M $NaOH_{aq.}$ (30 mL), water (30 mL), dried with anhydrous sodium sulfate

and concentrated. The product was isolated as white wax and characterized by ^{1}H NMR analysis (300 MHz, $CDCl_3$). δ: 0.88 (*t, J*=8.8 Hz, 6H, CH_2CH_3), 1.18-1.38 (*s*, 60H, $(CH_2)_{15}CH_3$), 1.47 (*m*, 4H, $NCH_2CH_2(CH_2)_{15}Me$), 2.57 (*t, J*=7.0 Hz, 4H, $NCH_2CH_2(CH_2)_{15}Me$), 2.70 (*s*, 4H, $CH_2NCH_2CH_2(CH_2)_{15}Me$).

III.3.2.3. Synthesis of DOD-BPED*

N,N'-dioctadecylethylenediamine (1.50 g, 2.65 mmol), 2-chloromethyl-4-methoxy-3,5-dimethylpyridine hydrochloride (1.30 g, 5.44 mmol), and tributylhexadecylphosphonium bromide (0.135 g, 0.266 mmol) were dissolved in THF (30 mL), and then 5 N $NaOH_{aq.}$ (4 mL) was added. The biphasic mixture was refluxed at 60 °C for 5 d. After separation of the organic phase from the aqueous, it was washed with brine until the pH ~ 9. The organic layer was dried with $MgSO_4$ and the solvent was removed *via* rotary evaporator. The resulting solid was characterized via ^{1}H NMR (300 MHz, $CDCl_3$). δ: 0.80 (*t, J*=6.7 Hz, 6H, CH_2Me), 0.98-1.33 (*m*, 64H, $(CH_6)_{15}Me$), 2.14 (*s*, 6H, 5-Py-CH_3), 2.20 (*s*, 6H, 3-Py-CH_3), 2.26 (*t, J*=7.5 Hz, 4H, $CH_2CH_2(CH_2)_{15}Me$), 2.42 (*s*, 4H, $CH_2NCH_2(CH_2)_{16}Me$), 3.53 (*s*, 4H, 2-Py-CH_2), 3.64 (*s*, 6H, 4-Py-OCH_3), 8.04 (*s*, 2H, 5-Py*H*).

III.3.2.4. Synthesis of DOD-BPED

N,N'-dioctadecylethylenediamine (0.500 g, 0.885 mmol), 2-(chloromethyl)pyridine hydrochloride (0.298 g, 1.82 mmol), and tributylhexadecyl-phosphonium bromide (0.045 g, 0.089 mmol) were dissolved in THF (20 mL), and then 5

N $NaOH_{aq.}$ (1.5 mL) was added. The reaction was performed and worked up in the same way as DOD-BPED*. The resulting solid was characterized via ^{1}H NMR (300 MHz, $CDCl_3$). δ: 0.80 (*t*, *J*=6.7 Hz, 6H, CH_2*Me*), 0.98-1.33 (*m*, 64H, $(CH_6)_{15}$Me), 2.14 (*s*, 6H, 5-Py-CH_3), 2.20 (*s*, 6H, 3-Py-CH_3), 2.26 (*t*, *J*=7.5 Hz, 4H, $CH_2CH_2(CH_2)_{15}$Me), 2.42 (*s*, 4H, $CH_2NCH_2(CH_2)_{16}$Me), 3.53 (*s*, 4H, 2-Py-CH_2), 3.64 (*s*, 6H, 4-Py-OCH_3), 8.04 (*s*, 2H, 5-Py*H*).

III.3.2.5. ATRP of *n*BA

An example ATRP procedure formulated with 2000 ppm of $Cu^{III}Br_2$/BPMODA catalyst and targeted degree of polymerization (DP) equal to 200 is given as follows; see Table III.1 for specific reaction conditions. A 10 mL Schlenk flask was charged with *n*-BA (5 mL, 35 mmol), EBiB (0.44 mL of 76.9 mg/mL solution in anisole, 0.17 mmol) BPMODA (0.79 mL of 100 mg/mL solution in anisole, 174 mmol), $CuBr_2$ (0.78 mL of 20 mg/mL solution in acetonitrile, 70 mmol), anisole (1.8 mL) and a stir bar. The reaction mixture was degassed by at least three freeze-pump-thaw cycles and filled with nitrogen again. With positive pressure of N_2, CuBr (19.9 mg, 140 mmol) was added to the 10 mL Schlenk flask. The flask was evacuated and refilled with nitrogen at least 6 times. The Schlenk flask was placed in a 60 °C oil bath. Samples were taken periodically to measure conversion *via* ^{1}H NMR and number average molecular weights *via* GPC.

III.3.2.6. SARA ATRP of *n*BA

An example SARA ATRP procedure formulated with 50 ppm of $CuBr_2$/BPMODA catalyst and targeted DP = 200 is given as follows; see Table III.3 for specific reaction

conditions. A 10 mL Schlenk flask was charged with Cu^0 wire (1 cm) and a stir bar, after which, the flask was degassed and backfilled with nitrogen (N_2) six times. A mixture of anisole (1.5 mL), EBiB (0.44 mL of 76.9 mg/mL solution in anisole, 0.17 mmol), BPMODA (0.24 mL of 10 mg/mL solution in anisole, 5.2 μmol), and $CuBr_2$ (0.39 mL of 1 mg/mL solution in anisole, 1.7 μmol) was added to a glass vial and purged with nitrogen for 20 min. Previously deoxygenated *n*-BA (5 mL, 35 mmol) was added to the vial. Immediately, the reaction mixture was transferred *via* an airtight syringe to the Schlenk flask, which was placed in a thermostated oil bath at 60 °C. Samples were taken periodically to measure conversion *via* ^{1}H NMR and number average molecular weights *via* GPC.

III.3.2.7. ARGET ATRP of BMA

An example ARGET ATRP procedure formulated with 50 ppm of $CuBr_2$/DOD-BPED& catalyst and targeted DP = 200 is given as follows; see Table III.5 for specific reaction conditions. A 10 mL Schlenk flask charged with a stir bar was degassed and backfilled with nitrogen (N_2) six times. A mixture of anisole (1.4 mL), EPBA (28 μL, 0.16 mmol), DOD-BPED* (0.41 mL of 10 mg/mL solution in anisole, 4.7 μmol), and $CuCl_2$ (0.21 mL of 1 mg/mL solution in anisole, 1.6 μmol) was added to a glass vial and purged with nitrogen for 20 min. Previously deoxygenated BMA (5 mL, 31 mmol) was added to the vial. Immediately, the reaction mixture was transferred *via* an airtight syringe to the Schlenk flask, which was placed in a thermostated oil bath at 60 °C. Previous deoxygenated $Sn^{II}(EH)_2$ (0.64 mL of 10 mg/mL solution in anisole, 15.7 μmol) was added

to the Schlenk flask to start the polymerization. Samples were taken periodically to measure conversion *via* ^{1}H NMR and number average molecular weights *via* GPC.

III.3.2.8. Partition experiments

Calibration curves were generated for $Cu^{III}Br_2$/BPMODA* (1/1 ratio) catalyst in monomer (*n*BA) and $Cu^{III}Br_2$/Me_6TREN (1/1.5 ratio) catalyst in water. Stock solutions were prepared of varying catalyst concentrations (8, 5, 2.5, 1, and 0.2 mM) whose absorbance was determined using UV-Vis. A linear relationship was obtained correlating absorbance with catalyst concentration.

Solutions of $Cu^{III}Br_2$/BPMODA and $Cu^{III}Br_2$/BPMODA* (1/1 ratio) in *n*-BA were prepared at various concentrations (2.5 and 1 mM). The solutions were mixed with deionized water in a 30/100 (w/w) ratio and were stirred at either r.t. or 80 °C for 1 h. The organic phase was separated from the aqueous phase, after which the absorbance was measured *via* UV-Vis spectrometer at 780 nm. Me_6TREN was added to the aqueous phase at a ratio of $CuBr_2$/Me_6TREN (1/1.5), assuming 100% of the catalyst was transferred to the aqueous phase, after which the concentration of the catalyst was determined by the absorbance at 800 nm. In the case of BPMODA, only the absorption of the aqueous phase was measured, from which the concentration of catalyst remaining in the organic phase was calculated.

III.3.2.9. A(R)GET ATRP of *n*BA in miniemulsion with BPMODA

An example AGET ATRP in miniemulsion procedure formulated with 2000 ppm of $CuBr_2$/BPMODA catalyst and targeted DP = 200 is given as follows; see Table III.3 for specific reaction conditions. $CuBr_2$ (17 mg, 0.078 mmol) and BPMODA (17.4 mg, 0.078 mmol) were dissolved in *n*-BA (5.0 g, 39.1 mmol) in a round bottom flask at 60 °C to form a solution of the copper complex. The solution was then cooled to room temperature prior to dissolving the initiator EBiB (26 μL, 0.195 mmol) and hexadecane (0.14 mL, 0.826 mmol) in the solution. A 5 mM solution of Brij 98 in deionized water (20.2 mL) was added to the organic *n*-BA solution and was subjected to sonication in an ice bath (Heat Systems Ultrasonics W-385 sonicator; output control set at 8 and duty cycle at 70% for 1 min). The resulting stable miniemulsion was purged with nitrogen for 30 min. A predeoxygenated aqueous solution of AA (0.7 mL, containing 6.9 mg AA) was injected into the miniemulsion over a period of 3 min to activate the catalyst and start the polymerization Samples were taken periodically to measure the conversion gravimetrically and to determine the number-average molecular weights by GPC.

III.3.2.10. ARGET ATRP of BMA in miniemulsion with DOD-BPED*

An example ARGET ATRP in miniemulsion procedure formulated with 250 ppm of $CuBr_2$/DOD-BPED* catalyst and targeted DP = 2000 is given as follows; Table III.7 for specific reaction conditions. $CuBr_2$ (2.0 mg, 8.8 μmol) and DOD-BPED* (7.6 mg, 8.8 μmol) were dissolved in BMA (5.0 g, 35.2 mmol) in a round bottom flask at 60 °C to form a solution of the copper complex. The solution was then cooled to room temperature prior to dissolving the initiator EPBA (43 μL, 17.6 μmol) and hexadecane (0.14 mL, 63 μmol)

in the solution. A 5 mM solution of Brij 98 in deionized water (20 mL) was added to the organic BMA solution and was subjected to sonication in an ice bath (Heat Systems Ultrasonics W-385 sonicator; output control set at 8 and duty cycle at 70% for 1 min). The resulting stable miniemulsion was purged with nitrogen for 30 min. A predeoxygenated aqueous solution of AA (0.6 mL, containing 0.6 mg AA) was injected into the miniemulsion over a period of 3 min to activate the catalyst and start the polymerization Samples were taken periodically to measure the conversion gravimetrically and to determine the number-average molecular weights by GPC.

III.3.3. Analyses

Molecular weight and molecular weight distributions of the formed polymers were measured by gel permeation chromatography (GPC) using Polymer Standards Services (PSS) columns (guard, 10^5, 10^3, and 10^2 Å), with THF eluent at 35 °C, flow rate 1.00 mL/min, and differential refractive index (RI) detector (Waters, 2410). Diethyl ether was used as the internal standard to correct for any fluctuation of the THF flow rate. The number-average molecular weights (M_n) and molecular weight distribution (M_w/M_n) were determined with a calibration based on linear polystyrene standards using WinGPC 6.0 software from PSS. Absorbance of catalyst solutions was measured by UV-Vis (Agilent, 8453)**.** ^{1}H NMR spectra were recorded in $CDCl_3$ as a solvent using Bruker 300 MHz spectrometer. Electrochemical analysis voltammograms were recorded at 25 °C with a Gamry Reference 600 potentiostat. 19.6 mL of MeCN containing 0.2 M $TBAClO_4$ supporting electrolyte was prepared using previously dried reagents. To this solution was added 0.4 mL of a 0.05 M solution of $Cu^{III}(OTf)_2$/ligand or $Cu^{III}(OTf)_2$/ligand.

Measurements were carried out under a nitrogen atmosphere at a scan rate of 25 mV/s using platinum disk working electrode and platinum mesh counter electrode. Potentials were recorded versus a saturated calomel electrode (SCE, from Gamry) separated from the working solutions by a porous Vycor tip. After each of CV measurement, 80 μL of a 0.25 M solution of TEABr was added to solution to complex from $Cu^{III}(OTf)_2$/ligand to $Cu^{III}(Br)_2$/ligand and each of the solution was carried to measure CV.

III.4. Results and discussion

III.4.1. BPMODA*

III.4.1.1. Ligand design and characterization

As BPMODA has proven itself to be an excellent ligand for aqueous dispersed polymerizations, the logical process for generating a highly active, yet hydrophobic ligand, was to alter the structure of BPMODA to increase activity. Previous studies on 2,2'-bypridine and TPMA ligands demonstrated that increasing the electron donating properties of ligand substituents resulted in rate enhancements of the polymerizations.[17,22] The addition of methoxy- and two methyl groups on each pyridinyl ring, for a total of six electron donating groups, was expected to increase the activity of BPMODA without greatly affecting the hydrophobicity of the ligand. The synthesis of BPMODA* was straightforward and based on that of BPMODA, as reported in the literature: the coupling of 2-chloromethyl-4-methoxy-3,5-dimethylpyridine hydrochloride with the primary amine, octadecyl amine.

It has been reported that half-wave potential ($E_{1/2}$) values are correlated to K_{ATRP}, which provides insight into the activity of a catalyst complex.[25-27] Cyclic voltammetry (CV) was used to determine the $E_{1/2}$ value of BPMODA and BPMODA*, -0.098 and -0.204 V (vs. SCE), respectively. From this correlation, it can be concluded that the supplemental electron donating substituents present on BPMODA* should increase the K_{ATRP} value 10^{-7}, for BPMODA, to ca. 10^{-5}. The two orders of magnitude increase in K_{ATRP} value causes BPMODA* to have a similar activity to TPMA. To test the suggested increase in catalytic activity of BPMODA*, several polymerizations were conducted under homogeneous, normal ATRP conditions.

III.4.1.2. Homogenous polymerizations

Normal ATRP was conducted at three different ratios of Cu^{I}/L to Cu^{III}/L (80:20, 95:5, and 99:1) for BPMODA and BPMODA*. All polymerizations were carried out in 20% anisole at 60 °C with a targeted DP = 200; conditions and results are summarized in Table III.1. Regardless of the ligand used, a well-controlled polymerization was obtained. Every polymerization demonstrated both linear first-order kinetics, indicating a constant amount of radicals, and linear growth of number average molecular weights (M_n) with monomer conversion (Figure III.2). Experimental M_n values ($M_{n,GPC}$) strongly correlated with theoretical values while M_w/M_n decreased with monomer conversion, whose final values were below 1.15. The singular distinction between the polymerizations with each ligand is the rate of polymerization (R_p). From the first-order kinetic plots it is evident that the rate of polymerization is much faster when BPMODA* is used as the ligand. It is important to note the increase in R_p does not come with any loss in control over the

polymerization. This data supports the conclusion of the C.V.: BPMODA* does have a higher K_{ATRP} value compared to BPMODA due to the addition of six electron donating groups. However, higher K_{ATRP} values did not originate in decreased values of k_{da} as evidenced by narrow molecular weight distributions.

Figure III.2 also demonstrates the effects of catalyst concentration on the polymerizations with BPMODA*. Those polymerizations conducted with higher percentages of deactivator ($CuBr_2$/L) present at the beginning of the reaction showed the slowest R_p. As the percentage of initial deactivator was decreased (5 and 1%) a corresponding increase in the rate of polymerization was seen. The lack of deactivator present during the initial stages of these polymerizations did result in larger M_w/M_n values at early monomer conversions, however, the final M_w/M_n values were nearly identical (1.08-1.09).

Table III.1. Normal ATRP of *n*-BA with BPMODA and BPMODA*.

Entry[a,b]	**CuBr**	**$CuBr_2$**	**t (h)**	**Conv.**[c]	$M_{n,GPC}$	$M_{n,th}$	M_w/M_n
1	0.80	0.20	48	0.56	14 500	14 400	1.04
2*	0.80	0.20	24	0.88	17 900	22 600	1.08
3	0.95	0.05	49	0.62	15400	15 800	1.09
4*	0.95	0.05	7.5	0.82	19 300	20 900	1.08
5	0.99	0.01	48	0.63	12 800	16 000	1.13
6*	0.99	0.01	6	0.84	18 400	21 400	1.09

[a] All polymerizations were conducted in 20% (v/v) anisole at 60 °C with [*n*-BA]:[EBiB]:[Ligand] = 200:1:1. [b] Entries labeled with (*) utilized BPMODA*, all other entries utilized BPMODA. [c] Determined by ^{1}H NMR.

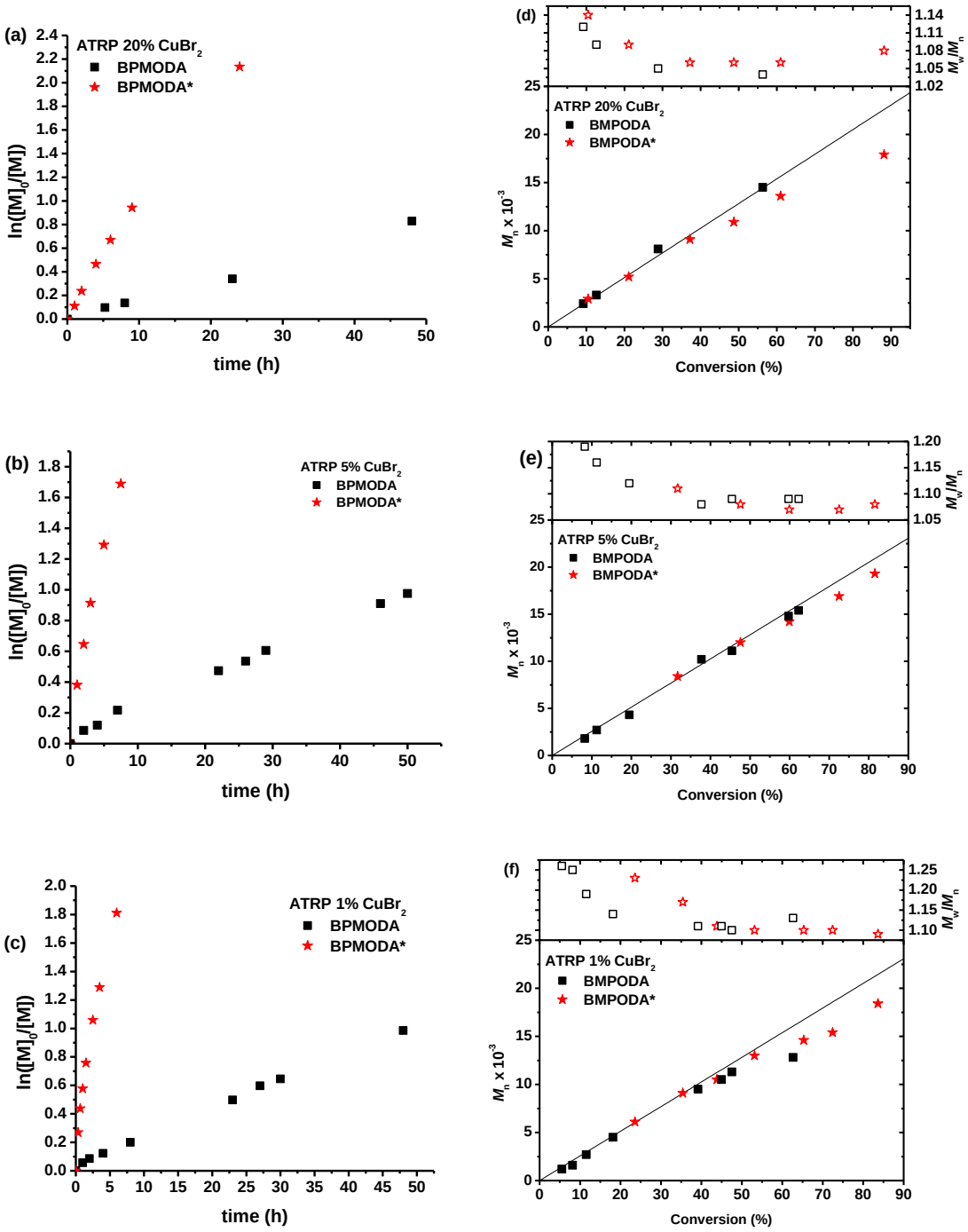

Figure III.2. First order kinetic plots (a-c) and evolution of M_n and M_w/M_n with conversion (d-f) for the normal ATRP of *n*-BA at = 80:20; 99:5; and 99:1 for BPMODA and BPMODA*. All polymerizations were conducted with [*n*-BA]:[EBiB]:

[CuBr]:[$CuBr_2$] :[Ligand]: = 200:1:X:Y:1 (X = 0.80, 0.95, 0.99 and Y = 0.20, 0.05, 0.01) in 20% (v/v) anisole at 60 °C.

Both ligands were then tested under SARA ATRP conditions, which require significantly less catalyst (50 ppm), in contrast to normal ATRP (5000 ppm), along with Cu^0 wire as a reducing agent. It was expected that BPMODA, a ligand with a low K_{ATRP} value, would result in a poorly controlled polymerization, while BPMODA*, with a K_{ATRP} value similar to that of TPMA, would afford a well-controlled ATRP. To test this hypothesis, a third polymerization was carried out under SARA ATRP conditions which employed TPMA.

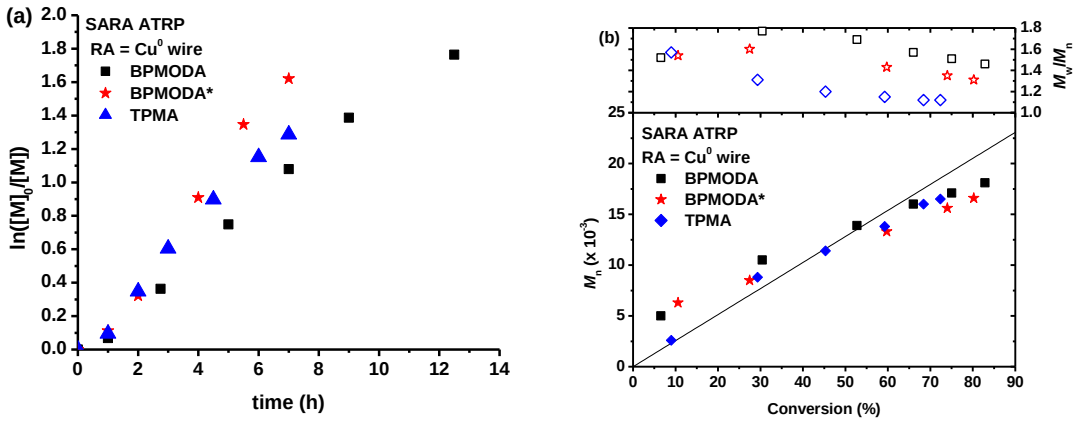

Figure III.3. First-order kinetic plots (a) and evolution of M_n and M_w/M_n with monomer conversion (b) for the SARA ATRP of *n*-BA with BPMODA, BPMODA*, or TPMA. All polymerizations were conducted with [*n*-BA]:[EBiB]:[$CuBr_2$]:[Ligand]:[Cu^0 wire] = 200:1:0.01:0.03:1 cm in 20% (v/v) anisole at 60 °C.

Figure III.3 shows the linear first order kinetics by each of the three ligands tested. BPMODA* and TPMA had very similar R_p, while BPMODA was the slowest. The difference in R_p under SARA ATRP conditions was not as dramatic as was seen in normal

ATRP, which is attributed to the presence of the reducing agent. The rate of polymerization is dependent on the rate at which Cu^0 wire reduces $Cu^{II}Br_2$/L to $Cu^{I}Br$/L and the least reducing catalyst should be more quickly converted to its lower oxidation state. While the $M_{n,GPC}$ values increased linearly with monomer conversion for each ligand, it is evident that TPMA afforded the most well-controlled polymerization. When TPMA was utilized, there was the strongest correlation between $M_{n,GPC}$ and $M_{n,th}$, along with the lowest M_w/M_n values. Although BPMODA* did not afford as much control as TPMA, it did offer a more controlled polymerization than BPMODA. Both ligands demonstrated M_w/M_n values which decreased with monomer conversion, however, the values were broader than those given by TPMA. Nevertheless, BPMODA* offered more control than BPMODA.

III.4.1.3. Partition experiments

Before starting polymerization under miniemulsion type conditions, the partition coefficient for each complex was determined at various catalyst concentrations. UV-Vis was used to determine the absorbance of both the organic and aqueous layers, from which the concentration of the catalyst and respective partition coefficient ($\lambda = [Cu]_{org}/[Cu]_{aq}$) was determined (Table III.2). At each concentration tested, a higher percentage catalyst, for both ligands, was transferred to the aqueous phase when stirred at 80 °C. The electron donating groups present on BPMDOA* do not appear to have an effect on the partition coefficient as similar amounts of catalyst remained in the organic phase.

Table III.2. Partitioning of $CuBr_2$/BPMODA and $CuBr_2$/BPMODA* in *n*-BA/Water (w/w) = 30/100.

30/100 (w/w) (org:Aq)		**[$CuBr_2$/L] Initial Conc. 2.5 mM**		**1 mM**	
		Reg	Star	Reg	Star
λ	r.t.	1.96	9.04	2.93	4.20
λ	80 °C	0.26	2.23	1.33	0.48
$[Cu]_{org}/[Cu]_{int}$	r.t.	66.2	90.0	74.5	80.8
$[Cu]_{org}/[Cu]_{int}$	80 °C	20.9	69.0	57.2	32.4

III.4.1.4. Heterogeneous Polymerizations

Polymerizations were carried out under miniemulsion conditions with both BPMODA and BPMODA*. To start, ligand and copper were dissolved in monomer to form the catalyst by stirring at 60 °C for 30 – 60 min. The solubility of BPMODA* in monomer was significantly better as compared to BPMODA. To form the catalyst in *n*-BA with BPMODA, it was required to stir at 60 °C for 1 h and the final solution was very cloudy. On the other hand, BPMODA* required only 30 min to fully form the catalyst in *n*-BA and the final solution was translucent, as seen in Figure III.4. This increased solubility of BPMODA* in monomer is advantageous not only for ease of polymerization set-up but also for consistency of results as it is much easier to see if the catalyst is fully dissolved with BPMODA*.

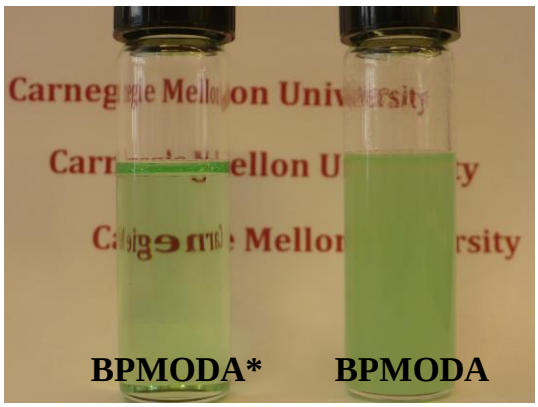

Figure III.4. 500 ppm catalyst solutions in *n*-BA with BPMODA* and BPMODA.

Though AGET ATRP (catalyst ~ 2000 ppm) with BPMODA in miniemulsion is common and well-studied, it was important to compare the newly synthesized ligand under identical conditions, after which the catalyst concentration was systematically lowered until ARGET ATRP conditions were reached; Table III.3 and Figure III.5 summarize these results. Linear first order kinetics were observed for both ligands when 2000 ppm of catalyst was utilized (Figure III.5a). Both polymerizations exhibited $M_{n,GPC}$ values which strongly correlated the $M_{n,th}$ values as well as low M_w/M_n values. However, the molecular weight distributions at early monomer conversion is the distinguishing mark between the ligands. While both ligands offer M_w/M_n values which decrease with monomer conversion, BPMODA* affords polymers with significantly lower M_w/M_n values at the beginning states of the polymerization. For example, BPMODA showed a M_w/M_n = 2.69 at 20% monomer conversion, while BPMODA* showed a M_w/M_n = 1.54 at 16% monomer conversion. As AGET ATRP operates under similar mechanistic conditions to SARA ATRP, the rates of polymerizations for the ligands were similar due to the presence of the reducing agent, ascorbic acid. As the concentration of catalyst was lowered, similar trends were seen. At

both 1000 and 500 ppm of catalyst, BPMODA* resulted in polymerizations with lower M_w/M_n values at all monomer conversions.

Table III.3. A(R)GET ATRP of *n*-BA in miniemulsion with BPMODA and BPMODA*.[a]

Entry[b]	$CuBr_2$ (ppm)	Ligand	AA	Conv.[c]	$M_{n,th}$	$M_{n,GPC}$	M_w/M_n[d]	M_w/M_n[e]
1	0.4 (2000)	0.4	0.2	0.55	14 100	15 300	2.69	1.23
2*	0.4 (2000)	0.4	0.2	0.54	13 800	13 500	1.54	1.15
3	0.2 (1000)	0.2	0.1	0.87	22 400	18 000	2.49	1.60
4*	0.2 (1000)	0.2	0.1	0.54	14 000	14 000	1.62	1.18
5	0.1 (500)	0.1	0.05	0.87	22 300	18 500	1.61	1.48
6*	0.1 (500)	0.1	0.05	0.84	21 600	18 200	1.45	1.33
7	0.05 (250)	0.05	0.025	0.88	22 000	21 000	2.64[f]	2.61
8*	0.05 (250)	0.05	0.025	0.93	23 800	18 900	1.66	1.51

[a] [*n*-BA]:[EBiB] = 200:1, [Brij98]/[Hexadecane]= 2.3/3.6 wt% vs *n*-BA, T = 80 °C; [b] entries labeled with (*) used BPMODA*, all others used BPMODA; [c] determined by gravimetry; [d] monomer conversion < 45% unless otherwise noted; [e] M_w/M_n values of final polymer sample. [f] monomer conversion = 66 %.

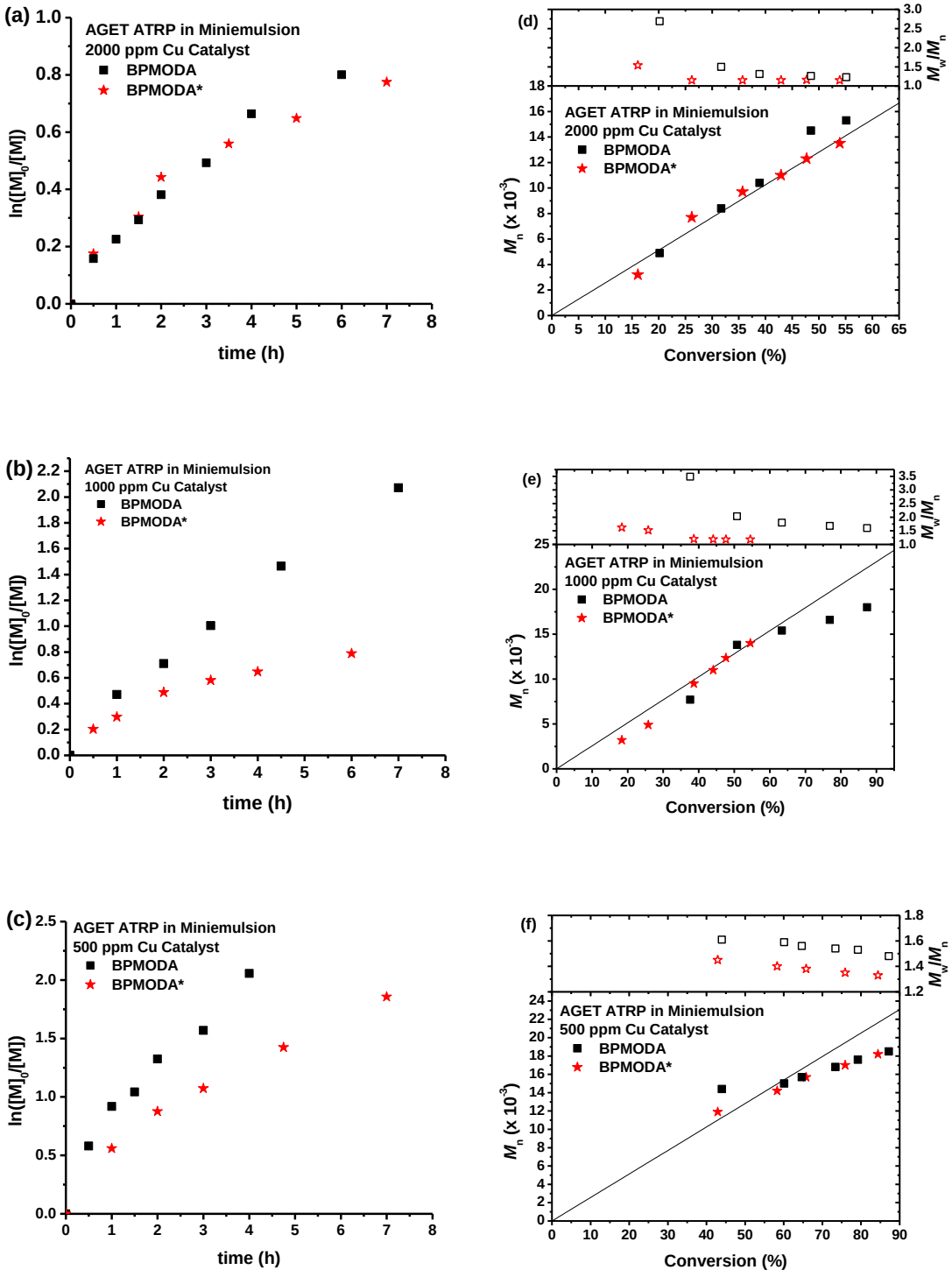

Figure III.5. First-order kinetic plots (a-c) and evolution of molecular weights and M_w/M_n with conversion (d-f) of AGET ATRP of *n*-BA with BPMODA and BPMODA* in

miniemulsion. [a] [*n*-BA]:[EBiB] = 200:1, [Brij98]/[Hexadecane]= 2.3/3.6 wt% vs *n*-BA, T = 80 °C.

In an attempt the find the "limit" for each ligand, the catalyst concentrations were reduced even further. 250 ppm of catalyst resulted in very different polymerizations for each ligands. The first order kinetic plot can be seen in Figure III.6, which demonstrates the kinetic plots for BPMODA are not linear at this concentration. The plot levels off, indicating the polymerization has stopped. The number average molecular weight does not grow linearly with monomer conversion and the polymerization stops at 90% conversion. Additionally, the M_w/M_n values are quite large (>2.5) throughout the polymerization. However, when an identical polymerization was carried out with BPMODA*, a significant increase in control was seen. BPMODA* afforded linear first order kinetics, $M_{n,GPC}$ values which had a reasonable correlation to the theoretical values and M_w/M_n <1.5 throughout the polymerization. While the polymerization with BPMODA* at 250 ppm of catalyst was not ideal, it did offer much more control than BPMODA.

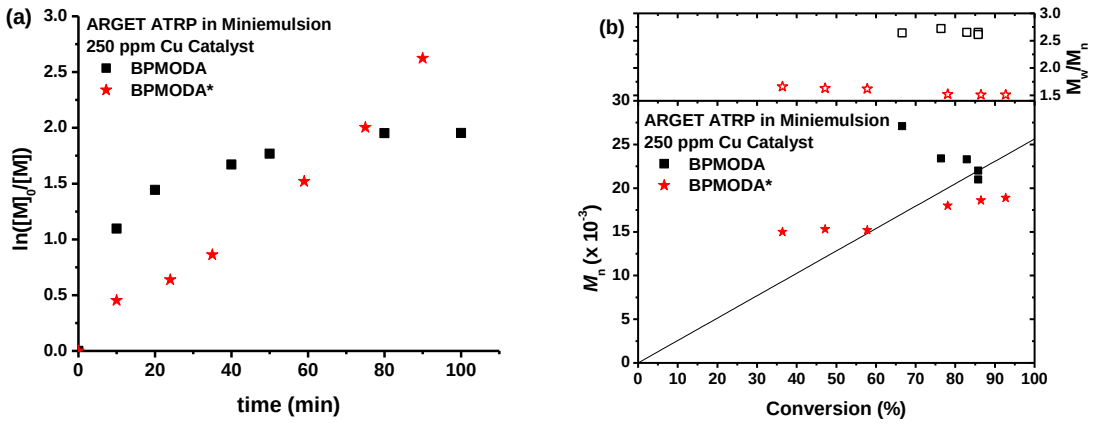

Figure III.6. First-order kinetic plot (a-c) and evolution of molecular weight and M_w/M_n with conversion (d-f) of AGET ATRP of *n*-BA with BPMODA and BPMODA* in

miniemulsion. [a] [*n*-BA]:[EBiB] = 200:1, [Brij98]/[Hexadecane]= 2.3/3.6 wt% vs *n*-BA, T = 80 °C.

The previous set of miniemulsion polymerizations maintained the ratio of ascorbic acid and ligand to copper throughout all polymerizations. While this allowed a systematic study of the ligands over a range of catalyst concentrations, it did not allow for the optimal polymerization conditions at low catalyst concentrations. For example, ARGET ATRP utilizes an excess of ligand compared to copper, ensuring the catalyst is formed. To fully realize the potential of BPMODA*, a series of polymerizations were conducted with conditions more suited toward low catalyst concentrations.

III.4.2. DOD-BPED*

III.4.2.1. Ligand design and characterization

When considering the design of a second ligand, hydrophobicity and K_{ATRP} value were increased as compared to BPMODA* through the number of aliphatic chains present as well as the denticity of the ligand. The structure of DOD-BPED* (Figure III.1) was based on *N,N'*-dimethyl-*N,N'*-bis(2-pyridylmethyl)ethane-1,2-diamine (BPED), a tetradentate ligand known to have a K_{ATRP} value similar to that of TPMA.[26] Two octadecyl chains were incorporated into the BPED-based structure affording increased hydrophobicity over BPMODA* which contains only one aliphatic chain. In addition to being tetradentate, as compared to the less active tridentate structure of BPMODA*, six electron donating groups were also included on two pyridine rings to further increase activity. [26,22,17]

It has been reported that half-wave potentials ($E_{1/2}$ values) measured by cyclic voltammetry (CV) are correlated to K_{ATRP} thereby providing insight into the activity of a catalyst complex.[25-27] DOD-BPED*, when complexed with $CuBr_2$, is insoluble in aceteonitrile preventing the measurement of the $E_{1/2}$ and K_{ATRP} values by CV. Utilizing a solvent other than acetonitrile for CV will provide a trend in $E_{1/2}$ value changes with ligand structure as given in Table III.4. For example, the $E_{1/2}$ value of BPMODA* is more negative, indicating a more active ligand, than BPMODA due to the presence of electron dontating groups on BPMODA*. When measured in DMF, a similar trend for the BPMDOA to BPMODA* structure change was observed: -0.07 and -0.14 V (vs SCE), respectively. Comparison of the cyclic voltammograms of *N′*,*N″*-dioctadecyl-*N′*,*N″*-bis(2-pyridylmethyl)ethane-1,2-diamine (DOD-BPED) ($E_{1/2}$ = -0.13 V) with that of DOD-BPED* ($E_{1/2}$ = -0.17 V) resulted in a more negative $E_{1/2}$ values for DOD-BPED* due to the electron donating groups within the structure. This shift toward a more negative $E_{1/2}$ value indicates a higher K_{ATRP} value for DOD-BPED* than for DOD-BPED.

Table III.4. $E_{1/2}$ values of BPMODA, BPMODA*, DOD-BPED and DOD-BPED* in selected solvents.

Ligand	**$E_{1/2}$ in MeCN**	**$E_{1/2}$ in DMF**
TPMA	-0.24 V[26]	-0.21 V
BPMODA	-0.098 V	-0.07 V
BPMODA*	-0.204 V	-0.14 V
DOD-BPED	not soluble	-0.13 V
DOD-BPED*	not soluble	-0.17 V

III.4.2.2. Homogenous polymerizations

$CuBr_2$/DOD-BPED* was first tested as a catalyst under homogeneous ARGET ATRP conditions and compared with $CuBr_2$/TPMA and $CuBr_2$/BPMODA. Butyl methacrylate (BMA) was polymerized at a targeted DP = 200 with 50 ppm of $CuBr_2$/L catalyst and $Sn^{III}(EH)_2$ as the reducing agent. Specific reaction conditions and results are summarized in Table III.5 and Figure III.7. Linear first-order kinetics as well as similar rates of polymerization (R_p) were observed for all ligands. While all polymerizations demonstrated good correlation between experimental ($M_{n,exp}$) and theoretical ($M_{n,th}$) molecular weights, the final M_w/M_n values of 1.12, 1.38 and 1.42 for TPMA, DOD-BPED* and BPMODA, respectively, signify the polymerization with BPMODA was the least controlled. ARGET ATRPs conducted with $CuBr_2$/TPMA are established and known to offer a high degree of control at catalyst concentrations as low as 10 ppm and such was the case in this work. While the polymerization with DOD-BPED* resulted in a larger M_w/M_n value as compared to TPMA, the linear first-order kinetics and good correlation of $M_{n,exp}$ and $M_{n,th}$ values are promising results for successful heterogeneous polymerizations with low catalyst concentrations.

Table III.5. ARGET ATRP of BMA with TPMA and DOD-BPED*

Entry[a]	**t (h)**	**Conv.**[b]	$M_{n,th}$	$M_{n,GPC}$	M_w/M_n
TPMA	8	0.35	9 800	11 000	1.12
DOD-BPED*	7.5	0.27	7 700	7 600	1.38
BPMODA	7	0.30	8 600	10 500	1.42

[a] All polymerizations were conducted with [BMA]:[EBPA]:[$CuBr_2$]:[Ligand]:[$Sn^{III}(EH)_2$] = 200:1:0.01:0.03:0.1, 20% (v/v) anisole, T =60 °C. [b] Determined by ^{1}H NMR.

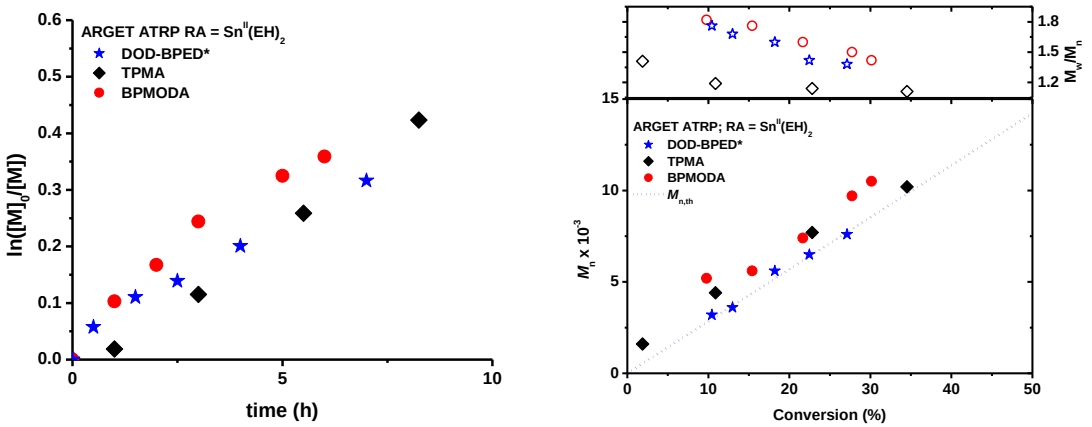

Figure III.7. First-order kinetic plots (a) and evolution of M_n and M_w/M_n with monomer conversion (b) for the ARGET ATRP of BMA with DOD-BPED*, TPMA, or BPMODA. All polymerizations were conducted with [BMA]:[EBPA]:[$CuBr_2$]:[Ligand]:[$Sn^{III}(EH)_2$] = 200:1:0.01:0.03:0.1, 20% (v/v) anisole, T =60 °C.

III.4.2.3. Heterogeneous polymerizations

Polymerizations under heterogeneous miniemulsion conditions were conducted with $CuBr_2$/DOD-BPED* catalyst whose concentration was systematically decreased from 250 to 50 ppm at a targeted DP = 2000 as detailed in Table III.6 (entries 1-3) and Figure III.8a,b. Although lower catalyst concentrations resulted in a decreased rate of polymerization (R_p), linear first-order kinetics was observed for each polymerization. All polymerizations demonstrated linear growth of molecular weight with monomer conversion in addition to good correlation between $M_{n,exp}$ and $M_{n,th}$ values. When 250 or 100 ppm (entries 1 and 2) of $CuBr_2$/DOD-BPED* catalyst was employed, M_w/M_n values were low (ca. 1.23 and 1.24, respectively). Only a slight increase of the final M_w/M_n value (ca. 1.33) was observed when a mere 50 ppm (entry 3) of catalyst was utilized.

Table III.6. ARGET ATRP of BMA in Miniemulsion with DOD-BPED*.[a]

Entry	BMA	EBPA	$CuBr_2$ (ppm)	Ligand	AA	conv[b]	$M_{n,th}$	$M_{n,GPC}$	M_w/M_n
1	2000	1	0.5 (250)	0.5	0.25	0.54	152 800	173 700	1.23
2	2000	1	0.2 (100)	0.2	0.1	0.44	124 700	124 900	1.24
3	2000	1	0.1 (50)	0.1	0.05	0.28	80 600	78 200	1.33
4	5000	1	0.5 (50)	0.5	0.25	0.37	261 300	248 900	1.33
5	10000	1	1 (50)	1	0.5	0.37	527 700	755 500	1.39

[a][Brij 98]/[hexadecane] = 2.3/3.6 wt % vs BMA, T = 80 °C. [b]Determined by gravimetry.

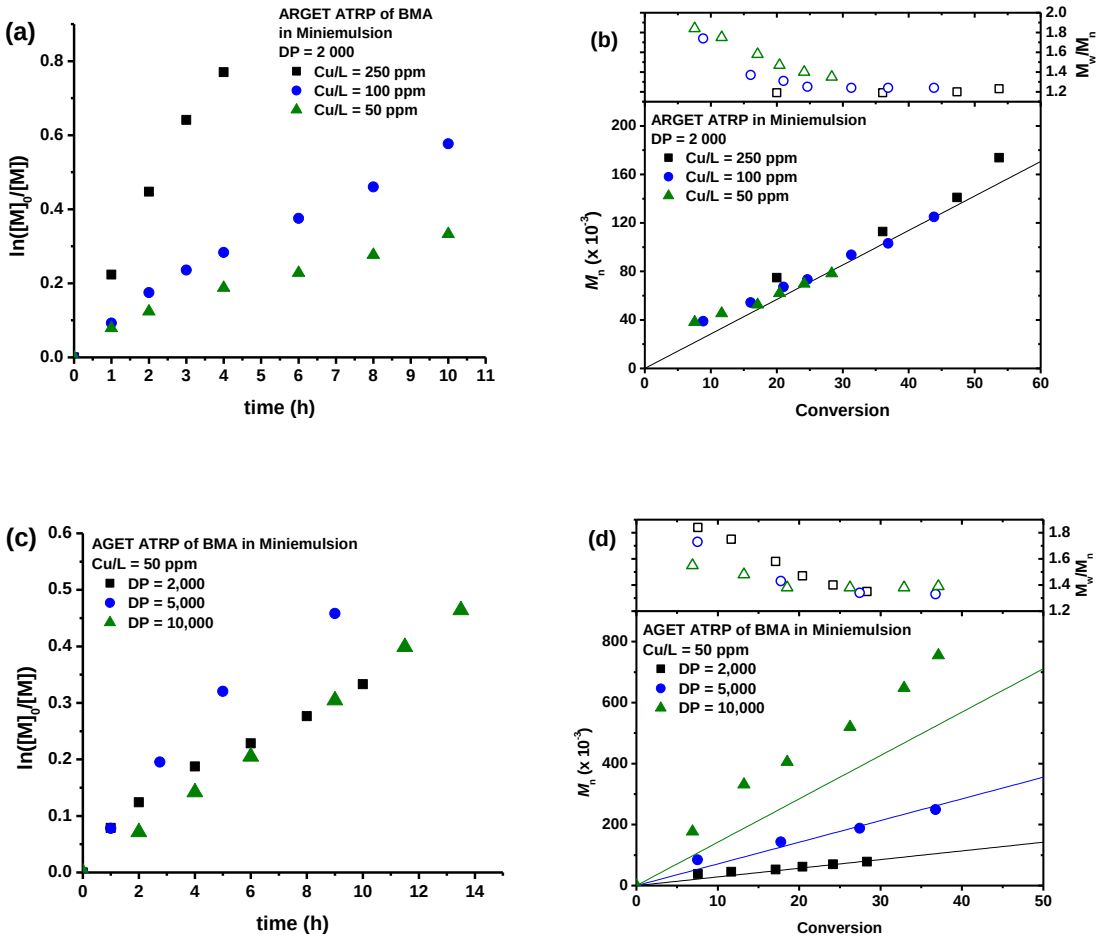

Figure III.8. First-order kinetic plots (a,c) and evolution of M_n and M_w/M_n with monomer conversion (b,d) for the ARGET ATRP of BMA DOD-BPED* under miniemulsion conditions. All polymerizations were conducted with [Brij 98]/[hexadecane] = 2.3/3.6 wt % vs BMA, T = 80 °C. Specific reaction conditions in Table 2.

Maintaining the catalyst concentration at 50 ppm, the targeted degree of polymerizations were systematically increased from DP = 2000 to DP = 10000 while keeping monomer conversion below 50% to avoid any particle aggregation. Table III.6 (entries 3-5) and Figure III.8c,d summarize these results. All polymerizations demonstrated linear first-order kinetics as well as linear growth of molecular weight with

monomer conversion. M_w/M_n values decreased with monomer conversion reaching final M_w/M_n values = 1.35, 1.33, and 1.39 for DP = 2000, 5000, and 10000, respectively. The synthesis of large polymers with low M_w/M_n values may be attributed to the more active ligand, DOD-BPED*, which allows for low catalyst concentrations during the polymerization thereby reducing the Cu^IX/L induced catalytic radical termination effect.[28] However, this may also be due to compartmentalization where radical-radical termination is limited due to the separation of radicals in the miniemulsion system.[29] The generation of a polymer with $M_{n,exp}$ > 700,000 and narrow MWD values while utilizing only 50 ppm of catalyst (Table III.6, entry 5) is an extraordinary advance of ATRP in aqueous dispersed media.

III.5. Conclusions

In summary, careful ligand design is an important tool for the improvement and expansion of ATRP success. This chapter demonstrates that the modification of traditionally used BPMODA, a ligand with low catalyst activity, was achieved through the addition of electron donating groups, which resulted in a ca. 100 fold increase in the K_{ATRP} value. Homogenous polymerizations under normal ATRP conditions confirmed BPMODA* to have a higher R_p without loss of control. Additionally, the hydrophobicity of BPMODA was not been compromised by the supplementary EDGs as demonstrated by partition experiments. Heterogeneous polymerizations conducted over a range of catalyst concentrations (2000 - 250 ppm) with BPMODA* consistently resulted in polymerizations with increased control throughout the polymerizations, particularly at early monomer conversions. This chapter also details the synthesis of a second ligand, DOD-BPED*, for

use in miniemulsion ARGET ATRP. Well controlled polymerizations were achieved with as low as 50 ppm of $CuBr_2$/DOD-BPED* catalyst. Moreover, while maintaining this level of catalyst concentration, it was shown that DOD-BPED* can successfully polymerize BMA at a targeted DP = 10000. Most significantly, very high molecular weight polymers of $M_{n,exp}$ > 700,000 with low M_w/M_n values were achieved using only 50 ppm of $CuBr_2$/DOD-BPED* catalyst.

III. 6. Acknowledgements

I would like to thank Joanna Burdyńska not only for the synthesis of BPMODA*, DOD-BPED and DOD-BPED*, but also for many helpful discussions. I would also like to thank Sangwoo Park for his contributions; performing countless CVs as well as his keen eye for detail during the publishing process. A special thanks goes to Dr. Jim Spanswick for all of his hard work on the patent for these active ligands.

III. 7. References

1. Min, K.; Matyjaszewski, K. *Macromolecules* **2005,** *38,* 8131-8134.
2. Kagawa, Y.; Kawasaki, M.; Zetterlund, P. B.; Minami, H.; Okubo, M. *Macromol. Rapid Commun.* **2007,** *28*, 2354-2360.
3. Min, K.; Gao, H. F.; Matyjaszewski, K. *J. Am. Chem. Soc.* **2005,** *127,* 3825-3830.
4. Min, K.; Jakubowski, W.; Matyjaszewski, K. *Macromol. Rapid Commun.* **2006,** *27,* 594-598.
5. Bombalski, L.; Min, K.; Dong, H. C.; Tang, C. B.; Matyjaszewski, K. *Macromolecules* **2007,** *40,* 7429-7432.

6. Min, K.; Yu, S.; Lee, H. I.; Mueller, L.; Sheiko, S. S.; Matyjaszewski, K. *Macromolecules* **2007,** *40*, 6557-6563.

7. Qiu, J.; Gaynor, S. G.; Matyjaszewski, K. *Macromolecules* **1999,** *32*, 2872-2875.

8. Jousset, S.; Qiu, J.; Matyjaszewski, K. *Macromolecules* **2001,** *34*, 6641-6648.

9. Eslami, H.; Zhu, S. P. *Polymer* **2005,** *46*, 5484-5493.

10. Eslami, H.; Zhu, S. P. *J. Polym. Sci., Part A: Polym. Chem.* **2006,** *44*, 1914-1925.

11. Min, K.; Gao, H.; Yoon, J. A.; Wu, W.; Kowalewski, T.; Matyjaszewski, K. *Macromolecules* **2009,** *42*, 1597-1603.

12. Cunningham, M. F. *Prog. Polym. Sci.* **2008,** *33*, 365-398.

13. Min, K.; Matyjaszewski, K. *Cent. Eur. J. Chem.* **2009,** *7*, 657-674.

14. Oh, J. K. *J. Polym. Sci., Part A: Polym. Chem.* **2008,** *46*, 6983-7001.

15. Jakubowski, W.; Matyjaszewski, K. *Angew. Chem., Int. Ed.* **2006,** *45*, 4482-4486.

16. Matyjaszewski, K.; Jakubowski, W.; Min, K.; Tang, W.; Huang, J.; Braunecker, W. A.; Tsarevsky, N. V. *Proc. Natl. Acad. Sci. U.S.A.* **2006,** *103*, 15309-14.

17. Magenau, A. J. D.; Kwak, Y.; Schroeder, K.; Matyjaszewski, K. *ACS Macro Lett.* **2012,** *1*, 508-512.

18. di Lena, F.; Matyjaszewski, K. *Prog. Polym. Sci.* **2010,** *35*, 959-1021.

19. Cheng, C.; Shu, J.; Gong, S.; Shen, L.; Qiao, Y.; Changqing, F. *New J. Chem.* **2010,** *34*, 163-170.

20. Stoffelbach, F.; Griffete, N.; Bui, C.; Charleux, B. *Chem. Commun.* **2008**, 4807-4809.

21. Simms, R. W.; Cunningham, M. F. *Macromolecules* **2007,** *40*, 860-866.

22. Schroeder, K.; Mathers, R. T.; Buback, J.; Konkolewicz, D.; Magenau, A. J. D.; Matyjaszewski, K. *ACS Macro Lett.* **2012,** *1*, 1037-1040.

23. Xia, J. H.; Matyjaszewski, K. *Macromolecules* **1999,** *32*, 2434-2437.

24. Xia, J. H.; Gaynor, S. G.; Matyjaszewski, K. *Macromolecules* **1998,** *31*, 5958-5959.

25. Qiu, J.; Matyjaszewski, K.; Thouin, L.; Amatore, C. *Macromol. Chem. Phys.* **2000,** *201*, 1625-1631.

26. Tang, W.; Kwak, Y.; Braunecker, W.; Tsarevsky, N.; Coote, M. L.; Matyjaszewski, K. *J. Am. Chem. Soc.* **2008,** *130*, 10702-10713.

27. Braunecker, W.; Tsarevsky, N.; Gennaro, A.; Matyjaszewski, K. *Macromolecules* **2009,** *42*, 6348-6360.

28. Wang, Y.; Soerensen, N.; Zhong, M.; Schroeder, H.; Buback, M.; Matyjaszewski, K. *Macromolecules* **2013,** *46*, 683-691.

29. Cunningham, M. F. *Progress in Polymer Science* **2002,** *27*, 1039-1067.

CHAPTER IV

TUNING DISPERSITY IN DIBLOCK COPOLYMERS USING ARGET ATRP*

IV.1. Preface

ATRP is generally considered as the preferred method to synthesize well-defined polymers with controlled molecular weight and narrow molecular weight distribution as discussed in the first three chapters. However, control over molecular weight distribution, or dispersity, could also be an attractive asset of a controlled polymerization for many potential applications. Until the development of controlled radical polymerizations, it was nearly impossible to synthesize symmetrically disperse polymers.

As discussed in Chapter I, polymers with controlled, symmetric dispersity have proven to provide a unique set of characteristics and, in some cases, perform better than their narrow molecular weight distribution analogues. For example, certain phase domains

*Work in this chapter has been published in the following manuscript: Plichta, A.; Zhong, M.; Li, W.; Elsen, A. M.; Matyjaszewski, K., "Tuning Dispersity in Diblock Copolymers Using ARGET ATRP." *Macromolecular Chemistry and Physics* **2012**, *213*, 2659-2668. Copyright © 2012 Wiley-VCH.

may exhibit increased stability, traditionally unstable phase domains may become the equilibrium domain, and micelle formation in solution may change dramatically upon increased molecular weight distributions.

In this chapter, poly(methyl acrylate)-*b*-polystyrene copolymers with controlled molecular weight distribution of each block were synthesized *via* activators regenerated by electron transfer (ARGET) atom transfer radical polymerization (ATRP). Polymers with tunable dispersity, in the range of M_w/M_n 1.32 to 2.0, were achieved by adjusting the concentration of the copper catalyst and reaction temperature, thereby controlling the rate of the reversible deactivation reaction and hence the number of monomer units added during each activation cycle. High chain end functionality was retained with increased dispersity and the livingness of the macroinitiators was confirmed by chain extension to form diblock copolymers with controlled dispersity in each block. Liquid chromatography under critical conditions (LCCC) was employed to determine whether any macroinitiator remained in the final product.

The experiments of this project were conducted by Dr. Mingjiang Zhong and Dr. Andrzej Plichta while Dr. Wenwen Li carried out the LCCC characterization. I came on to the project to analyze and organize the data in the proper way to demonstrate the importance of retaining chain end functionality while generating polymers with broad molecular weight distrubition. Additionally, I wrote the manuscript and coordinated publication of this project. This development of "controlled" molecular weight distribution will be utilized in the next chapter for the study of gradient copolymers and was very useful in determining how molecular weight distribution can affect the quality of gradient architecture.

IV.2. Introduction

The synthesis of block copolymers was first reported by Szwarc et al. in 1956 with the preparation of a polystyrene-***b***-polyisoprene copolymer by anionic polymerization. Since that report, block copolymers have become a fundamental aspect of polymer chemistry.[1,2] Block copolymers not only exhibit properties resulting from the contribution of each block, but if these blocks are incompatible, they may also undergo microphase separation to form nanostructured materials.[3] This phase separation behavior results in generation of properties that provide materials suitable for many applications, including thermoplastic elastomers, contact lenses, nanolithography, nanowires, and photonic crystals.[4]

ATRP allows polymerization of a library of functional monomers (e.g., styrenics, (meth)acrylates, and acrylamides), with control over composition (e.g., statistical, block, and gradient), and architectures (e.g., brushes and stars), with precise control over the number-average molecular weight (M_n) and molecular weight distributions (MWD), or dispersity (M_w/M_n). The equilibrium constant of ATRP is defined as $K_{ATRP} = k_a/k_{da}$, where k_a and k_{da} are the rate constants of the activation and deactivation, respectively, and their values depend on (1) the ligand, which takes part in formation of the catalytic complex with a transition metal halide, (2) the halogen atom ($K_{ATRP,Cl} < K_{ATRP,Br}$) and (3) the monomer (alkyl halide chain end) and (4) reaction conditions (e.g., solvent, pressure,[5] and temperature).[6]

When the ATRP equilibrium is established, the rate of polymerization, $R_{p,ATRP}$, is provided by equation IV.1.

$$R_p = k_p \frac{k_a}{k_{da}} [M][R\text{-}X]_0 \frac{[Mt^n/L]}{[X\text{-}Mt^{n+1}/L]} \quad (IV.1)$$

$R_{p,ATRP}$ in ATRP depends on K_{ATRP}, the initial concentration of the halogen based initiator, and the ratio of the concentration of activator (Cu^I/L) to deactivator (X-Cu^{II}/L), but not on the absolute concentration of catalyst, as described in equation IV.2.[7,8] Generally, the targeted values for K_{ATRP} are very low, (10^{-11} to 10^{-5}),[9] which ensures that only a small number of active radical species are present at any moment, thereby preventing/reducing termination reactions and retaining high chain end functionality. As the rate of termination, $R_t = 2k_t[P^\bullet]^2$, is proportional to the square of [$P^\bullet$] the impact of termination is diminished.

$$\frac{M_w}{M_n} = 1 + \frac{1}{DP_n} + \frac{k_p[R\text{-}X]_0}{k_{da}[X\text{-}Mt^{n+1}/L]}\left(\frac{2}{p} - 1\right) \quad (IV.2)$$

As expressed in equation (IV.2), the dispersity of molecular weights, defined as M_w/M_n, is determined by the deactivator concentration and lowering said concentration should increase the M_w/M_n of the final polymers. However, when less than 100 ppm of catalyst is utilized in a standard ATRP, the polymerization stops at low monomer conversion (<10%) due to unavoidable termination reactions and complete conversion of Cu^I/L to X-Cu^{II}/L species. Therefore, procedures were developed to compensate for the termination in which a fraction of the deactivator is continuously reduced to regenerate the activator. The procedures include use of a reducing agent, as in ARGET ATRP,[10] addition of metallic copper as in supplemental activators and reducing agent (SARA),[11-14] decomposition of free radical initiators, as in initiators for continuous activator regeneration (ICAR) ATRP,[15] or by directly applying a reducing potential to the reaction medium as in electrochemically mediated ATRP (*e*ATRP).[16] All of these methods are

proven to continuously rejuvenate the catalyst and drive the reaction to high conversion. Consequently, catalyst concentrations well below 100 ppm have been successfully utilized in well controlled polymerizations.

In ARGET systems, the ATRP starts with the transition metal complex in its higher oxidation state, X-Cu^{II}/L and the addition of a reducing agent, such as tin^{II}2-ethylhexanoate ($Sn^{II}(EH)_2$), glucose, or ascorbic acid reduces a fraction of X-Cu^{II}/L to Cu^{I}/L and generates the dynamic ATRP equilibrium.[17] The mechanism for ARGET ATRP is shown in Scheme IV.1.

Scheme IV.1. Mechanism of ARGET ATRP.

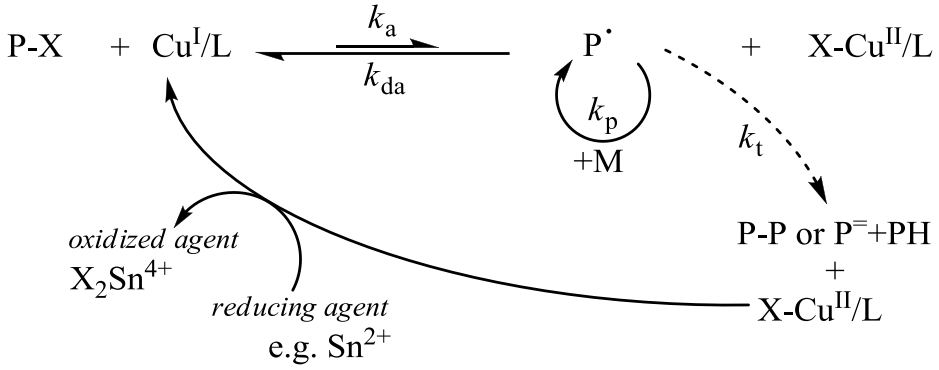

The selection of ligands that generate catalysts with higher K_{ATRP} values, such as tris(2-pyridylmethyl)amine (TPMA)[18] or tris[2-(dimethylamino)ethyl]amine (Me_6TREN),[19] are necessary in ARGET ATRP to generate and retain an appropriate activator to deactivator ratio that provides the desired polymer in a reasonable time frame. ATRPs conducted under ARGET conditions generally afford copolymers with low dispersities (< 1.2) and targeted degree of polymerization ($DP_n = [M]_0/[R\text{-}X]_0$) in the

presence of efficient deactivation (k_{da}) by X-Cu^{II}/L. However, ultimately at lower catalyst concentrations MWD should become broader. Therefore, systematically decreasing the catalyst concentration should result in polymers with segments displaying higher dispersity.

Polymerization procedures which allow the synthesis of segmented copolymers with controlled dispersity in the polymeric blocks, while maintaining end-group functionality, have become the subject of increased interest in recent years due to their unusual properties and phase separation behavior.[20-28] A symmetrically broad MWD can be obtained in the presence of various "scrambling" reactions, e.g. transesterification during ring opening polymerization of lactones,[29] or can be induced by a slow feeding of an anionic initiator.[30] Applied physical blending also leads to polymers with broader MWD.[31]

The subject of this chapter is to analyze the effect of varying the concentration of copper-based catalysts on MWD and number average molecular weight (M_n) of poly(methyl acrylate) (PMA) and polystyrene (PSt) block copolymers obtained in ARGET ATRP systems. As disclosed below, at very low catalyst concentrations polymers with broad MWD were formed. Broad-narrow diblock copolymers were generated from these disperse polymers, by chain extension with a second monomer.

IV.3. Experimental

IV.3.1. Materials

Styrene (St) (Aldrich Reagent Plus, 99%) and methyl acrylate (MA) (Aldrich, 99%) were passed through column filled with basic alumina and purged by bubbling with N_2 (duration ~ 3 min/mL) just before use. Anisole (Sigma-Aldrich, Reagent Plus, 99%) was purged by bubbling with N_2 and stored under N_2. Tris[2-(dimethylamino)ethyl]amine (Me_6TREN) (ATRP Solutions, 99%), $Sn^{II}(EH)_2$ (Sigma, ~95%), ethyl 2-bromoisobutyrate (EBiB) (Acros, 98%) and solvents for polymer purification and analysis: tetrahydrofuran (THF) (Sigma-Aldrich, ACS reagent >99%), acetone (Sigma-Aldrich, ACS reagent >99.5%), hexanes (Fluka), toluene (Fluka) were used as supplied. Copper (I) bromide (Acros, 98 %) was washed with glacial acetic acid to remove any soluble oxidized species, filtered, washed twice with anhydrous ethyl ether, dried and kept under vacuum in the presence of copper wire.

IV.3.2. Synthetic procedures

IV.3.2.1. Disperse homopolymers by ARGET ATRP

Specific reaction conditions for ARGET ATRP procedures with ppm of Cu for of MA and S polymerizations are provided in Tables IV.1 and IV.2, respectively. Specific conditions for an ARGET ATRP targeting DP_n = 484 with 0.1 ppm of Cu follow: deoxidized MA (6 mL, 66.7 mmol) and anisole (1 mL) were transferred via purged syringes to 10 mL Schlenk flask which was previously evacuated and filled up with N_2 5 times. The other components were added via purged syringes in the form of stock solutions in deoxidized anisole (total volume of 1 mL): CuBr/Me_6TREN (0.1 mol ppm related to monomer, $6.67 \cdot 10^{-6}$ mmol), EBiB (0.138 mmol), Me_6TREN ($1.38 \cdot 10^{-2}$ mmol), and $Sn^{II}(EH)_2$ (10 mol % of initiator, $1.38 \cdot 10^{-2}$ mmol). Total volume of solvent was always 25

vol. % of reaction mixture. After all components were added, an initial sample was collected, and the sealed flask was placed in thermostated oil bath at 60 °C. Samples were taken after appropriate time intervals and analyzed by gas chromatography (GC) and gel permeation chromatography (GPC) to follow the progress of the reaction and measure the MWD and M_n of the polymer samples. Usually, the reactions were stopped at 60 % of monomer conversion by opening the flask and exposing the catalyst to the air. Then the reaction mixture was diluted with THF, passed through 0.2 μm filter before the polymer was precipitated by addition of the solution into cold hexanes. The precipitate was filtered and dried under vacuum overnight at room temperature. The pure product was characterized by GPC.

IV.3.2.2. Chain extension by ARGET ATRP chain extension

The appropriate macroinitiator was placed in 25 mL Schlenk flask, followed by gas evacuation and refilling with N_2 5 times. Deoxygenated anisole (solvent) was transferred via a purged syringe to the flask and after sealing the flask was stirred overnight with a magnetic stirrer to dissolve the polymer. Deoxidized monomer then was transferred via purged syringe to the flask under nitrogen. The other components (catalyst complex, ligand, reducing agent) were added via purged syringes in the form of stock solutions in anisole as described for homopolymer synthesis. The complete compositions and reaction conditions for chain extension polymerizations are listed in Table IV.3 and are listed here for each entry:

(1) ARGET ATRP $[T1\text{-}2]_0/[S]_0/[CuBr]_0/[Me_6TREN]_0/[Sn^{II}(EH)_2]_0$ = 1/590/0.0295(50ppm)/0.5/0.5, 40 vol. % of anisole, temp. 80 °C, terminated after 1230 min. at p_S = 49%;

(2) normal ATRP $[T1\text{-}3]_0/[S]_0/[CuCl]_0/[CuCl_2]_0/[PMDETA]_0$ = 1/800/0.8/0.2/1, 67 vol. % of anisole, temp. 80-90 °C, terminated after 7080 min. at p_S = 41%;

(3) ARGET ATRP $[T1\text{-}6]_0/[S]_0/[CuBr]_0/[Me_6TREN]_0/[Sn^{II}(EH)_2]_0$ = 1/337/0.0337(100ppm)/0.5/0.5, 70 vol. % of anisole, temp. 80 °C, terminated after 1200 min. at p_S = 42%;

(4) ARGET ATRP $[T6\text{-}3]_0/[S]_0/[CuBr]_0/[Me_6TREN]_0/[Sn^{II}(EH)_2]_0$ = 1/1144/0.114(100ppm)/0.5/0.5, 80 vol. % of anisole, temp. 80 °C, terminated after 1740 min. at p_S = 35%;

(5) ARGET ATRP $[T4\text{-}4]_0/[MA]_0/[CuBr]_0/[Me_6TREN]_0/[Sn^{II}(EH)_2]_0$ = 1/393/0.0393(100ppm)/0.3/0.3, 80 vol. % of anisole, temp. 60 °C, terminated after 1320 min. at p_{MA} = 47%;

(6) ARGET ATRP $[T4\text{-}4]_0/[MA]_0/[CuBr]_0/[Me_6TREN]_0/[Sn^{II}(EH)_2]_0$ = 1/393/0.00196(5ppm)/0.3/0.3, 80 vol. % of anisole, temp. 60 °C, terminated after 1350 min. at p_{MA} = 40%;

(7) ARGET ATRP $[T4\text{-}4A]_0/[MA]_0/[CuBr]_0/[Me_6TREN]_0/[Sn^{II}(EH]_2]_0$ = 1/1504/0.0752(50ppm)/0.3/0.3, 47 vol. % of anisole, temp. 60 °C, terminated after 1140 min. at p_{MA} = 37%.

After all components were added to the flask, an initial sample was collected, and the sealed flask was placed in thermostated oil bath. Samples were taken periodically to follow monomer conversion, and obtain the polymer average molecular weight and its

distribution of each sample by GC and GPC. The reactions were stopped by opening the flask and exposing the catalyst to the air, after which the reaction mixture was diluted with THF, passed through 0.2 μm filter. The copolymer was precipitated by addition of the purified solution into cold hexanes, filtered and dried under vacuum overnight at room temperature. The pure product was characterized by the means of GPC, ^{1}H NMR and liquid chromatography under critical conditions (LCCC).

IV.3.3. Analyses

Molecular weight and molecular weight distributions were determined by GPC. The GPC was conducted with a Waters 515 pump and Waters 410 differential refractometer using PSS columns (Styrogel 105, 103, 102 Å) in THF as an eluent at 35 °C and at a flow rate of 1 mL/min. Linear polystyrene standards were used for calibration. Monomer conversion was determined using a Shimadzu GC 14-A gas chromatograph equipped with a FID detector using a J&W Scientific 30 m DB WAX Megabore column and anisole as an internal standard. Injector and detector temperatures were kept constant at 250 °C. Analysis was carried out isothermally: for MA polymerization – at 40 °C for 2 min followed by an increase of temperature to 180 °C at a heating rate of 20 °C/min and holding at 180 °C for 2 min.; for S polymerization – at 60 °C for 2 min followed by an increase of temperature to 180 °C at a heating rate of 20 °C/min and holding at 180 °C for 2 min. Conversion was calculated by detecting the decrease in the area of the monomer peak relative to the peak areas of the standards. ^{1}H NMR spectroscopy was used for determination of copolymer composition and was performed using a Bruker 300 MHz instrument with $CDCl_3$ as a solvent.

LCCC was used to estimate the homopolymer content in the prepared block copolymers, *LCCC for PS*.[32] The samples were analyzed under the critical condition for polystyrene (PS) using a Waters 600 controller and pump. The mobile phase was a mixture of tetrahydrofuran (THF) and acetonitrile (51%/49%, v/v) and the flow rate was set at 0.5 mL/min. The columns used for separation were 2 sets of Macherey & Nagel, Nucleosil columns 300-5 C18 (particle size 5 μm, pore size 300 Å and column dimensions 250 × 4 mm i.d.) and 1000-7 C18 (particle size 7 μm, pore size 1000 Å and column dimensions 250 × 4 mm i.d.). The column oven temperature was set at 32 ºC. The detector was an evaporative light scattering detector (ELSD, Polymer Laboratories, PL-ELS 1000, nitrogen flow 1.2 L/min, evaporator temperature 90 ºC). Data acquisition was accomplished using PSS-WINGPC 7 from Polymer Standards Service (PSS; Mainz, Germany). Sample preparation: the homo- or co-polymers were dissolved in THF/acetonitrile (50%/50% v/v, ~0.5 mg/mL), and the injection volume each time was 20 μL. *LCCC for PMA*.[33] The samples were analyzed under the critical condition for PMA using a Waters 600 controller and pump. The mobile phase was a mixture of methyl ethyl ketone (MEK) and cyclohexane (88 %/12 %, v/v) and the flow rate was set at 0.5 mL/min. The columns used for the separation were 2 sets of Macherey & Nagel Nucleosil columns, 100-5 (particle size 5 μm, pore size 100 Å and column dimensions 250 × 4 mm i.d.) and 300-5 (particle size 5 μm, pore size 300 Å and column dimensions 250 × 4 mm i.d.), and the column oven temperature was set at 32 ºC. The detector was an evaporative light scattering detector (ELSD, Polymer Laboratories, PL-ELS 1000, nitrogen flow 1.2 L/min, evaporator temperature 90 ºC). Data acquisition was accomplished using PSS-WINGPC 7 from Polymer Standards Service (PSS; Mainz, Germany). Sample preparation: The homo- or co-polymers were dissolved

in MEK/cyclohexane (90%/10% v/v, ~0.5 mg/mL), and the injection volume each time was 20 μL.

IV.4. Results and discussion

IV.4.1. ARGET ATRP of methyl acrylate (MA)

Polymerizations of MA were carried out at 60 °C in 25 vol.% of anisole under ARGET ATRP conditions catalyzed by 0.1 to 5 mol ppm CuBr/Me_6TREN complex relative to monomer. $Sn^{II}(EH)_2$ was used as the reducing agent and ethyl 2-bromoisobutyrate (EBiB) as initiator with a molar ratio of 0.1:1. These conditions were examined at two targeted DP_n, 242 and 1089 respectively. The results are summarized in Table IV.1. The entries marked in bold font were used as macroinitiators for further chain extension polymerizations.

Table IV.2. Polymerization conditions and results for ARGET ATRP of MA.

Entry[a)]	[Cu] (ppm)[b)]	Targeted DP_n	Crude samples taken from reaction mixture					After precip. [d)]	
			t (min)	*p* (%)[c)]	$M_{n,\,GPC}$	M_w/M_n	I_{eff}	$M_{n,\,GPC}$	M_w/M_n
1	5	242	150	51.8	**11,800**	**1.68**	0.92		
			180	62.1	14,600	1.65	0.88		
2	2	242	180	59.1	15,000	1.96	0.82		
			270					**20,900**	**1.71**
3	0.5	242	180	69.4	15,500	2.00	0.94		
4	5	1089	1440	55.5	45,300	1.32	> 1		
5	1	1089	180	38.9	39,400	1.79	0.93	**42,200**	**1.74**

[a)] All polymerizations were carried out in 25 % (v/v) anisole at 60 °C with $[EBiB]_0/[Me_6TREN]_0/[Sn^{II}(EH)_2]_0$ = 1/0.1/0.1. The entries marked in bold were used for further chain extension polymerizations; [b)] [Cu] expressed as a mol ppm related to monomer; [c)] *p* = monomer conversion; [d)] Characterized after precipitation from hexanes and drying under vacuum.

Polymerizations which targeted DP_n = 242, were carried out with various catalyst loadings, 5, 2, 1, and 0.5 ppm. The evolution of M_n, initiation efficiency and M_w/M_n with monomer conversion are shown in Figure IV.1(a). When 5 ppm of catalyst was utilized at DP_n = 242, there was a good correlation between experimental and theoretical M_n. At the same time, M_w/M_n values were initially high (1.8 – 2.0), but diminished with monomer conversion. When the catalyst level was decreased below 5 ppm for the same DP_n = 242, the experimental M_n values were higher than theoretical values. The initiation efficiency, $I_{eff} = M_{n,th}/M_{n,exp}$, was lower than 1, indicating that only a fraction of the initiator introduced to the system was activated. As the polymerization progressed, the M_n decreased and I_{eff} increased, whereas M_w/M_n oscillated just below 2.0.

When DP_n = 1089 was targeted (Figure IV.1(b)), the effect of lowering the catalyst concentration (5 and 1 ppm CuBr) on M_n and I_{eff} was not as significant. In each case, there was poor I_{eff} at low monomer conversion, however, I_{eff} reached unity at conversion of MA = 40%. M_w/M_n decreased with monomer conversion for both catalyst concentrations. The broader MWD at 1 ppm catalyst could be attributed to insufficient concentration of deactivator present in the system. These polymerizations had linear first order kinetic plots, as shown in Figure IV.2.

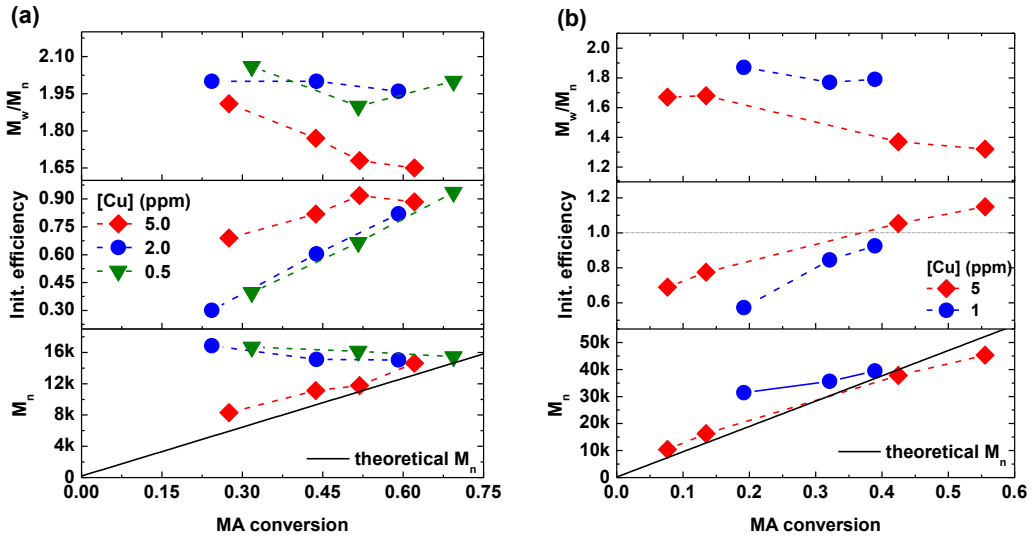

Figure IV.1. Evolution of M_n (bottom panel), I_{eff} (middle panel) and M_w/M_n (top panel) *vs.* MA conversion for ARGET ATRP of MA at 60 °C. Conditions: (a) Targeted DP_n = 242, $[MA]_0/[EBiB]_0/[CuBr]_0/[Me_6TREN]_0/[Sn^{II}(EH)_2]_0$ = 242/1/0.0012/0.1/0.1 (diamond, 5.0 ppm CuBr, T1-1), 242/1/0.00048/0.1/0.1 (circle, 2.0 ppm CuBr, T1-2), 242/1/0.00012/0.1/0.1 (down triangle, 0.5 ppm CuBr, T1-3); (b) Targeted DP_n = 1089, $[MA]_0/[EBiB]_0/[CuBr]_0/[Me_6TREN]_0/[Sn^{II}(EH)_2]_0$ = 1089/1/0.0054/0.1/0.1 (diamond, 5.0 ppm CuBr, T1-4), 1089/1/0.0011/0.1/0.1 (circle, 1.0 ppm CuBr, T1-5).

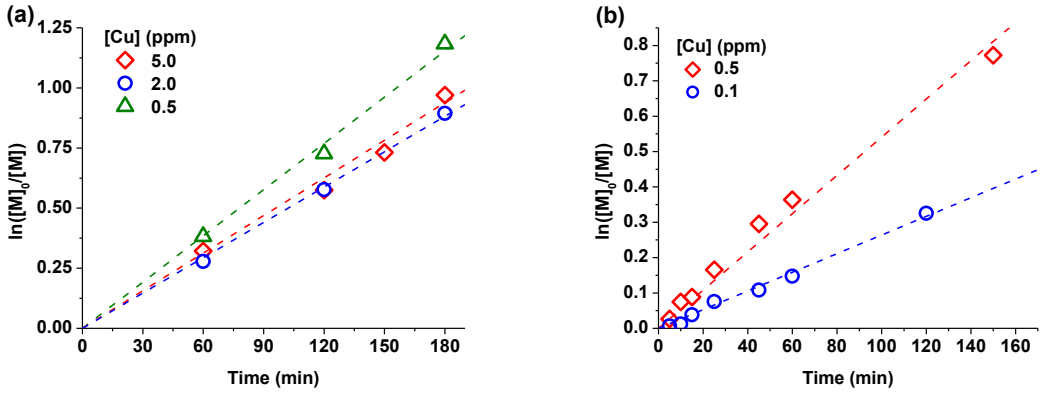

Figure IV.2. Semi-logarithmic kinetic plot for ARGET ATRP of MA at 60 °C. Conditions: (a) Targeted DP_n = 242, $[MA]_0/[EBiB]_0/[CuBr]_0/[Me_6TREN]_0/[Sn^{II}(EH)_2]_0$ = 242/1/0.0012/0.1/0.1 (diamond, 5 ppm CuBr, T1-2), 242/1/0.00048/ 0.1/0.1 (circle, 2.0 ppm CuBr, T1-3), 242/1/0.00012/0.1/0.1 (up triangle, 0.5 ppm CuBr, T1-4); (b) Targeted DP_n = 484, $[MA]_0/[EBiB]_0/[CuBr]_0/[Me_6TREN]_0/[Sn^{II}(EH)_2]_0$: 484/1/0.00024/0.1/0.1 (diamond, 0.5 ppm CuBr, T1-9), 484/1/ 0.000048/0.1/0.1 (circle, 0.1 ppm CuBr, T1-10)/ dashed lines represent linear fit.

IV.4.2. ARGET ATRP of Styrene (S)

S was polymerized under ARGET ATRP conditions catalyzed by 0.5 mol ppm of CuBr/Me_6TREN complex, relative to monomer. The reaction temperature was varied over the range of 80 - 100 °C, with 25 vol.% anisole as solvent, $Sn^{II}(EH)_2$ was employed as the reducing agent and ethyl 2-bromoisobutyrate (EBiB) as the initiator. In contrast to MA polymerizations, the molar ratio of $[Sn^{II}(EH)_2]_0/[R\text{-}X]_0$ was not constant and was varied from 0.1 to 0.3. Targeted DP_n changed in the range 355 – 400. The results are summarized in Table IV.2.

Table IV.2. Polymerization conditions and results for ARGET ATRP of S

Entry [a]	[Cu] (ppm) [b]	Targeted DP_n [c]	*T* (°C)	$[Sn^{II}(EH)]_0/[R\text{-}X]_0$	Crude samples from reaction mixture					After precip. [d]	
					t (min)	*p* (%)	$M_{n,GPC}$	M_w/M_n	I_{eff}	$M_{n,GPC}$	M_w/M_n
1	0.5	400	80	0.1	6900	52.9	22,300	1.45	0.9		
2	0.5	400	90	0.1	3090	51.8	19,700	1.67	> 1		
3	0.5	400	90	0.3	2400	53.0	23,400	1.63	0.94	24,300	1.43
4	0.5	360	100	0.3	1695	42.8	30,900	2.01	0.52	**31,600**	**1.97**
4A [e]	0.5	355	100	0.3	1410	54.5	21,100	1.57	0.96	**22,200**	**1.61**

[a] All polymerizations were carried out in 25 % (v/v) anisole with $[EBiB]_0/[Me_6TREN]_0$= 1/0.1. The entries marked in bold were used for further chain extension; [b] [Cu] expressed as a mol ppm related to monomer; [d] Characterized after precipitation from hexanes and drying under vacuum. [e] Same conditions as entry 4, but with targeted DP_n = 360 and $[Me_6TREN]_{entry4A} = 3[Me_6TREN]_{entry4}$.

Figure IV.3 shows M_n, I_{eff}, and M_w/M_n for the ARGET ATRP of S catalyzed by 0.5 ppm CuBr/Me_6TREN complex. For all experiments presented in Figure IV.3, $M_{n,GPC}$ is initially significantly larger than the theoretical values, signifying low I_{eff}. However, at 30% monomer conversion, I_{eff} increased to unity and experimental $M_{n,GPC}$ neared the predicted values. M_w/M_n values, were initially high and leveled off at 1.8 – 1.9 when conversion of styrene = 10 to 30%, and gradually decreased after $I_{eff} \approx 1$ at conversion of styrene > 30%. The most dynamic changes in M_w/M_n were for the sample polymerized at the lowest temperature (80 °C) with low concentrations of reducing agent. Semi-logarithmic kinetic plots for S polymerization with 0.5 ppm CuBr at different temperatures and various quantities of $Sn^{II}(EH)_2$ are linear. Although M_w/M_n decreased with styrene conversion and the values were moderate in comparison to the other samples, they were higher than those obtained in a well-controlled ARGET ATRP process, which may be attributed to very low catalyst concentrations.

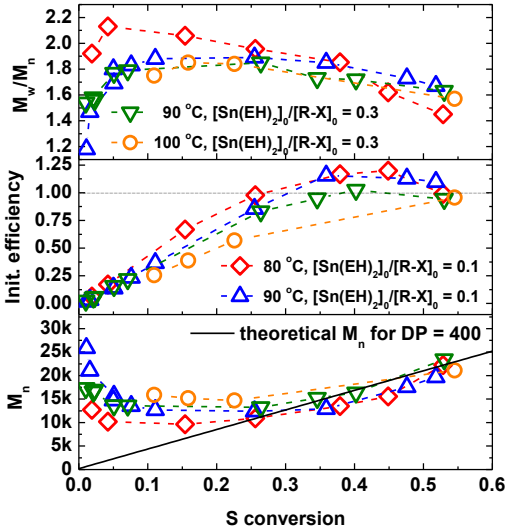

Figure IV.3. Evolution of M_n (bottom panel), I_{eff} (middle panel) and M_w/M_n (top panel) *vs.* S conversion (theoretical M_n for quantitative initiation DP_n = 400 (black solid line in bottom panel)). Conditions: $[S]_0/[EBiB]_0/[CuBr]_0/[Me_6TREN]_0/[Sn^{II}(EH)_2]_0$ = 400/1/0.0002/0.1/0.1 at 80 °C (diamond, T4-1), 400/1/0.0002/0.1/0.1 at 90 °C (up triangle, T4-2), 400/1/0.0002/0.1/0.3 at 90 °C (down triangle, T4-3), 355/1/0.00018/0.1/0.3 at 100 °C (circle, T4-4A).

IV.4.3. Chain extension to form diblock copolymers from broad dispersity macroinitiators

It was demonstrated in the previous sections that homopolymers with controlled, yet relatively high dispersity could be prepared *via* ARGET ATRP in the presence of low level of copper catalysts (< 5 ppm). The livingness of the formed polymers was studied through a chain extension process, which also offered access to block copolymers with controlled MWDs in each of the two blocks. Some of the obtained poly(methyl acrylates)

(PMA_B) and polystyrenes (PS_B) homopolymers with broad MWDs were utilized as macroinitiators in chain extension processes to form broad-narrow or broad-broad diblock copolymers (DBC_{BN} or DBC_{BB}, resp.). Such copolymers might undergo phase separation process forming structures of uncommon morphologies stabilized by the high M_w/M_n.[25,34]

The majority of the chain extension polymerizations were carried out under ARGET ATRP conditions with 50 – 100 ppm of copper with respect to the monomer. This catalyst concentration ensured well controlled processes, so the extended block was of low dispersity. Usually, the targeted DP_n was high but the reactions were quenched at low monomer conversion to avoid termination process. The results for chain extension of PMA_B (entries 1 – 4) and PS_B (entries 5 – 7) are shown in Table IV.3. The entries are labeled to indicate the specific macroinitiator utilized, defined as broad or narrow, followed by the chain extended polymer, defined as broad or narrow, and the M_w/M_n value of the final copolymer. For example, $(PMA1_B\text{-}PS_N)_{1.12}$ corresponds to PMA macroinitiator, entry 1, which was chain extended with a well-defined PS, whose final M_w/M_n = 1.12.

Table IV.3. Results of broad-narrow MWD block copolymers obtained by ARGET ATRP.

Entry [a)]	Macroinitiator – first block				Copolymer		Extended Block			Homopol.
	Source	M_n [b)]	M_w/M_n [b)]	wt.% [c]	M_n [b)]	M_w/M_n [b)]	M_n [d)]	M_w/M_n [e)]	wt.% [c)]	content wt% [f)]
	PMA							PS		
$(PMA1_B\text{-}PS_N)_{1.12}$	T1-1	11,800	1.68	27	55,900	1.12	44,100	1.13	73	0
$(PMA2_B\text{-}PS_N)_{1.20}$	T1-2	20,900	1.71	35	46,500	1.20	25,600	1.27	65	12
$(PMA5_B\text{-}PS_B)_{1.50}$	T1-5	42,200	1.74	75	49,300	1.50	7,100	2.34	25	20
$(PMA5_B\text{-}PS_B)_{1.31}$	T3-3	49,300	1.50	41	96,400	1.31	54,200	1.53	59	0
	PS							PMA		
$(PS4_B\text{-}PMA_B)_{1.43}$	T2-4	31,600	1.97	57	46,600	1.43	15,000	1.62	43	10
$(PS4_B\text{-}PMA_B)_{1.58}$	T2-4	31,600	1.97	63	43,100	1.58	11,500	2.42	37	40
$(PS4A_B\text{-}PMA_N)_{1.17}$	T2-4A	22,200	1.61	30	63,600	1.17	41,400	1.23	70	-

[a)] Copolymers obtained by chain extension polymerization started from appropriate macroinitiator (source, e.g. T1-1 stands for Table IV.1, entry 1); conditions for each process are listed in Experimental section; [b)] from GPC (THF); [c)] from ^{1}H NMR; [d)] calculated by deduction M_n of macroinitiator from M_n of copolymer; [e)] calculated based on Fukuda's equation (11); [f)] Determined by LCCC as fraction of macroinitiator in copolymer sample.

Gel permeation chromatography (GPC) measurements were performed to acquire M_n and M_w/M_n values of the copolymers and calculate values for the extended block. Through the deduction of $M_{n,\text{macroinitiator}}$ from $M_{n,\text{DBC}}$, $M_{n,\text{extended block}}$ was determined. M_w/M_n was determined using Fukuda's equation (IV.3) where ω_A and ω_B are the weight fraction of block A and block B, respectively.[35,36] The weight fraction of each block was estimated based on ^{1}H NMR spectrometry.

$$[\frac{M_w}{M_n}]_{AB} = \omega_A^2([\frac{M_w}{M_n}]_A - 1) + \omega_B^2([\frac{M_w}{M_n}]_B - 1) + 1 \quad \text{(IV.3)}$$

The first series of chain extensions was based on the polymerization of S from PMA. Table VI.3, entry 1 ($(PMA1_B\text{-}PS_N)_{1.12}$) outlines the use of PMA macroinitiator with M_n = 11 800 and M_w/M_n = 1.68, from which S was polymerized. The overall dispersity decreased significantly during the chain extension reaching a final value of 1.12. Equation (VI.3) determined the M_w/M_n of the extended block to be 1.13. The GPC traces reproduced in Figure IV.4(a), top panel, show that the MWD narrowed and cleanly shifted towards higher MW. One can assume from the GPC traces that there were very little 'dead' PMA chains, meaning no inactive end groups, in the macroinitiator. The successful extension of all chains was confirmed by liquid chromatography under critical conditions (LCCC) (Figure IV.4(b), top panel, dashed line), as no PMA homopolymer was detected. LCCC is based on selecting an appropriate composition of mobile phase, that separates macromolecules depending on chemical composition (polarity) but not molecular weight of the polymer for which the critical conditions (mobile phase) are set.

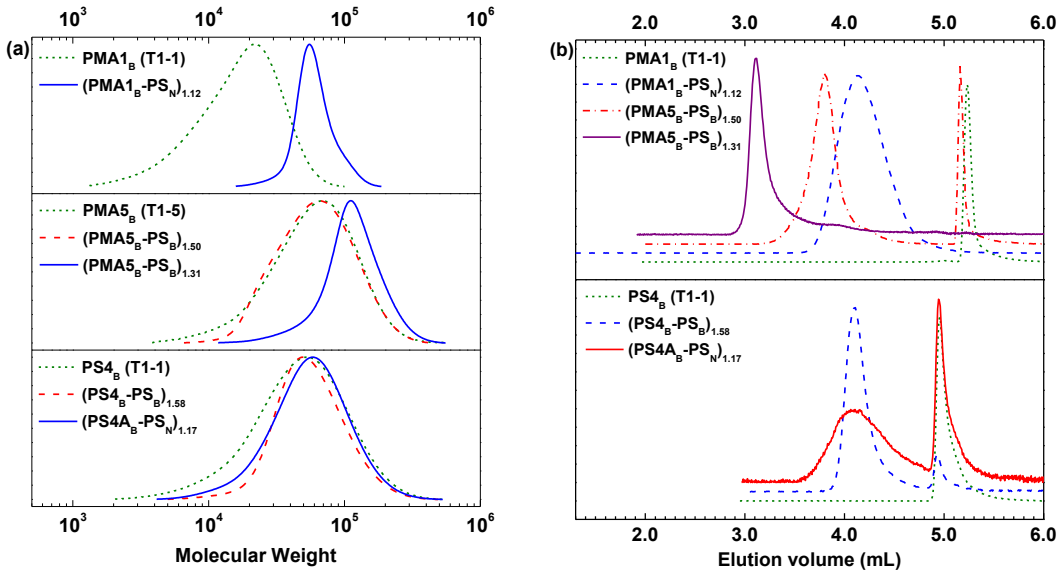

Figure IV.4. (a) GPC traces for chain extension processes of PMA macroinitiators with S (top and middle panels) and PS macroinitiator with MA (bottom panel); (b) LCCC traces of PMA macroinitiators (dotted line) and the products of their chain extension with S (top panel) and PS macroinitiator (dotted line) and the products of its chain extension with MA (bottom panel). Conditions (legends direct to appropriate tables and entries); $(PMA1_B\text{-}PS_N)_{1.12}$, $[T1\text{-}1]_0/[S]_0/[CuBr]_0/[Me_6TREN]_0/[Sn^{II}(EH)_2]_0 = 1/590/0.0295/0.5/0.5$; $(PMA5_B\text{-}PS_B)_{1.50}$, $[T1\text{-}5]_0/[S]_0/[CuBr]_0/[Me_6TREN]_0/[Sn^{II}(EH)_2]_0 = 1/337/0.0337/0.5/0.5$; $(PMA5_B\text{-}PS_B)_{1.31}$, $[T3\text{-}3]_0/[S]_0/[CuBr]_0/[Me_6TREN]_0/[Sn^{II}(EH)_2]_0 = 1/1144/0.114/0.5/0.5$; $(PS4_B\text{-}PS_B)_{1.43}$, $[T2\text{-}4]_0/[MA]_0/[CuBr]_0/[Me_6TREN]_0/[Sn^{II}(EH)_2]_0 = 1/393/0.0393/0.3/0.3$; $(PS4_B\text{-}PS_B)_{1.58}$, $[T2\text{-}4]_0/[MA]_0/[CuBr]_0/[Me_6TREN]_0/[Sn^{II}(EH)_2]_0 = 1/393/0.00196/0.3/0.3$.

$(PMA2_B\text{-}PS_N)_{1.20}$ and $(PMA5_B\text{-}PS_B)_{1.50}$ showed incomplete chain extension. LCCC confirmed there was residual macroinitiator remaining in the block copolymers (e.g., top panel, dashed-dotted red line, PMA peak at elution volume 5.1-5.3 mL). There are two possible reasons for this observation: either incomplete initiation or the presence of 'dead'

PMA chains. The chain extended sample, $(PMA5_B\text{-}PS_B)_{1.50}$, was employed for a sequential chain extension with S, $(PMA5_B\text{-}PS_B)_{1.31}$, to identify the nature of the residual PMA. The resulting chain extended copolymer contained a minority of PMA_B block and LCCC did not show any PMA homopolymer present. The GPC trace (Figure IV.4(a), middle panel solid line), shifted significantly, contrary to the first chain extension, $(PMA5_B\text{-}PS_B)_{1.50}$. This experiment proved that the initial PMA_B macroinitiators were almost fully end-functionalized, although they were generated in the presence of only 1 or 5 ppm of catalyst, providing poor control over M_n and M_w/M_n.

The presence of unextended PMA_B macroinitiator in the initial chain extension was due to the broad MWD in sample T1-5 and reduced accessibility of the transferable atom in the higher molar mass macromolecules. From the ^1H NMR and LCCC results, it can be estimated that 55 wt.% of PMA_B was chain extended to $(PMA5_B\text{-}PS_B)_{1.50}$. In the second chain extension reaction, $(PMA5_B\text{-}PS_B)_{1.31}$, the probability of chain extension was enhanced by targeting a much higher polymerization degree in the second chain extension reaction.

The second series of diblock copolymers examined were generated by MA chain extension from PS_B macroinitiators, Table VI.3, entries 5 – 7. The chain extensions $(PS4_B\text{-}PMA_B)_{1.43}$ and $(PS4_B\text{-}PMA_B)_{1.58}$ were started from the same macroinitiator, with moderate M_n = 31,600 and high M_w/M_n =1.97, and catalyzed with 100 and 5 ppm of copper, respectively. The higher concentration of copper resulted in a well controlled polymerization while the lower concentration provided less control. DBCs with a majority of PS and similar M_n were obtained; however, the M_w/M_n in second block differed (Figure IV.4(a), bottom panel). (PS_B-*b*-PMA_N) was characterized by M_w/M_n = 1.43 and a M_w/M_n

$_{PMA}$ = 1.62, whereas (PS_B-*b*-PMA_B) displayed a M_w/M_n of 1.58 and $M_w/M_{n\ PMA}$ = 2.42. Both samples contained unreacted PS_B homopolymer amounting to 10% and 40%, (Figure IV.4(b), bottom panel). This phenomenon is likely attributable to the same reason as in PMA_D extension, e.g. $(PMA5_B\text{-}PS_B)_{1.50}$. The final copolymer, $(PS4A_B\text{-}PS_N)_{1.17}$, exhibited M_n of 63600 and a low value of M_w/M_n = 1.17; the majority of the copolymer was comprised of PMA_N. The M_w/M_n vs. M_n plot, which represents all broad dispersity homopolymers with preserved chain-end functionalities described in this chapter and their resulting block copolymers, is given in Figure IV.5.

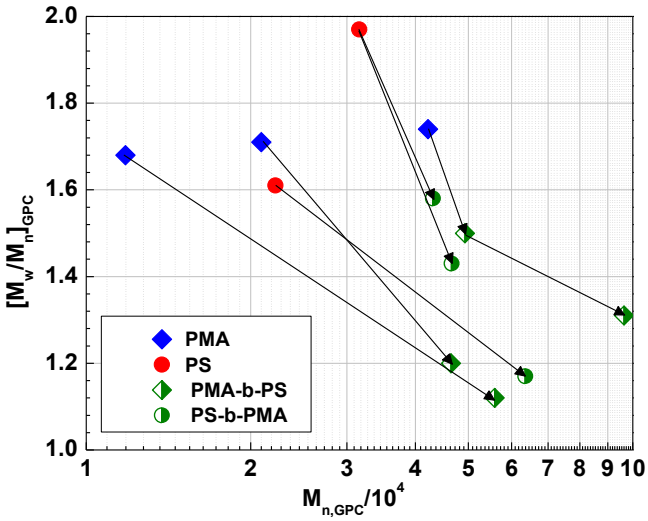

Figure IV.5. The M_w/M_n *vs.* M_n map of all homopolymers utilized for block copolymer synthesis.

IV.5. Conclusions

ARGET ATRP methodology with varied copper catalyst concentrations permits the synthesis of methyl acrylate and styrene homopolymers with controlled dispersity under

ARGET ATRP conditions. PMA and PS with tunable M_w/M_n values ranging from 1.32 – 2.0 were synthesized, with preserved chain end functionalities. The dispersity was tuned by adjusting the concentration of a copper based catalyst complex, targeting different degrees of polymerization at different reaction temperatures. Several trends were identified: (a) all polymerizations studied provided linear first order kinetics with respect to monomer, (b) M_w/M_n values typically decreased as monomer conversion increased, (c) low initiation efficiency resulted in experimental M_n values larger than predicted at low monomer conversions, (d) initiation efficiency typically increased toward unity with increasing monomer conversion.

The nature of ARGET ATRP affords low termination rates as a limited number of active species are present at any given time, allowing for high chain end functionality. Regardless of their dispersity, the synthesized homopolymers retained this functionality through successful chain extensions to form block copolymers. A series of diblock broad-narrow and broad-broad copolymers were prepared, which were characterized by ^{1}H NMR, GPC and LCCC. The latter analysis established that chain extension efficiency depends on targeting a high degree of polymerization for the second (extended) block, but does not depend upon catalyst concentration used for macroinitiator synthesis. The obtained block copolymers may exhibit unusual morphological features due to the controlled increase of M_w/M_n in one block as previously reported.

IV.6. Acknowledgements

I would like to thank Dr. Mingjiang Zhong and Dr. Andrzej Plitcha, for their synthetic work as well as Dr. Wenwen Li for her characterization of materials with LCCC.

Additionally, Mingjiang was extremely helpful during the publication process as he often improved figures and gave thoughtful insight to the organization of the manuscript.

IV.7. References

1. Szwarc, M. *Nature* **1956,** *178*, 1168-1169.
2. Szwarc, M.; Levy, M.; Milkovich, R. *Journal of the American Chemical Society* **1956,** *78*, 2656-2657.
3. Bates, F. S.; Fredrickson, G. H. *Annual Review of Physical Chemistry* **1990,** *41*, 525-557.
4. Matyjaszewski, K.; Gnanou, Y.; Leibler, L., Eds. *Macromolecular Engineering: From Precise Macromolecular Synthesis to macroscopic Materials Properties and Applications*; Wiley-VCH: Weinheim, 2007.
5. Morick, J.; Buback, M.; Matyjaszewski, K. *Macromolecular Chemistry and Physics* **2011,** *212*, 2423-2428.
6. Seeliger, F.; Matyjaszewski, K. *Macromolecules* **2009,** *42*, 6050-6055.
7. Braunecker, W. A.; Matyjaszewski, K. *Progress in Polymer Science* **2007,** *32*, 93-146.
8. Zhong, M. J.; Matyjaszewski, K. *Macromolecules* **2011,** *44*, 2668-2677.
9. Tang, W.; Tsarevsky, N. V.; Matyjaszewski, K. *Journal of the American Chemical Society* **2006,** *128*, 1598-1604.
10. Jakubowski, W.; Matyjaszewski, K. *Angewandte Chemie-International Edition* **2006,** *45*, 4482-4486.

11. Magenau, A. J. D.; Kwak, Y.; Matyjaszewski, K. *Macromolecules* **2010,** *43*, 9682-9689.

12. Percec, V.; Guliashvili, T.; Ladislaw, J. S.; Wistrand, A.; Stjerndahl, A.; Sienkowska, M. J.; Monteiro, M. J.; Sahoo, S. *J. Am. Chem. Soc.* **2006,** *128*, 14156-14165.

13. Matyjaszewski, K.; Tsarevsky, N. V.; Braunecker, W. A.; Dong, H.; Huang, J.; Jakubowski, W.; Kwak, Y.; Nicolay, R.; Tang, W.; Yoon, J. A. *Macromolecules (Washington, DC, United States)* **2007,** *40*, 7795-7806.

14. Matyjaszewski, K.; Coca, S.; Gaynor, S. G.; Wei, M.; Woodworth, B. E. *Macromolecules* **1997,** *30*, 7348-7350.

15. Matyjaszewski, K.; Jakubowski, W.; Min, K.; Tang, W.; Huang, J. Y.; Braunecker, W. A.; Tsarevsky, N. V. *Proceedings of the National Academy of Sciences of the United States of America* **2006,** *103*, 15309-15314.

16. Magenau, A. J. D.; Strandwitz, N. C.; Gennaro, A.; Matyjaszewski, K. *Science* **2011,** *332*, 81-84.

17. Jakubowski, W.; Matyjaszewski, K. *Macromolecules* **2005,** *38*, 4139-4146.

18. Xia, J. H.; Matyjaszewski, K. *Macromolecules* **1999,** *32*, 2434-2437.

19. Xia, J. H.; Gaynor, S. G.; Matyjaszewski, K. *Macromolecules* **1998,** *31*, 5958-5959.

20. Leibler, L.; Benoit, H. *Polymer* **1981,** *22*, 195-201.

21. Listak, J.; Jia, X.; Plichta, A.; Zhong, M.; Matyjaszewski, K.; Bockstaller, M. R. *Journal of Polymer Science Part B-Polymer Physics* **2012,** *50*, 106-116.

22. Cooke, D. M.; Shi, A.-C. *Macromolecules* **2006,** *39*, 6661-6671.

23. Matsen, M. W. *Physical Review Letters* **2007,** *99*, 148304.

24. Sides, S. W.; Fredrickson, G. H. *Journal of Chemical Physics* **2004,** *121*, 4974-4986.

25. Listak, J.; Jakubowski, W.; Mueller, L.; Plichta, A.; Matyjaszewski, K.; Bockstaller, M. R. *Macromolecules* **2008,** *41*, 5919-5927.

26. Lynd, N. A.; Meuler, A. J.; Hillmyer, M. A. *Progress in Polymer Science* **2008,** *33*, 875-893.

27. Hustad, P. D.; Marchand, G. R.; Garcia-Meitin, E. I.; Roberts, P. L.; Weinhold, J. D. *Macromolecules* **2009,** *42*, 3788-3794.

28. Hillmyer, M. A. *Journal of Polymer Science Part B: Polymer Physics* **2007,** *45*, 3249-3251.

29. Lynd, N. A.; Hillmyer, M. A. *Macromolecules* **2005,** *38*, 8803-8810.

30. Lynd, N. A.; Hillmyer, M. A. *Macromolecules* **2007,** *40*, 8050-8055.

31. Noro, A.; Iinuma, M.; Suzuki, J.; Takano, A.; Matsushita, Y. *Macromolecules* **2004,** *37*, 3804-3808.

32. Min, K.; Gao, H. F.; Matyjaszewski, K. *Journal of the American Chemical Society* **2005,** *127*, 3825-3830.

33. Gao, H.; Min, K.; Matyjaszewski, K. *Macromolecular Chemistry and Physics* **2006,** *207*, 1709-1717.

34. Matyjaszewski, K. *Isr. J. Chem.* **2012,** *52*, 206-220.

35. Fukuda, T. *Journal of Polymer Science Part A: Polymer Chemistry* **2004,** *42*, 4743-4755.

36. Almdal, K. In *Developments in Block Copolymer Science and Technology*; John Wiley & Sons, Ltd, 2004; pp. 31-69.

CHAPTER V

EXPLORING QUALITY IN GRADIENT COPOLYMERS*

V.1. Preface

In Chapter IV it was demonstrated that reducing the catalyst concentration to extreme levels (< 5 ppm) under ARGET ATRP conditions results in polymers with symmetrically broad molecular weight distributions. Additionally, the increase of dispersity was accomplished without disrupting the chain end functionality, allowing for chain extension to block copolymers. It was the purpose of this chapter was to expand this study of molecular weight distribution to gradient copolymers, specifically, to determine the effects of molecular weight distribution on the quality of gradient copolymers.

Gradient copolymers are an important class of materials due to their unique properties including special interfacial phase behaviors, increased critical micelle

*Work in this chapter has been published in the following manuscript: Elsen, A. M.; Li, Y.; Li, Q.; Sheiko, S. S.; Matyjaszewski, K. "Exploring Quality in Gradient Copolymers" *Macromolecular Rapid Communications* **2014,** *35*, 133-140**.**

concentrations, reeling-in micelle effects, and broadened glass transition temperatures (T_g). These rare properties suggested the use of gradient copolymers as polymer blend compatibilizers, additives for sound and vibration dampening, and stabilizers for emulsions.

ARGET ATRP was employed with decreasing levels of catalyst concentrations to generate copolymers with increasing M_w/M_n values. The copolymers were transformed into molecular bottlebrushes to enable visualization and analysis of individual molecules by AFM. Quality of gradient copolymers was evaluated utilizing AFM through the correlation of average height profiles with instantaneous compositions, determined by ^{1}H NMR, as well as the deviation of individual brushes from this average value.

These results established MWD values as an excellent trait to assess quality within gradient copolymers, an important knowledge for the research presented in the following chapter. Chapter VI details the synthesis of gradient copolymers, in addition to random and block copolymers, to be utilized as copolymeric surfactants. Understanding that MWD is an assessment of the gradient architecture quality allowed us to synthesize well-defined gradient copolymers.

For the work in this chapter, I conducted all synthetic experiments including the synthesis of gradient backbones, macroinitiators and molecular bottlebrushes. AFM characterization of the molecular bottlebrushes was accomplished by my collaborators at UNC Chapel Hill: Yuanchao Li, Qiaoxi Li and Prof. Sergei S. Sheiko.

V.2. Introduction

Gradient copolymers have received increasing attention due to their ability to achieve properties which are unavailable by homopolymers and traditional copolymers.[1,2] Unlike block copolymers, which comprise an instantaneous switch between monomer units, gradient copolymers have a continuous compositional drift from one chain end to the other.[3] Resulting from this unique architecture based on copolymer composition, gradient copolymers may exhibit special interfacial phase behaviors, increased critical micelle concentrations, reeling-in micelle effects, and broadened glass transition temperatures (T_g).[4-13] The degree to which these properties occur may be tuned by the specific composition of monomers and gradient quality. These rare properties suggested the use of gradient copolymers as polymer blend compatibilizers, additives for sound and vibration dampening, and stabilizers for emulsions.[6,14]

Two main methods exist to synthesize gradient copolymers via controlled/living polymerization: spontaneous and forced methods.[1] The spontaneous gradient, or batch method, takes advantage of differences in reactivity ratios (r_1 *and* r_2) between monomers to spontaneously generate a smooth change in monomer composition along the polymer chain. The reactivity ratios can be used to estimate the severity/quality of the gradient or the composition of the polymer chains. On the other hand, forced gradient may utilize monomers with similar reactivity ratios but requires a continuous feeding of one monomer into a solution of a second monomer throughout the polymerization.

Requirements for the synthesis of precise gradient copolymers include fast initiation, uniform chain growth and facile cross-propagation. Such requirements allow all polymer chains to initiate at once while propagating at the same pace, allowing a consistent gradient composition among all chains. Atom transfer radical polymerization (ATRP) is an excellent candidate for synthesizing gradient copolymers due to its controlled/living nature and has proven to successfully synthesize a variety of such copolymers.[1,15-17]

The uniformity of polymer chains, i.e. MWD, depends on the dynamics of exchange between active and dormant species and more precisely on the ratio of rates of deactivation and propagation. This can be relatively easily controlled by concentration of the deactivating species. Activators regenerated by electron transfer (ARGET) ATRP[18-20] is capable of tuning the molecular weight distributions of synthesized polymers by the catalyst concentration. [21,22]

Recently reported computational studies indicated that copolymers with large final M_w/M_n values are characterized by poor gradient quality;[23] it was the goal of this work to examine this correlation between M_w/M_n values and gradient quality experimentally. Synthesis of methacrylate/acrylate gradient copolymers was carried out by batch copolymerization under ARGET ATRP conditions in the presence of systematically decreasing catalyst concentrations ($Cu^{II}X_2$/L) resulting in decreasing quality of molecular weight distribution. The gradient copolymers were then used as backbone macroinitiators to synthesize molecular bottlebrushes with gradient grafting density of the side chains. Taking advantage of molecular imaging with atomic force microscopy (AFM), the average instantaneous composition was characterized through profiling of brush height. The

uniformity, or quality, of gradient within the brushes was characterized through deviation of each brush from the average height profile.

V.3. Experimental

V.3.1. Materials

2-(Trimethylsilyl-oxy)ethyl methacrylate (HEMA-TMS, 99%, Scientific Polymer) and *n*-butyl acrylate (nBA, 99%, Aldrich) were passed through a basic alumina column prior to use. Tetrahydrofuran (THF, 99.9%, Fisher Scientific) was distilled under N_2 prior to use. Acetonitrile (MeCN, 99.5%, Aldrich), anisole (99%, Aldrich), 2-bromoisobutyryl bromide (BiB, 98%, Aldrich), copper(I) bromide (CuBr, 99.99%, Aldrich), copper(II) bromide ($CuBr_2$, 99.999%, Aldrich), chloroform ($CHCl_3$, 99.9%, Fisher Scientific), 4,4′-dinonyl-2,2′-dipyridyl (dNbpy, 97%, Aldrich), 2-ethyl bromoisobutyrate (EBiB, 98%, Aldrich), hexanes (99.5%, Pharmco Aaper) methanol (MeOH, 99.8%, Pharmco Aaper), *N,N,N',N'',N*''-pentamethyldiethylenetriamine (PMDETA, 99%, Aldrich), potassium fluoride (KF, 99%, Aldrich), tetrabutylammonium fluoride in THF (1M) (TBAF, 95%, Aldrich), tin(II) ethylhexanoate ($Sn^{II}(EH)_2$, 99%, Aldrich), were all used as received.

V.3.2. Synthetic procedures

V.3.2.1. Synthesis of gradient copolymer backbone

An example ARGET ATRP procedure formulated with 500 ppm of $CuBr_2$/PMEDTA catalyst and targeted DP = 300 for both monomers is given as follows;

see Table V.1 for specific reaction conditions. A 10 mL Schlenk flask equipped with a stir bar was evacuated and back-filled with N_2 six times. A solution of $CuBr_2$ (0.15 mL of 20 mg/mL solution in acetonitrile, 14 μmol), PMDETA (0.18 mL of 20 mg/mL solution in anisole, 21 μmol), and anisole (5.0 mL) was bubbled under N_2 for 20 min. A second solution of *n*BA (2 mL, 13.9 mmol), HEMA-TMS (3 mL,13.9 mmol), and EBiB (0.12 mL of 76.9 mg/mL solution in anisole, 47 μmol) was also bubbled under N_2 for 20 min. Each solution was transferred to the flask under nitrogen atmosphere. Finally, a degassed solution of $Sn^{II}(EH)_2$ (1.1 mL of 10 mg/mL solution in anisole; 28 μmol) was added to the flask to start the polymerization. The flask was placed in a 80 °C oil bath. Samples were taken periodically to measure conversion via ^1H NMR and number average molecular weights via GPC. The polymerization was stopped by exposure to air and the final reaction mixture was flushed through a neutral alumina column to remove any residual copper.

V.3.2.2. Functionalization to gradient macroinitiator

An example of macroinitiator functionalization procedure formulated with PHEMA-TMS-*grad*-PBA_{500} is given as follows. A 250 mL round bottomed flask equipped with a stir bar was charged with PHEMA-TMS-*grad*-PBA_{500} (2.11 g, 10.4 mmol), KF (730 mg, 12.6 mmol). The flask was purged with N_2 for 1 h. Dry THF (20 mL) was added to the flask followed by the dropwise addition of TBAF (31 mg, 90 mmol). When the polymer was dissolved, the flask was placed in an ice bath. Over a period of 15 min., BiB (1.9 mL, 15.6 mmol) was added. The reaction mixture was allowed to stir overnight, naturally coming to room temperature. The functionalized polymer was precipitated into methanol/water (80:20). The precipitated polymer was dissolved in 100 mL of chloroform

and passed through a column of basic alumina. Remaining chloroform was removed via rotary evaporator. The polymer was dissolved in THF required and precipitated three times from methanol and three times from hexanes. The final polymer, PBIBEM-*grad*-PBA_{500} was dried under vacuum for 24 h. ^1H NMR was used to confirm full functionalization occurred.[16]

V.3.2.3. Synthesis of gradient brushes

An example ATRP procedure formulated with PBIBEM-*grad*-PBA_{500} is given as follows; see Table V.1 for specific reaction conditions. A 25 mL Schlenk flask was charged with *n*-BA (20 mL, 140 mmol), PBIBEM-*grad*-PBA_{500} (28 mg, 0.10 mmol), PMDETA (8.7 mg, 50 μmol), $CuBr_2$ (0.11 mL of 10 mg/mL solution in acetonitrile, 5 μmol), anisole (2.2 mL) and a stir bar. The reaction mixture was degassed by at least three freeze-pump-thaw cycles and filled with nitrogen again. With positive pressure of N_2, CuBr (6.4 mg, 45 μmol) was added to the 25 mL Schlenk flask. The flask was evacuated and refilled with nitrogen at least 6 times. The Schlenk flask was placed in a 50 °C oil bath. Samples were taken periodically to measure conversion via ^1H NMR and number average molecular weights via GPC. The polymerization was stopped by exposure to air and the final polymer, PBIBEM(-*graft*-PBA)-*grad*-PBA500 was precipitated into cold methanol.

V.3.3. Analyses

Molecular weight and molecular weight distributions of the formed polymers were measured by gel permeation chromatography (GPC) using Polymer Standards Services

(PSS) columns (guard, 10^5, 10^3, and 10^2 Å), with THF eluent at 35 °C, flow rate 1.00 mL/min, and differential refractive index (RI) detector (Waters, 2410). Diphenyl ether was used as the internal standard to correct for any fluctuation of the THF flow rate. The number-average molecular weights (M_n) and dispersity index (M_w/M_n) were determined with a calibration based on linear polystyrene standards using WinGPC 6.0 software from PSS. ^{1}H NMR spectra were recorded in $CDCl_3$ as a solvent using Bruker 300 MHz spectrometer. Samples for AFM measurements were prepared by spin casting from dilute solutions onto freshly cleaved mica substrates. Imaging of individual molecules was conducted using a multimode AFM with NanoScope V controller (Bruker) in PeakForce QNM mode. Silicon probes with a resonance frequency of 50-90 kHz and a spring constant of ~0.4 N/m were used. The analysis of length and height distributions was performed using a custom software program developed in-house.

V.4. Results and discussion

V.4.1. Copolymer synthesis

As detailed in Table V.1, three copolymers of HEMA-TMS and *n*BA were synthesized via the spontaneous method with increasing values of MWD (c.a. 1.24, 1.4, and 1.65) by introducing different concentrations of catalyst (c.a. 500, 50, and 25 ppm) comprised of $CuBr_2$ and PMDETA into the polymerization set-up. All polymerizations were carried out in 50% anisole at 80 °C with a targeted degree of polymerization (DP) = 300 for both monomers while utilizing $Sn^{II}(EH)_2$ as the reducing agent. The resulting polymers are identified by the following notation: PHEMA-TMS-*grad*-PBA_{500}, where the subscript number represents the ppm amount of catalyst used during polymerization.

Table V.1. Synthesis and characterization of gradient copolymers, PHEMA-TMS-*grad*-$PBA_{500,\ 50,\ or\ 25}$ and resulting gradient bottlebrushes, P(BiBEM-*graft*-BA)-*grad*-$PBA_{500,\ 50\ or\ 25}$.

	PHEMA-TMS -*grad*-PBA_X [a]					P(BiBEM-*graft*-BA)-*grad*-PBA_X [d]		
X ppm	**$CuBr_2$**	**Conv[b]**	**Conv[c]**	**$M_{n,GPC}$**	**M_w/M_n**	**$M_{n,GPC}$**	**M_w/M_n[e]**	**DP_{SC}[f]**
500	0.3	0.92	0.68	70 100	1.24	230 000 [g]	1.37	30
50	0.03	0.95	0.75	80 300	1.40	113 900	1.50	23
25	0.015	0.94	0.71	66 600	1.65	196 700	2.13	14

[a] All polymerizations were conducted in 50% (v/v) anisole at 80 °C with [*n*BA]:[HEMA-TMS]:[EBiB]:[$CuBr_2$]:[PMDETA]:[$Sn^{II}(EH)_2$] = 300:300:1:Y:(1.5Y):0.6. [b] Conversion of HEMA-TMS determined by ^{1}H NMR. [c] Conversion of *n*BA determined by ^{1}H NMR. [d] All polymerizations were conducted with [*n*BA]:[PBIBEM]:[dNbpy]:[CuBr]:[$CuBr_2$] = 1400:1:1:0.475:0.025, T = 70 °C unless otherwise noted; [e] determined by GPC; [f] determined by ^{1}H NMR; [g] [*n*BA]:[PBIBEM]:[PMDETA]:[CuBr]:[$CuBr_2$] = 1400:1:0.5:0.45:0.05, T = 50 °C.

Each polymerization demonstrated linear first-order kinetics for both monomers; HEMA-TMS has the larger reactivity ratio ($r_{HEMA\text{-}TMS}$ = 1.9) as compared to *n*BA (r_{nBA} = 0.35),[16] which resulted in a faster rate of polymerization for HEMA-TMS. Evolution of number average molecular weight ($M_{n,exp}$) values with monomer conversion correlated well with theoretical values ($M_{n,th}$) only for the polymerization which employed the highest amount of catalyst: PHEMA-TMS-*grad*-PBA_{500}. The polymerizations carried out with 50 and 25 ppm of catalyst initially had experimental M_n values larger than theoretical values and significantly so in the case of 25 ppm (Figure V.1a-c). This limited control, as further

indicated by increased M_w/M_n values, (ca. 1.24, 1.40 and 1.65 for 500, 50, and 25 ppm, respectively) with decreasing quantities of catalyst present, was expected and desired.

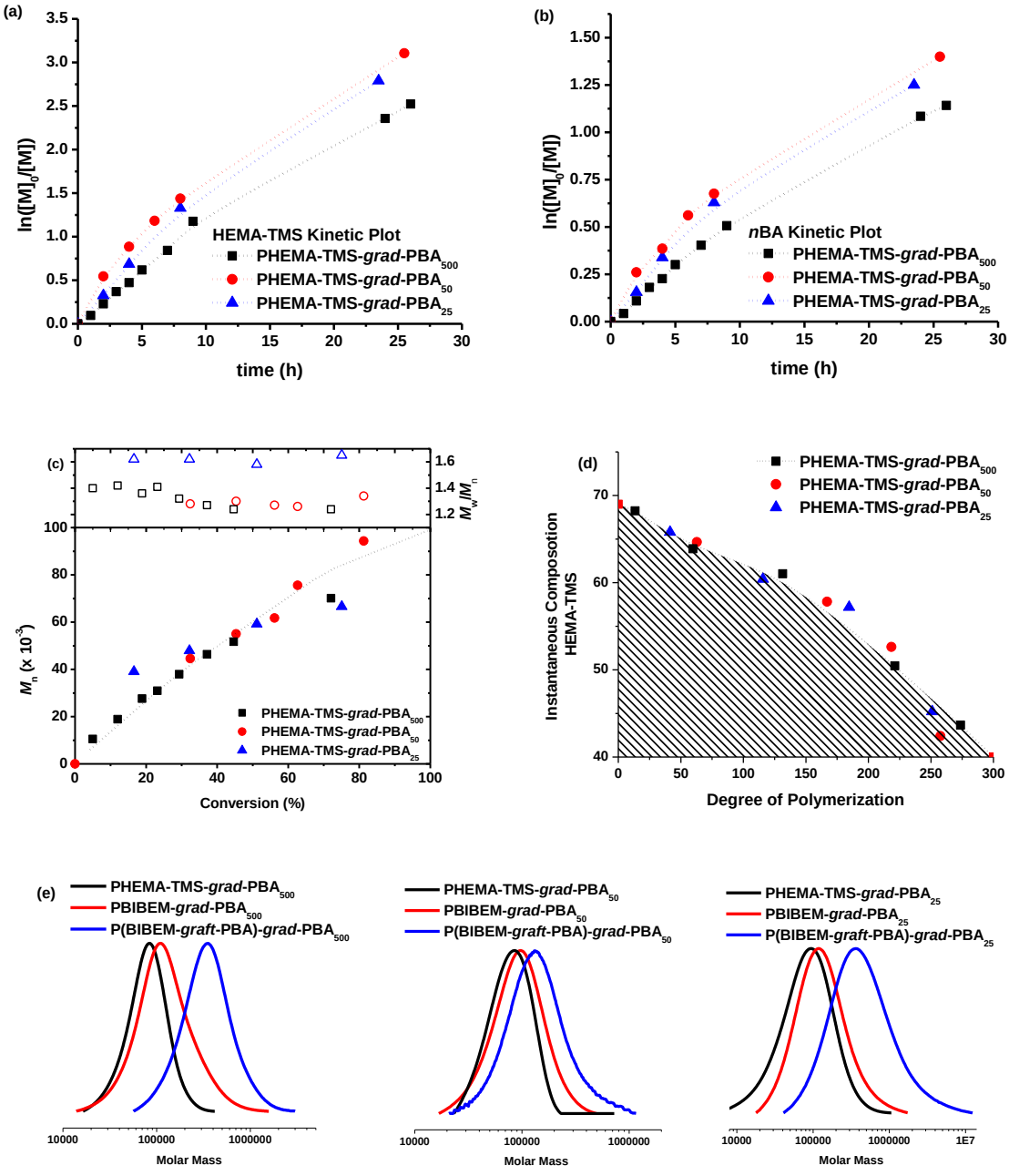

Figure V.1. First-order kinetic plot of (a) HEMA-TMS, (b) *n*BA, (c) evolution of molecular weight with conversion, (d) instantaneous composition of HEMA-TMS for all

PHEMA-TMS-*grad*-PBA_X copolymers where X = 500, 50, or 25 and (e) GPC traces showing evolution of molecular weight with molecular brush synthesis.

The instantaneous composition (IC) of the copolymers was calculated from the monomer conversion using the equation $IC_{HEMA\text{-}TMS} = \Delta_{HEMA\text{-}TMS}/(\Delta_{HEMA\text{-}TMS} + \Delta_{BA})$, where Δ is the change in conversion since the previous sample. While the three copolymers exhibit similar overall instantaneous compositions as displayed in Figure V.1d, it is important to remember that this was an average value for all chains, not a specific chain in particular. Therefore, other methods were required to characterize the true quality of individual gradient copolymers. While the Kerr effect has proven to be an effective characterization of gradient architecture,[24] AFM was chosen for this research as it is an excellent method to characterize dimensions of individual molecules on a surface. However, linear molecules are difficult to image due to limited lateral and vertical resolution, therefore previous reports have taken advantage of the bottlebrush architecture to quantify both dimensions and composition of polymer molecules including the correlation of brush gradient with height profiling.[17,16,25,26]

V.4.2. Molecular bottlebrush synthesis

To fully realize the effect of limited control on gradient architecture, the backbones were converted into bottlebrushes for AFM imaging. The functionality on HEMA-TMS repeat units was transformed into an ATRP initiating site (2-bromoisobutyryloxyethyl methacrylate, BiBEM) from which *n*BA side chains were grafted under normal ATRP conditions.[16] Table V.1 outlines the reaction conditions for each successful spontaneous

gradient brush synthesis. The polymerizations of *n*BA from PBiBEM-*grad*-PBA_{50} and PBiBEM-*grad*-PBA_{25} targeted DP = 400 with dNbpy as the ligand and 95% CuBr and 5% $CuBr_2$ at 70 °C. $CuBr_2$ was added to provide sufficient amount of deactivator and to reduce the concentration of active radicals at initial stages of the polymerization. The polymerization of *n*BA at a targeted DP = 1400 from PBiBEM-*grad*-PBA_{500} with PMDETA as the ligand offered the best control.

^{1}H NMR was used to determine the length of the side chains (DP_{SC}) based on monomer conversion of *n*BA and the number of initiating sites as determined by HEMA-TMS conversion during backbone synthesis. In each case, the length of the side chains was under 50 repeat units. GPC was also used to analyze the polymers as well as monitor the reactions. Figure V.1e shows the traces for the starting materials (PHEMA-TMS-*grad*-PBA_x), macroinitiators (PBiBEM-*grad*-PBA_x), and bottlebrushes (P(BiBEM-*graft*-BA)-*grad*-PBA_x) for all catalyst concentrations (x = 500, 50, or 25 ppm). A slight shift in M_n values was observed when the copolymers were transformed into the macroinitiators, while more significant shift in the molecular weight was observed after the formation of molecular bottlebrushes. A monomodal peak in GPC was observed for each bottlebrush, indicating the brush formation was a controlled polymerization.

V.4.3. AFM analysis

Characterization of gradient copolymers through molecular imaging by AFM is possible by the changing density of grafted side chains along the backbone. High concentrations of HEMA-TMS repeat units incorporated at the "head" of the gradient chain resulted in a high density of grafted side chains in the bottlebrushes.[27] Above a certain

grafting density there are space constraints which prevent all chains from adsorbing to the mica surface even while the backbone is fully extended, forcing a portion of the chains to stack on top of one another forming a characteristic cap along the backbone.[28,29] The cap of desorbed side chains results in overall increase of the height profile of the brush backbone as well as formation of the bulky "head" region in the gradient bottlebrush. Due to the gradient architecture of the backbone, the grafting density continually decreased along with the backbone, forming the flexible "tail" region. These theoretical predictions are consistent with the AFM image along with top and side-view representations in Figure V.2, which demonstrates the changes in height profile with gradient backbone architecture.

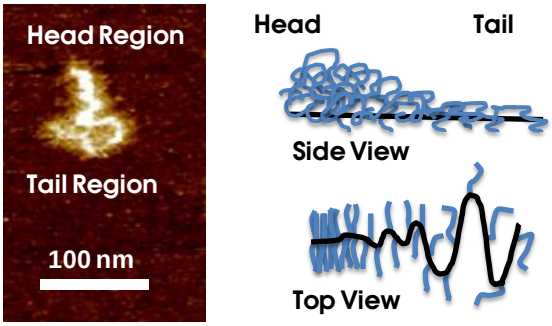

Figure V.2. AFM height image with top and side view representations of gradient molecular bottlebrushes on a surface.

The molecular bottlebrushes were spin cast from dilute chloroform solutions on to freshly cleaved mica substrates for AFM measurement. AFM was first utilized to confirm DP_{SC} through width profiles (D); increased side chain length resulted in an increase in bottlebrush width. As detailed in Table V.2, D = 30, 25, and 15 nm for P(BiBEM-*graft*-BA)-*grad*-$PBA_{500,\ 50,\ or\ 25\ ppm}$, which corresponds well with DP_{SC} given in Table V.1 for each sample. The length distribution (L_w/L_n) was also measured by statistical analysis of

the AFM micrographs. The sample with the narrowest weight distribution (smallest M_w/M_n value), P(BiBEM-*graft*-BA)-*grad*-PBA_{500}, also had narrow length distributions, L_w/L_n = 1.07. As less catalyst was used during the backbone synthesis, the L_w/L_n values of the bottlebrushes correspondingly increased (ca. 1.14 and 1.21), indicating a broader distribution in length among the samples. This suggests the reduced control in the systems with lower catalyst concentrations which correspondingly results in poorer gradient quality.

Table V.2. AFM characterization of molecular brushes.

Brush Sample	M_w/M_n [a]	D [b] [nm]	L_w/L_n [b]	<s> [b] [nm]
P(BiBEM-*graft*-BA)-*grad*-PBA_{500}	1.37	30	1.07	0.20
P(BiBEM-*graft*-BA)-*grad*-PBA_{50}	1.50	25	1.13	0.24
P(BiBEM-*graft*-BA)-*grad*-PBA_{25}	2.13	15	1.21	0.33

[a] determined by GPC; [b] width (D), length distribution (L_w/L_n) and standard deviation of $IC_{HEMA\text{-}TMS}$ <s> of bottlebrush backbone as determined by AFM.

Figure V.3 shows height profiles of individual brush molecules along with the average height profiles obtained for each brush, P(BiBEM-*graft*-BA)-*grad*-$PBA_{500,\ 50,\ or\ 25}$. In absolute values, the average height profile for each brush sample was different due to the difference in side-chain length. For example, P(BiBEM-*graft*-BA)-*grad*-PBA_{500} has the longest side chains (DP_{SC} = 30) and therefore the tallest height profile, while P(BiBEM-*graft*-BA)-*grad*-PBA_{25} has the shortest side chains (DP_{SC} = 14) and correspondingly the lowest height profile. Assuming the surface-adsorbed bottlebrush adopts the shape of a half cylinder, the $IC_{HEMA\text{-}TMS}$ (dotted line, measured by ^{1}H NMR) is approximately proportional to the square of the average height profile ($\langle h^2 \rangle$, grayed area, measured by

AFM). The plots at the bottom of Figure V.3 demonstrate clear correlation between $\langle h^2 \rangle$ and $IC_{HEMA\text{-}TMS}$, which confirms gradient composition.

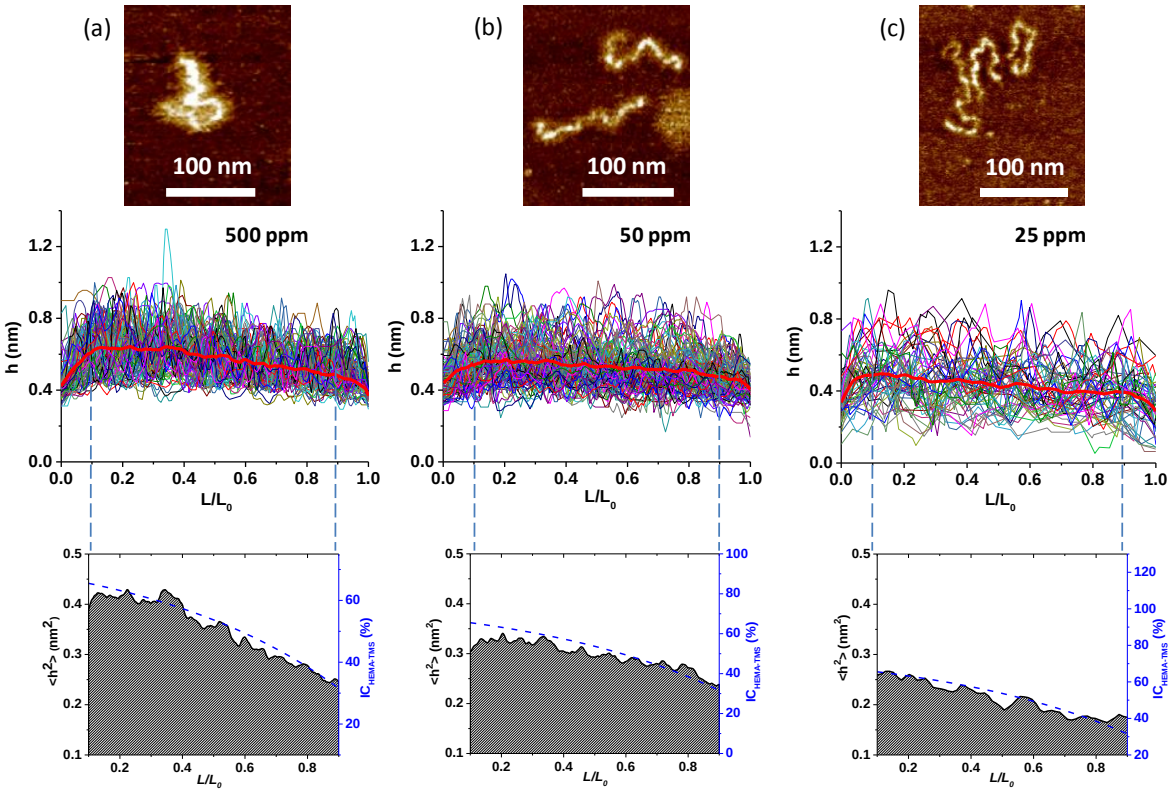

Figure V.3. AFM images (top), height profiles of individual molecules (50~100 chains) and their averages (red line) (middle), and average height square (h^2) profiles (bottom) from AFM analysis of typical molecules from P(BiBEM-*graft*-BA)-*grad*-PBA_X where X = 500 (a), 50 (b), or 25 (c). The average h^2 profiles demonstrate good agreement with the instantaneous copolymer composition (dashed line). The L/L_0 range in the bottom plots were cut by 0.1 L/L_0 at both ends to mask the intrinsic height decrease at the bottlebrush ends not relevant to the synthetically introduced gradient.

To analyze the quality of gradient found in each sample, the standard deviation of the instantaneous composition $IC_{HEMA\text{-}TMS}$ was analyzed as:

$$< s >= \sqrt{\frac{1}{N}\sum_{i=1}^{N}\left\{\int_{0.1}^{0.9}\left[f_a(l)\cdot\left(\frac{h_i^2(l)}{h_a^2(l)}-1\right)\right]^2 dl \Big/ \int_{0.1}^{0.9} dl\right\}} \quad \text{(V.1)}$$

where $h_i(l)$and $h_a(l)$are the height profile of an individual bottlebrush and the average height profile for an assembly of bottlebrushes, respectively, $l = L/L_0$is normalized distance along a brush backbone of a contour length L_0, and N is number of bottlebrushes analyzed. In equation V.1, $f_a(l)$ is the average $IC_{HEMA\text{-}TMS}$ along the brush backbone, which can be approximated by an exponential function $f_a(l) = 0.8 - 0.12e^{1.6\cdot l}$. It is necessary to point out that the backbone composition and height profiles have been analyzed within central section of bottlebrushes to circumvent the intrinsic decrease in height at the brush ends. In this analysis, the zero standard deviation would correspond to a system when all brushes demonstrate the same gradient of grafting density along their backbones. Any deviation from zero indicates broader dispersion of the gradient, i.e. decrease in quality of the gradient control. Table V.2 gives the <s> values for each brush, which demonstrates the gradient copolymer generated with the largest amount of catalyst, P(BiBEM-*graft*-BA)-*grad*-PBA_{500}, resulted in the lowest standard deviation. As shown in Figure V.4, the decrease in the catalyst concentration results in increase of both M_w/M_n and <s> values.

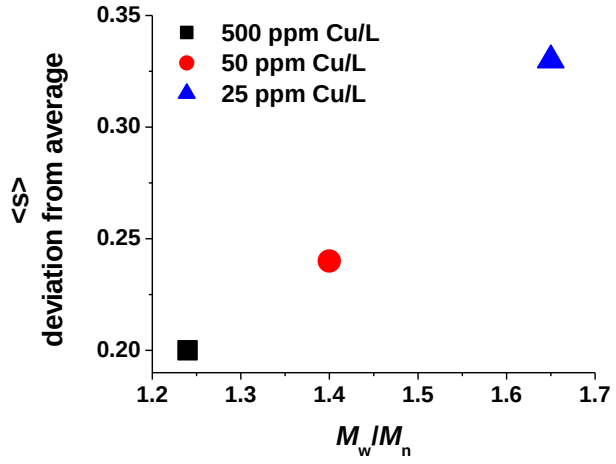

Figure V.4. Standard deviation of backbone composition <s> versus molecular weight polydispersity index M_w/M_n for molecular bottlebrushes synthesized with 500, 50, or 25 ppm of $CuBr_2$/L catalyst.

This empirical measurement of <s> corresponds to an average of the difference between the actual and mean heights measured within the individual macromolecules, at a given L/L_0 along the polymer backbone. Since the higher points are caused by the brush segments grown from the methacrylate monomers, <s> can be used to estimate the gradient quality from the local density of methacrylate vs. acrylate monomers. Recently, a theoretical evaluation of gradient quality, <GD>, was proposed.[23] The calculation of the <GD> value is conceptually very similar to the calculation of <s>, however, in determining <GD> the cumulative monomer composition was compared to the composition of the ideal gradient, not the average profile as was done in determining <s> in our paper. We believe that the empirically determined <s> parameter and <GD> should be strongly correlated, however, a quantitative transformation between <s> and <GD> is not possible, since the local density of chains will influence the height of a region of the macromolecule. This is

because a region of a lower brush density will allow the side chain to spread out more than a region with a higher brush density. Nevertheless, it is important to note that the <s> values followed the same trend as the <GD> values. In particular, this work showed that increasing MWD gave larger <s> values, and theoretical studies established that larger MWD values also lead to larger <GD> values.[23] Therefore, the experimental results are in agreement with the theoretical study, predicting that reduced control during polymerizations, as characterized by large MWD values, will result in poor gradient architecture.

V.5. Conclusions

Copolymers with increasing M_w/M_n values were generated by ARGET ATRP with decreasing levels of catalyst concentrations. Through transformation into molecular bottle brushes, AFM analysis was used to characterize the quality of gradient architecture present through height profiling. Average height profiles correlated well with instantaneous compositions determined by ^{1}H NMR. The standard deviation of height profile of each brush from the average value indicated that catalyst concentration during copolymer synthesis plays a role in the quality of gradient copolymer. P(BiBEM-*graft*-BA)-*grad*-PBA_{500} exhibited a low <s> value as well as narrow distribution of backbone lengths and molecular weights. However, the copolymers synthesized with lower catalyst concentrations (P(BiBEM-*graft*-BA)-*grad*-PBA_{50} and P(BiBEM-*graft*-BA)-*grad*-PBA_{25}) exhibited larger <s> values and broader distributions. In summary, this work confirms experimentally that MWD values are an excellent characteristic for assessing quality in gradient copolymers.

V.6. Acknowledgments

I would like to thank Dr. Dominik Konkolewicz and Dr. Dagmar D'hooge for helpful discussions on <GD>. Of course this project would not be complete without the incredible work by my collaborators at UNC Chapel Hill, Q. Li, Yuanchao Li and Prof. Seregi Sheiko. Yuanchao spent countless hours analyzing individual brushes via AFM, without which the manuscript would not be the complete work it is here. I also have to thank Joanna Burdyńska on many helpful discussions regarding the synthesis of macroinitiators and molecular bottlebrushes.

V.7. References

1. Matyjaszewski, K.; Ziegler, M. J.; Arehard, S. V.; Greszta, D.; Pakula, T. *Journal of Physical Organic Chemistry* **2000,** *13*, 775-786.
2. Zaremski, M. Y.; Kalugin, D. I.; Golubev, V. B. *Polymer Science* **2009,** *51*, 103-122.
3. Pakula, T.; Matyjaszewski, K. *Macromolecular Theory and Simulations* **1996,** *5*, 987-1006.
4. Shull, K. R. *Macromolecules* **2002,** *35*, 8631-8639.
5. Okabe, S.; Seno, K.; Kanaoka, S.; Aoshima, S.; Shibayama, M. *Macromolecules* **2006,** *39*, 1592-1597.
6. Mok, M. M.; Pujari, S.; Burghardt, W. R.; Dettmer, C. M.; Nguyen, S. T.; Ellison, C. J.; Torkelson, J. M. *Macromolecules* **2008,** *41*, 5818-5829.
7. Kim, J.; Mok, M. M.; Sandoval, R. W.; Woo, D. J.; Torkelson, J. M. *Macromolecules* **2006,** *39*, 6152-6160.

8. Jakubowski, W.; Juhari, A.; Best, A.; Koynov, K.; Pakula, T.; Matyjaszewski, K. *Polymer* **2008,** *49*, 1567-1578.

9. Sandoval, R. W.; Williams, D. E.; Kim, J.; Roth, C. B.; Torkelson, J. M. *Journal of Polymer Science: Part B: Polymer Physics* **2008,** *46*, 2672-2682.

10. Mok, M. M.; Kim, J.; Wong, C. L. H.; Marrou, S. R.; Woo, D. J.; Dettmer, C. M.; Nguyen, S. T.; Ellison, C. J.; Shull, K. R.; Torkelson, J. M. *Macromolecules* **2009,** *42*, 7863-7876.

11. Qin, S.; Saget, J.; Pyun, J.; Jia, S.; Kowalewski, T.; Matyjaszewski, K. *Macromolecules* **2003,** *36*, 8969-8977.

12. Lee, S. B.; Russell, A. J.; Matyjaszewski, K. *Biomacromolecules* **2003,** *4*, 1386-1393.

13. Buzin, A. I.; Pyda, M.; Costanzo, P.; Matyjaszewski, K.; Wunderlich, B. *Polymer* **2002,** *43*, 5563-5569.

14. Beginn, U. *Colloid Polymer Science* **2008,** *286*, 1465-1474.

15. Min, K.; Oh, J. K.; Matyjaszewski, K. *J. Polym. Sci., Part A: Polym. Chem.* **2007,** *45*, 1413-1423.

16. Lee, H.-i.; Matyjaszewski, K.; Yu, S.; Sheiko, S. S. *Macromolecules* **2005,** *38*, 8264-8271.

17. Boerner, H. G.; Duran, D.; Matyjaszewski, K.; da Silva, M.; Sheiko, S. S. *Macromolecules* **2002,** *35*, 3387-3394.

18. Matyjaszewski, K.; Jakubowski, W.; Min, K.; Tang, W.; Huang, J.; Braunecker, W. A.; Tsarevsky, N. V. *Proc. Natl. Acad. Sci. U.S.A.* **2006,** *103*, 15309-14.

19. Jakubowski, W.; Matyjaszewski, K. *Angew. Chem., Int. Ed.* **2006,** *45*, 4482-4486.

20. Jakubowski, W.; Min, K.; Matyjaszewski, K. *Macromolecules* **2006,** *39*, 39-45.

21. Listak, J.; Jakubowski, W.; Mueller, L.; Plichta, A.; Matyjaszewski, K.; Bockstaller, M. R. *Macromolecules* **2008,** *41*, 5919-5927.

22. Plichta, A.; Zhong, M.; Li, W.; Elsen, A. M.; Matyjaszewski, K. *Macromol. Chem. Phys.* **2012,** *213*, 2659-2668.

23. Van Steenberge, P. H. M.; D'hooge, D. R.; Wang, Y.; Zhong, M.; Reyniers, M.-F.; Konkolewicz, D.; Matyjaszewski, K.; Marin, G. B. *Macromolecules* **2012,** *45*, 8519-8531.

24. Hardrict, S. N.; Gurarslan, R.; Galvin, C. J.; Gracz, H.; Roy, D.; Sumerlin, B. S.; Genzer, J.; Tonelli, A. E. *J. Polym. Sci., Part B: Polym. Phys.* **2013,** *51*, 735-741.

25. Sheiko, S. S.; Sumerlin, B. S.; Matyjaszewski, K. *Prog. Polym. Sci.* **2008,** *33*, 759-785.

26. Lee, H. I.; Pietrasik, J.; Sheiko, S. S.; Matyjaszewski, K. *Prog. Polym. Sci.* **2010,** *35*, 24-44.

27. Pietrasik, J.; Sumerlin, B. S.; Lee, H. I.; Gil, R. R.; Matyjaszewski, K. *Polymer* **2007,** *48*, 496-501.

28. Panyukov, S.; Zhulina, E. B.; Sheiko, S. S.; Randall, G. C.; Brock, J.; Rubinstein, M. *J. Phys. Chem. B* **2009,** *113*, 3750-3768.

29. Lord, S. J.; Sheiko, S. S.; LaRue, I.; Lee, H.-I.; Matyjaszewski, K. *Macromolecules* **2004,** *37*, 4235-4240.

CHAPTER VI

ABA TRIBLOCK COPOLYMERS FROM TWO MECHANISTIC TECHNIQUES

VI.1. Preface

As discussed in Chapter IV, block copolymers with broadened molecular weight distributions have gained attention in recent years. While previous theoretical studies indicated that block copolymers with a disperse block may result in unique morphologies, it was difficult to confirm experimentally. Recent work has been able to overcome this hurtle with the invention of controlled radical polymerizations, for example an ABA triblock copolymer with disperse B block demonstrated a stable bicontinuous phase over a wide range of volume fractions. Materials with bicontinuous morphology are of noteworthy interest as they are excellent candidates for use in proton exchange membrane fuel cells (PEM-FC).

The following work outlines the use of two polymerization techniques, specifically, polycondensation and ATRP to generate ABA triblock copolymers. As polycondensation results in polymers with broad molecular weight distribution, the center of these triblock copolymers will be broad, while the outside blocks will have narrow molecular weight

distribution due to the control afforded from ATRP. Four types of samples were prepared based on poly(arylene ether ketone) or poly(arylene ether sulfone) center block with either poly(methyl methacrylate) or poly(pentafluorostyrene) outer block. Additionally, a series of triblock copolymers with a range of volume fractions were synthesized in order to target a variety of morphologies.

This work was done in collaboration with Natalia Agudelo Perez and Professor Betty Lopez from the University of Antioquia. Natalia synthesized the pre-polymers *via* polycondensation in Colombia and during her stay at CMU, we transformed them into macroinitiators and synthesized triblock copolymers *via* ATRP.

VI.2. Introduction

Current sources of energy for transportation, both personal and commercial, often rely on hydrocarbon based fuels. Finding an alternative fuel source to replace current systems has been of significant interest for many years, not only for environmental reasons but also due to increased demands on dwindling hydrocarbon sources.[1,2] Several alternative fuel sources are being studied to replace traditional combustion engines and one of the largest areas of concentration is fuel cells. A fuel cell is an electrochemical device which converts the chemical energy of a fuel, such as hydrogen, into electrical energy. Many different types of fuel cells are being explored including phosphoric acid, solid oxide, molten carbonate, and alkaline and all are viable fuel cells. Particularly, PEM-FCs are expected to be excellent power sources for transportation due to their high efficiency and energy density per volume and weight.[2,3]

Proton exchange membranes are particularly interesting for a number of reasons: their low operating temperatures allow for fast start up, even at low temperatures; they can quickly respond to power demands; solid, stable polymers operate without leaking, an issue in liquid electrolytes; and their only byproduct is water.[1-3] Through the use of thin polymer electrolytes (≤50 μm), PEMs provide short ion transport pathways, thereby reducing cell resistance. Reduction of cell resistance in turn increases the overall fuel cell performance and thin polymer electrolytes also decrease the total weight and volume of a fuel cell. PEMs are not thermal engines and the limitations associated with the Carnot cycle do not apply, which also increases the fuel efficiency.[1] The current state of PEM-FC research remains on the synthesis of new membranes that exhibit more robust and reliable performance.

Ideally, a proton exchange membrane should exhibit high proton conductivity (>0.01 $S \cdot cm^{-1}$) while having: no conductivity of electrons; very little or no dependence on the relative humidity or temperature; tolerance to carbon monoxide; hydrolytic stability under acidic conditions; a stable morphology; and low production and operation costs.[1] The current *golden standard* of PEMs is the industrially utilized Nafion®. Though Nafion® is the material to which all new PEMs are compared; it does not fulfill all of the aforementioned requirements. For example, Nafion® will fail as a PEM at high temperatures due to a loss of associated water and its high production and operation costs.[2,4,5] Therefore, much of the research is being done within this area to gain a replacement for Nafion®; in other words, a new *golden standard* of PEMs.

Poly(arylene ether sulfone)s (PAES) and derivatives thereof are another vast area of study for PEMs[6,4,7,8] due to their historical use as engineering thermoplastics, as well as

low production costs.[7] These materials possess excellent thermo and oxidative stability, with glass transition temperatures above 185 °C.[9] Introduced commercially in 1965, polysulfones were and are used in hair dryers, structural foams, electronics and cookware.[10,11] Astrel®, Victrex® and Udel® are all examples of commercial polysulfones.

A common modification of PAES for fuel cell applications is sulfonation, or the addition of pendent sulfonic acid groups to the aromatic backbone.[12,13] One significant disadvantage to the sulfonated PAES (s-PAES) system is the lack of control over the placement and number of acid groups and many studies show that ion conductivity is dependent on membrane morphology. Therefore, PEM research has focused on creating PAES-based materials which can self-assemble into defined morphology. As block copolymers are well known to self-assemble into a variety of morphologies, including spheres, cylinders, lamellae and bicontinuous,[14] this architecture would be the most common approach to achieve self-assembly of PAES. [6,15]

Research by McGrath *et al.* improved upon the traditional s-PAES systems by generating a hydrophobic-hydrophilic multi-block copolymer based on sulfonated and unsulfonated blocks of PAES. These samples exhibited sharper phase separation and larger topological features than a random copolymer analogue. Additionally, higher proton conductivity (0.8 versus 0.4 S/cm) was achieved though the multi-block copolymer had identical ion exchange capacity (IEC): 1.2 meq/g.[16]

Using dual mechanistic techniques is another avenue to pursue block copolymers of PAES.[17] An excess of one monomer during polycondensation polymerizations affords telechelic materials with relative ease, whose end groups may be transformed into initiating

sites for a second type of polymerization. Atom transfer radical polymerization (ATRP)[18-22] is a common method used in conjunction with polycondenstation to generate ABA triblock copolymers[23,24] for PEMs. For example, poly(2,3,5,6,-tetrafluorostyrene-4-phosphonic acid)[25] and poly(styrene-*co*-acrylonitrile)[26] were both successfully polymerized from difunctional PAES-based macroinitiators under ATRP conditions.

It has been a long-held opinion that the formation of well-ordered morphologies requires narrow molecular weight distribution (MWD) of the block copolymers. Theoretical studies on the implications of MWD in block copolymer phase behavior were conducted as early as 1980 by Leibler *et al*. and followed by many others,[27-33] while only recently has a surge in experimental studies occurred. In particular, embedding a disperse segment into the core of ABA copolymers resulted in classical morphologies but with dilated phase domains as well as phase coexistence. Additionally, shifts in the composition-dependent microphase windows consistent with increased interfacial curvature toward the polydisperse segment were observed along with a highly stable bicontinuous phase over a broad range of volume fractions. [34,35]

Herein, the synthesis of ABA block copolymers prepared by polycondensation and ATRP techniques is reported. Four types of samples prepared were poly(methyl methacrylate)-*b*-poly(arylene ether ketone)-*b*-poly(methyl methacrylate) (PKM), poly(pentaflurostyrene)-*b*-poly(arylene ether ketone)-*b*-poly(pentafluorstyrene) (PKF), poly(methyl methacrylate)-*b*-poly(arylene ether sulfone)-*b*-poly(methyl methacrylate) (PSM), and poly(pentaflurostyrene)-*b*-poly(arylene ether sulfone)-*b*-poly(pentafluorstyrene) (PSF). As polycondensation typically results in polymers with broad molecular weight distribution, the center of the triblock copolymers was broad, while

the outer blocks had narrow molecular weight distribution due to the control afforded from ATRP. It was the goal of this work to explore the effect of a disperse B block in ABA triblock copolymers on microphase separation. Therefore, triblock copolymers over a range of volume fractions were synthesized in order to target a range of morphologies. Furthermore, the materials will be tested as proton exchange membranes.

VI.3. Experimental

VI.3.1. Materials

Methyl methacrylate (MMA, 99%, Aldrich) and 2,3,4,5,6-pentafluorostyrene (PFS, 99%, Aldrich) was passed through a column filled with basic alumina prior to use. Bisphenol A (BPA, 99%, Aldrich), bis(4-fluorophenyl)sulfone (DFS, 99%, Aldrich), bromoisobutyryl bromide (BiB, 98%, Aldrich), copper(I) bromide ($Cu^{I}Br$, 99.999%, Aldrich), copper(II) bromide ($Cu^{II}Br_2$, 99.999%, Aldrich), 4,4′-difluorobenzophenone (DFK, 99%, Aldrich), *N,N,N',N'',N*''-pentamethyldiethylenetriamine (PMDETA, 99%, Aldrich), tin(II) 2-ethylhexanoate ($Sn^{II}(EH)_2$, 95%, Aldrich), potassium carbonate (K_2CO_3, 99%, Aldrich) and solvents were purchased from Aldrich were used as received. .

VI.3.2. Synthetic procedures

VI.3.2.1. Polycondensation of pre-polymer

An example of polycondensation formulated with DFS and BPA is given as follows; see Table VI.1 for specific reaction conditions. A 100 mL round bottomed flask equipped with a stir bar, Dean-Stark trap, condenser and gas inlet was charged with of DFS

(10 eq, 1.0127 g, 3,98 mmol), of BPA (11 eq, 1.0027 g, 4.39 mmol), of K_2CO_3 (26 eq, 1.4350 g, 10.38 mmol), 6.5 mL of toluene and 25 mL of NMP. The reaction mixture was allowed to reflux at 150 °C for 4 h under nitrogen. The water formed from azeotropic drying was removed and the polymerization was allowed to continue at 190 °C for 16 h. To ensure the polymers possessed terminal phenol groups, 10 mol% excess of BPA was added in 10 ml of toluene, and the reaction mixture refluxed for an additional 4 h at 160 °C. The viscous polymer solution was then cooled to ambient temperature, filtered and precipitated into an excess of water/methanol (v/v=1:1) with sufficient acetic acid to neutralize residual K_2CO_3. The precipitate was recovered via centrifugation and were further purified by precipitating twice from THF into methanol and dried under vacuum overnight at 60°C to afford 1.8 g of PS_9-OH. The material was characterized via GPC (M_n = 4,100 and M_w/M_n = 1.44) and ^{1}H NMR (300 MHz, $CDCl_3$), whose peak assignments are detailed in Figure VI.1. δ: 7.83(*m*, 4H, **a**), 7.25 (*m*, 4H, **d**), 7.11 (*d*, 2H, **g**), 6.97 (*m*, 8H, **b**, **c**), 6.75 (*d*, 2H, **f**), 1.75 (*s*, 6H, **e**).

VI.3.2.2. Functionalization to ATRP macroinitiator

An example of macroinitiator functionalization procedure formulated with PK_{17}-OH was based on previous literature[23] and is given as follows. A 20 mL round bottomed flask equipped with a stir bar was charged with PK_{17}-OH (1 eq, 1.0000 g, 0.187 mmol). The flask was purged with N_2 for 1 h. Dry pyridine (1.5 mL) was added to the flask and allowed to stir until all solid was dissolved. Over a period of 15 min., BiB (3 eq, 69 µL, 0.561 mmol) was added. The reaction mixture was allowed to stir at room temperature for 48 h. The functionalized polymer was precipitated into methanol/water (80:20) three times.

The final polymer, was dried under vacuum for 48 h which resulted in 0.7 g of PK_{17}-Br. The material was characterized via GPC (M_n = 10,300 and M_w/M_n = 1.7) and ^{1}H NMR (300 MHz, $CDCl_3$), whose peak assignments are detailed in Figure VI.1. δ: 7.82 (*m,* 4H, **a'**), 7.28 (*m*, 4H, **d'**), 7.03 (*m*, 8H, **b'**, **c'**), 2.08 (*s*, 6H, **f'**), 1.73 (*s*, 6H, **e'**). ^{1}H NMR was used to confirm full functionalization occurred via the disappearance of the proton *ortho* to hydroxyl (-OH) of the phenolic end groups, peak **f**, while a new peak, labeled as **f'**, appeared. This new peak is assigned to methyl protons (-CH_3) of 2-bromopropionyloxy groups of PK_{17}-Br.

VI.3.2.3. ARGET ATRP of MMA from macroinitiator

An example ARGET ATRP procedure formulated with $M_{63}PK_{17}M_{63}$ at a targeted DP = 200 is given as follows; see Table VI.2 for specific reaction conditions. A 10 mL Schlenk flask charged with the macroinitiator PK_{17}-Br (1eq, 165 mg, 23 μmol) and a stir bar was degassed and backfilled with nitrogen (N_2) six times. A mixture of anisole (2.8 mL), $CuBr_2$ (1.1 mg, 4.7 μmol)/TPMA (4.1 mg, 14μmol) complex in acetonitrile was added to a glass vial and purged with nitrogen for 20 min. Previously deoxygenated MMA (2 mL, 18.84 mmol) was added to the vial. Immediately, the reaction mixture was transferred *via* an airtight syringe to the Schlenk flask, which was placed in a thermostated water bath at 80 °C. Previous deoxygenated $Sn^{II}(EH)_2$ (0.43 mL of 10 mg/mL solution in anisole, 10.6 μmol) was added to the Schlenk flask to start the polymerization. Samples were taken periodically to measure conversion *via* ^{1}H NMR and number average molecular weights *via* GPC The polymerization was stopped by opening the flask and exposing the catalyst to air and was passed through a neutral alumina column to remove copper. The

polymer was precipitated three times into methanol and dried under vacuum at 60 ºC for three days. The final polymer had a M_n = 24,300 and M_w/M_n = 1.37.

VI.3.2.4. ATRP of PFS from macroinitiator

An example ATRP procedure formulated with $F_{57}PK_{18}F_{57}$ at a targeted DP = 400 is given as follows; see Table VI.3 specific reaction conditions. A 10 mL Schlenk flask was charged with PK_{18}–Br (100 mg), anisole (1.6 ml), PFS monomer (1.0 mL), $CuBr_2$ (3.2 mg, $1.4x10^{-2}$ mmol)/PMDETA (3.8 mg, $2.2x10^{-2}$ mmol) complex and a stir bar, the flask was sealed and five freeze–pump–thaw cycles were used to degas the system The reaction mixture was filled with nitrogen again. With positive pressure of N_2, CuBr (3.2 mg, $2.2x10^{-2}$ mmol) was added to the frozen solution mixture under nitrogen. The flask was evacuated and refilled with nitrogen at least 6 times. The reaction flask was charged with nitrogen at room temperature and an initial sample was taken via purged syringe, and the sealed flask was placed in thermostated oil bath at 110°C. Samples were taken at timed intervals and analyzed by GPC and ^{1}H-NMR to follow the progress of the reaction. The polymerization was stopped by opening the flask and exposing the catalyst to air and was passed through a neutral alumina column to remove copper. The polymer was precipitated three times into methanol and dried under vacuum at 60ºC for three days and was determined to have M_n = 30200 and M_w/M_n = 1.29.

VI.3.3. Analyses

Infrared of study of the PEEK, PEES and ABA block copolymers was performed in a FTIR Perkin Elmer spectrum one. Glass transition temperatures (T_g) of the samples

were acquired in a Temperature-Modulated Differential Scanning Calorimeter (TM-DSC) TA Instrument Q100. The thermal history of samples PEES and PEEK hermetically sealed in aluminum pans were erased by heating from room temperature to 360°C at 20°C/min, and then cooled to 20°C. Finally, the thermograms were acquired from 20°C to 360°C heating at 10°C/min. Molecular weight and molecular weight distributions of the formed polymers were measured by gel permeation chromatography (GPC) using Polymer Standards Services (PSS) columns (guard, 10^5, 10^3, and 10^2 Å), with THF eluent at 35 °C, flow rate 1.00 mL/min, and differential refractive index (RI) detector (Waters, 2410). Diethyl ether was used as the internal standard to correct for any fluctuation of the THF flow rate. The number-average molecular weights (M_n) and molecular weight distribution (M_w/M_n) were determined with a calibration based on linear polystyrene standards using WinGPC 6.0 software from PSS. ^{1}H NMR spectra were recorded in $CDCl_3$ as a solvent using Bruker 300 MHz spectrometer and was utilized determined molecular weight of pre-polymers, monitor the functionalization to macroinitiator, as well as to determine monomer conversion during ATRP reactions.

VI.4. Results and discussion

VI.4.1. Synthesis of PK-OH and PS-OH

Poly(arylene ether)s were synthesized by the nucleophilic aromatic substitution (S_NAr) of bisphenol A (BPA) and either difluorophenyl sulfone (DFS) or diflurophenyl ketone (DFK) in the presence of K_2CO_3 and a mixture of NMP/toluene, as depicted in Scheme VI.1, step 1. A range of molecular weights for both polyketone (PK-OH) and

polysulfone (PS-OH) were targeted using a stoichiometric imbalance (r) according with the Carothers equation (Eq VI.1)

$$P_n = \frac{1+r}{1-r} \quad \text{(VI.1)}$$

where, P_n is the targeted degree of polymerization, r is reactant ratio. These values, along with the characterization of the resulting polymers are given in Table VI.1. The subscript numbers present in the sample name refer to repeat units.

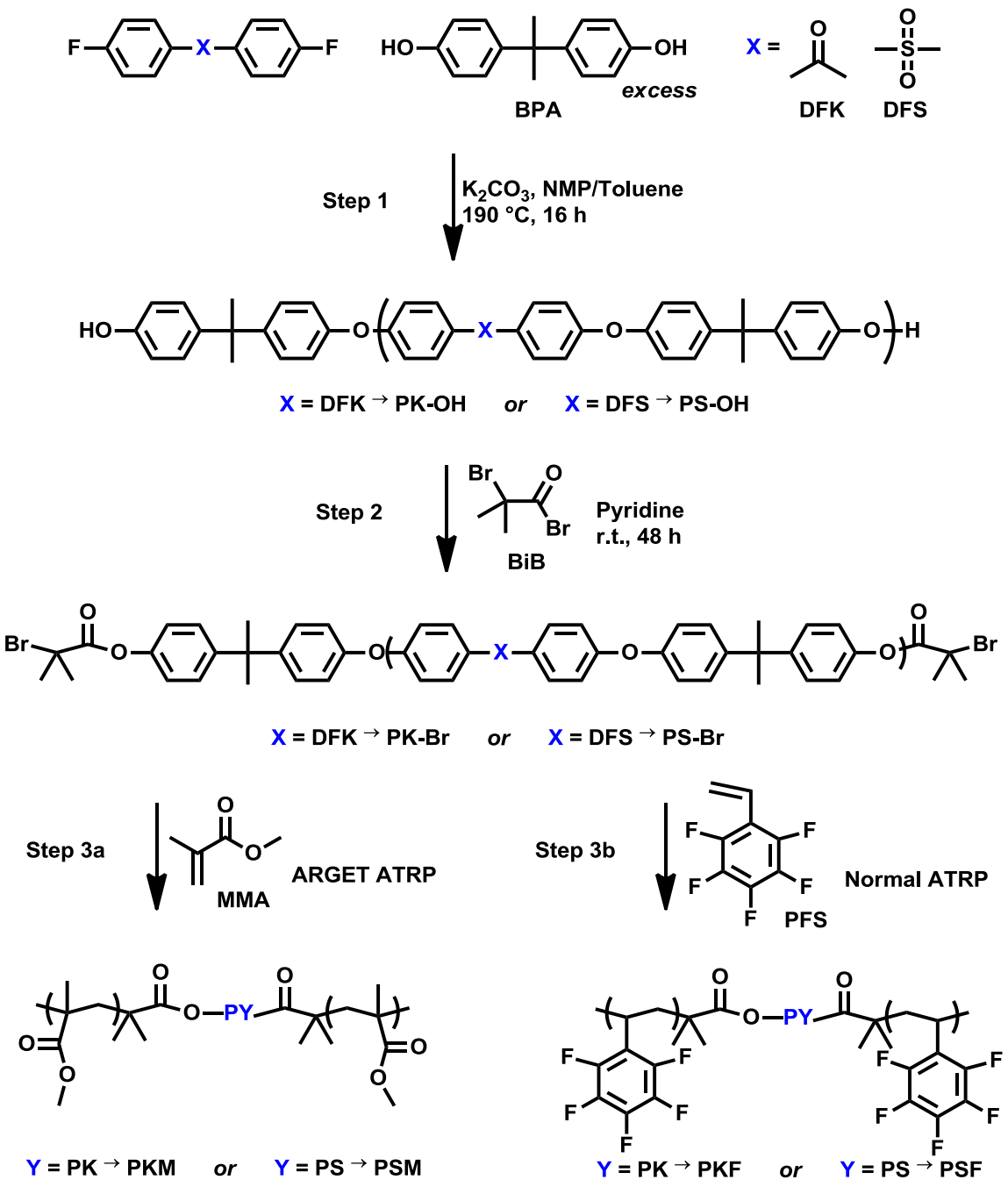

Scheme VI.1. Three step synthesis of triblock copolymers with either polyketone (PK) or polysulfone (PS) center blocks and either poly(methyl methacrylate) PMMA or poly(pentafluorostyrene) PPFS outer blocks.

Table VI.1. Polycondensation conditions and characterization of resulting PK-OH and PS-OH. [a]

Sample[b]	r^c	$P_{n,th}{}^d$	$M_{n,\,NMR}{}^e$	$M_{n,\,GPC}$	M_w/M_n	T_g (°C)
PK_{17}-OH	0.98805	39	7000	10700	1.53	144
PK_{18}-OH	0.98013	53	7400	18300	1.46	147
PS_9-OH	0.90685	12	4000	4100	1.44	144
PS_8-OH	0.90933	22	3800	5500	1.54	157

[a][BPA]:[K_2CO_3] = 0.63, T = 190 °C; [b] subscript number refers to experimental degree of polymerization; [c] r = [$mol_{DFS/K}$]/[mol_{BPA}]; [d] determined by equation VI.1; [e] determined by equation VI.2.

PS-OH and PK-OH were designed to be terminated with phenolic end groups by using an excess of BPA over DFS or DFK, respectively. This is an important design factor as it allows for functionalization at a later synthetic step. The aromatic protons located on the phenolic end groups may be differentiated from the aromatic protons of the repeat units (Figure VI.1), which may be utilized to determine the number–average molecular weight, M_n, of PK-OH and PS-OH by comparison of the signals labeled as **a** and **f**, when the integration of peak **f** = 1.00, using Eq VI.2. A_{Ha} is the integration of peak **a**, 4 is the number of protons which peak **a** represents, $MW_{r.u.}$ is the molecular weight of the repeat unit and 227.3 is the molecular weight of the BPA end group.

$$M_n = \left(\frac{A_{Ha}}{4}\right) MW_{r.u.} + 227.3 \qquad \text{(Eq VI.2)}$$

The discrepancies between $M_{n,NMR}$ and $M_{n,GPC}$ occur due to the use of polystyrene standards for molecular weight calibration in GPC. However, GPC was a useful tool as it

allowed the confirmation of a monomodal peak and measurement of molecular weight distribution. The polymers synthesized by conventional step-growth polymerization generated polymers with molecular weight distributions comparatively low for a step-growth process, which can be ascribed to fractionation of the material during the work-up procedure.

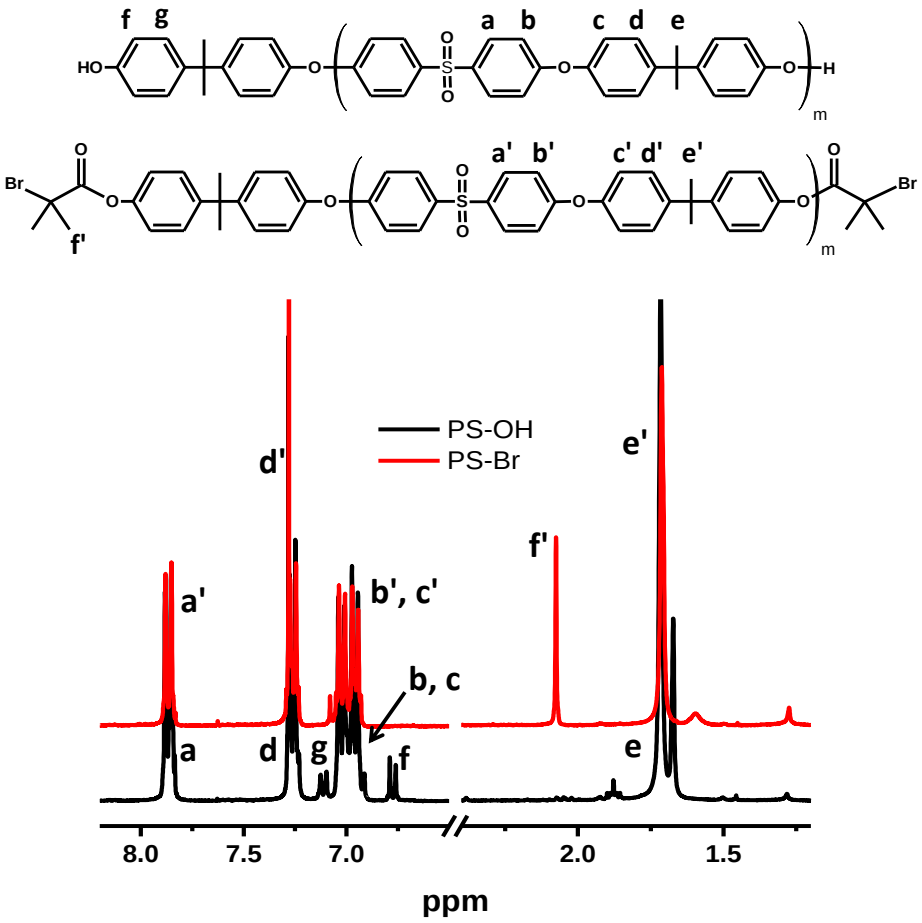

Figure VI.1. ^{1}H NMR spectra of the samples PS-OH and PS-Br.

The glass transition temperatures (T_g) of PK-OH and PS-OH were measured by differential scanning calorimetry (DSC) and are listed in Table VI.1. While PS-OH is traditionally amorphous, PK-OH samples have been well documented to result in

crystallizable materials with melting points (T_m) greater than 330°C. However, the non-polar 2-isopropylidene links present in the PK-OH samples have a comparatively low rotational barrier, which provided flexibility in the arylene ether segment. For this reason the PK-OH samples were not crystalline and did not exhibit crystallization or melting temperatures in the DSC trace.

VI.4.2. Synthesis of macroinitiators: PK-Br and PS-Br

The synthesis of well-defined triblock copolymers that include a traditional step-growth condensation polymer as the mid-block was achieved by the incorporation of controlled radical polymerization (CRP) functional groups at both chain ends of the polycondensation block and subsequent block copolymerization. The pre-polymers, PK-OH and PS-OH, were transformed into ATRP macroinitiators through end-group functionalization which was accomplished utilizing the phenolic end-groups. When reacted with 2-bromoisobutyryl bromide (BiB) in the presence of pyridine, the phenolic end groups of poly(arylene ether) were functionalized to α-haloesters (Scheme VI.1, step 2).

The functionalization of PS-OH and PK-OH was monitored *via* ^{1}H NMR and the proton *ortho* to hydroxyl (-OH) of the phenolic end groups. As seen in Figure VI.1, peak ***f***, corresponding to the end group protons, completely disappeared after the esterification, while a new peak, labeled as ***f'***, appeared. This new peak was assigned to methyl protons ($-CH_3$) of 2-bromoisobutyryloxy groups of PS-Br and PK-Br. These two factors indicate that the phenolic end groups of PS-OH and PK-OH were converted to 2-bromoisobutyryloxy groups. To confirm the functionalization to α-haloesters, FT-IR was

employed. The appearance of an absorption peak at 1750 cm^{-1}, ascribed to C=O stretching vibration of the ester groups, verified the transformation from pre-polymer to macroinitiator. FT-IR spectrum of the pre-polymers did not exhibit any absorbance at this wavelength. The chemical shifts in the ^{1}H NMR spectra in conjunction with the FT-IR spectra confirmed the full functionalization to the macroinitiator samples: PK-Br and PS-Br.

VI.4.3. Synthesis of ABA triblock copolymer

Utilizing di-functional ATRP macroinitiators, ABA triblock copolymers were synthesized under ATRP conditions. Polymerizing the outer blocks with a controlled radical polymerization technique afforded well defined "A" blocks in contrast to the symmetrically broad "B" block. Two monomers were employed for the synthesis of the triblock copolymers: MMA and PFS. These monomers were chosen as they would provide mechanical support if the materials were used as proton exchange membranes in fuel cells. In particular, fluorinated polymers have attracted significant attention due to a series of favorable properties, such as high thermal stability, hydrophobicity, good chemical resistance, low flammability as well as their optical and electrical properties. With each monomer, triblock copolymers were synthesized from PK-Br and PS-Br initiators. Additionally, several triblock copolymers were synthesized to afford a range of chemical compositions, or volume fractions of each block. This series of copolymers was prepared to analyze any morphology differences that accompany the various volume fractions.

The synthesis of PMMA-*b*-PK-*b*-PMMA (PKM) and PMMA-*b*-PS-*b*-PMMA (PSM) were carried out at 80 °C in 50 vol% of anisole under ARGET ATRP conditions,

as summarized in Table VI.2 and Scheme VI.1 (note: the subscript numbers refer to the number of repeat units for the respective blocks). The polymerizations were catalyzed by $CuBr_2$/TPMA complex with $Sn(EH)_2$ as the reducing agent and initiated by PK-Br and PS-Br, respectively. With the purpose of obtaining ABA copolymers with different compositions of polycondensation block (B) and PMMA block (A), either the molar ratio between PS-Br or PK-Br macroinitiator and PMMA, or target DP, was altered or the reaction time was accordingly increased or decreased.

Table VI.2. Polymerization conditions and results for ARGET ATRP of MMA from PK-Br or PS-Br macroinitiators.

Entry[a,b]	Target DP	Conv.[d]	$M_{n,th}$	$M_{n,GPC}$	M_w/M_n	f_{PC}[e]
$M_{271}PK_{17}M_{271}$[c]	800	0.67	61270	55400	1.37	11
$M_{134}PK_{17}M_{134}$	400	0.67	33820	35700	1.29	20
$M_{63}PK_{17}M_{63}$	200	0.63	19570	24300	1.37	34
$M_{49}PK_{17}M_{49}$	400	0.24	16710	25000	1.32	40
$M_{119}PS_9M_{119}$	400	0.59	27750	28600	1.24	14
$M_{72}PS_9M_{72}$	200	0.72	18470	28600	1.24	21
$M_{40}PS_9M_{40}$	400	0.20	12010	15400	1.15	32
$M_{26}PS_9M_{26}$	400	0.13	9120	12500	1.17	43

[a] All polymerization were carried out in 50% (v/v) anisole with $[Macroinitiator]_0/[CuBr_2]_0/[TPMA]_0/[Sn^{II}(EH)_2]_0$ =1/0.2/0.6/0.2 at 80°C. [b] Entries labeled with PK utilized PK-Br as macroinitiator and the other labeled with PS utilized PS-Br, the subscript numbers represent the degree of polymerization relative to each block. [c] In this entry was used molar ratio of $Sn^{II}(EH)_2$=0.45. [d] Determined by ^1H NMR. [e] Volume fractions

of the block copolymers were calculated with the densities of PMMA, PK and PS equivalent to 1.19, 1.26 and 1.24 g/cm^3, respectively.

Figure VI.2 displays the first-order kinetic plot and evolution of molecular weight and M_w/M_n values with monomer conversion of the polymerization of MMA from PK-Br and PS-Br. Three polymerizations were conducted with a range of targeted DP = 200, 400, and 800 for MMA from PK-Br while two polymerizations were conducted with PS-Br, targeting DP = 200 and 400. In each case, linear first-order kinetic was observed as well as good correlation between experimental and theoretical M_n values. While the M_w/M_n values of the pre-polymers were somewhat large (Table VI.1) due to the nature of polycondensation polymerization technique, the M_w/M_n values decreased with conversion of MMA, indicating well controlled polymerizations.

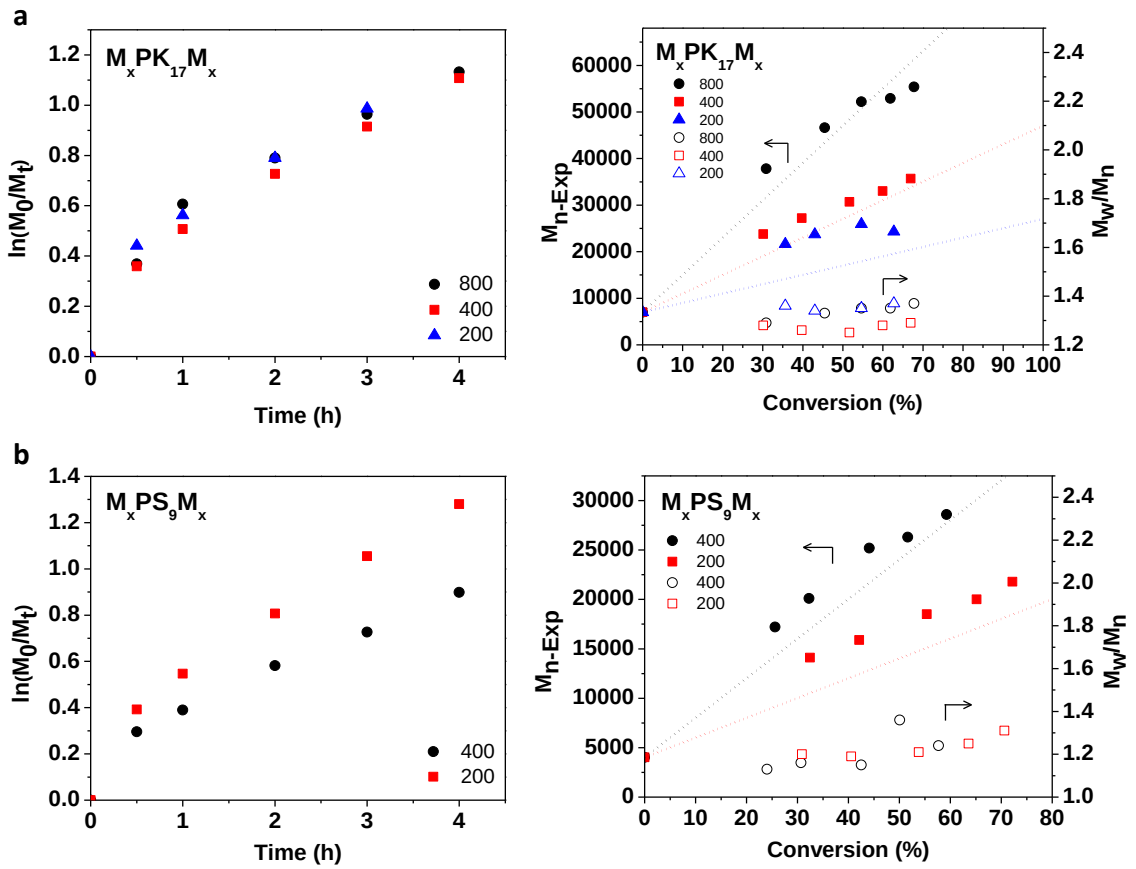

Figure VI.2. First order kinetic plots and evolution of M_n and M_w/M_n values with monomer conversion of (a) $M_xPK_{17}M_x$ with targeted DP = 200, 400 or 800 and (b) M_x PS_9 M_x with DP = 200 or 400.

The PPFS-PK-PPFS (PKF) and PPFS-PS-PPFS (PSF) triblock copolymers syntheses were achieved using normal ATRP (Scheme VI.1, step 3b) as outlined in Table VI.3 (note: the subscript numbers refer to the number of repeat units for the respective blocks). The polymerizations were conducted in 50 vol% of anisole with a CuBr/PMDETA catalyst complex. PMDETA was chosen as the ligand for these polymerizations as it is less active and therefore more suitable toward the high levels of

catalyst required for normal ATRP. From each macroiniatiator, PK-Br and PS-Br, two different degrees of polymerization of PFS were targeted: DP = 400 and 200.

Table VI.3. Polymerization conditions and results for normal ATRP of PFS from PK-Br or PS-Br macroinitiators.

Entry[a]	Target DP	Time (h)	Conv.[b]	$M_{n,th}$	$M_{n,GPC}$	M_w/M_n	f_{PC}[c]
$F_{57}PK_{18}F_{57}$	400	3	0.32	30640	28600	1.16	29
$F_{29}PK_{18}F_{29}$	200	3	0.27	16000	18400	1.22	45
$F_{29}PS_8F_{29}$	400	3	0.15	15110	14400	1.12	29
$F_{17}PS_8F_{17}$	200	3.3	0.17	10230	10300	1.19	42

[a] All polymerization were carried out in 50% (v/v) anisole with $[Macroinitiator]_0/[CuBr_2]_0/[PMDETA]_0/[CuBr]_0$ =1/0.8/1.2/1.2. [b] Determined by ^{1}H-NMR [c] Volume fractions of the block copolymers were calculated with the densities of PPFS, PK and PS equivalent to 1.55, 1.26 and 1.24 g/cm^3, respectively.

The first-order kinetic plot along with the evolution of molecular weight and M_w/M_n values with monomer conversion is displayed in Figure VI.3. All polymerizations exhibited linear first-order kinetics along with good correlation between experimental and theoretical molecular weights. Additionally, the M_w/M_n values decrease with conversion of PFS monomer, resulting in samples with narrow molecular weight distribution.

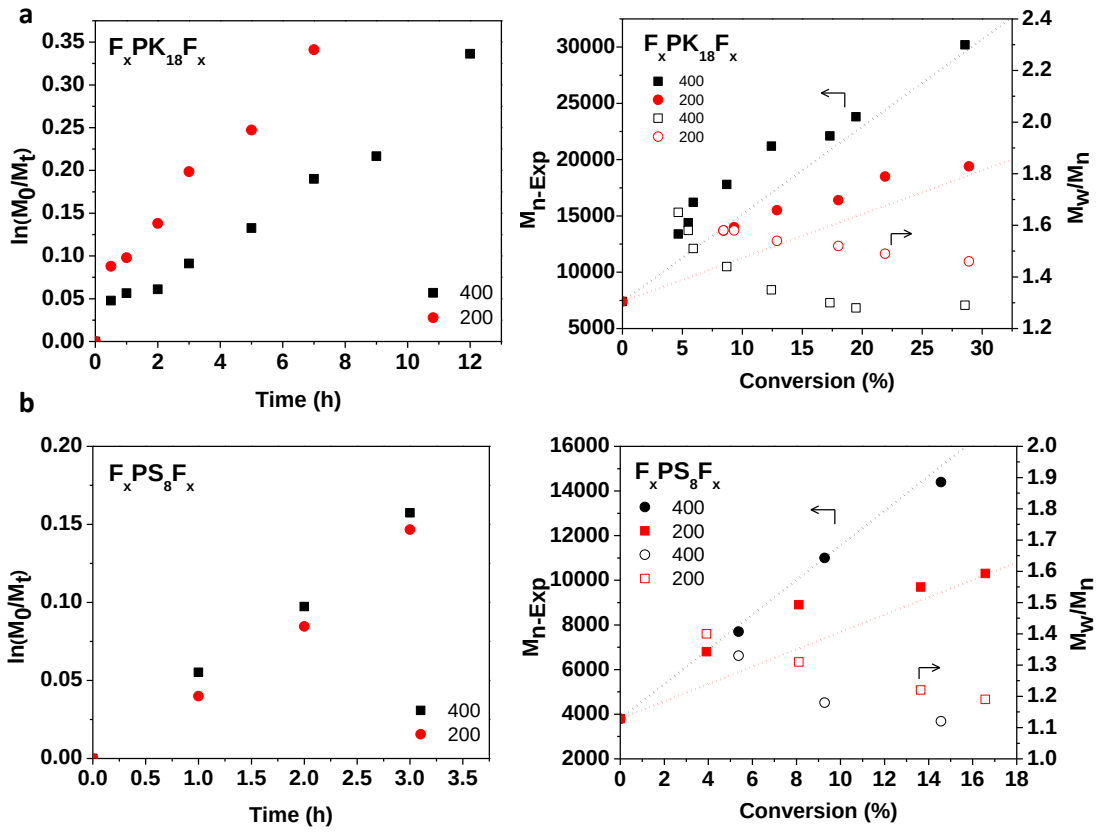

Figure VI.3. First order kinetic plot and evolution of M_n and M_w/M_n values with monomer conversion of (a) $F_xPK_{18}F_x$ with targeted DP = 200 or 400 and (b) $F_xPS_8F_x$ with DP = 200 or 400.

Example GPC traces for each type of polymerization, MMA or PFS from PK-Br or PS-Br is given in Figure VI.4. In each case, the broad molecular weight distribution of the macroinitiator was visible at the t = 0 h samples, however, as the reaction progressed, the molecular weight distribution decreased, signifying well controlled ATRPs. Furthermore, there was no remaining macroinitiator as the final traces for each polymerization demonstrated a clean shift in molecular weight as well as being monomodal.

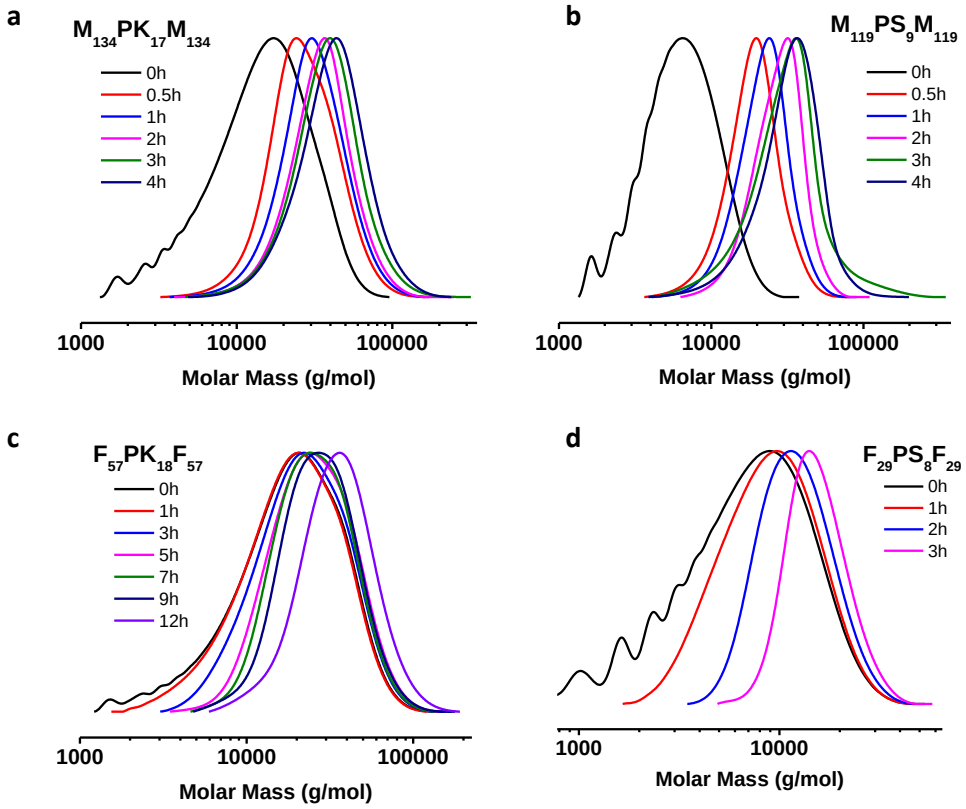

Figure VI.4. GPC traces for chain extension of a). PK macroinitiator with MMA, b). PS macroinitiator with MMA, c). PK macrointitor with PFS and d). PS macroinitiator with PFS

VI.4.4. Material characterization

Four samples, which contain identical center blocks with decreasing degrees of polymerization of the outer blocks ($PK_{17}M_x$, where x = 89, 80, 66, or 60), were chosen for characterization of morphology. The data for these samples is summarized in Table VI.2. Several different types of characterization methods were utilized including SAXS, WAXS, and TEM. Films were made from each of the four samples by dissolving the solid polymer

in 1.2 mL of toluene, followed by 8 days of solvent annealing and finally dried in a vacuum over for 24 h.

The first method used to characterize the four PKM samples was Small Angle X-ray Scattering to looks for micro-domain separation. As can be seen from Figure VI.5, the SAXS graph does not show many features, however there is one distinct peak at q = 0.082 (d = 76.62 A), which may be related to the crystallization of PK. It is interesting to note that the peak is strongest at the lowest volume fractions of PK. While no micro-domain separation occurred, WAXS and TEM were utilized to confirm the crystallization of PK.

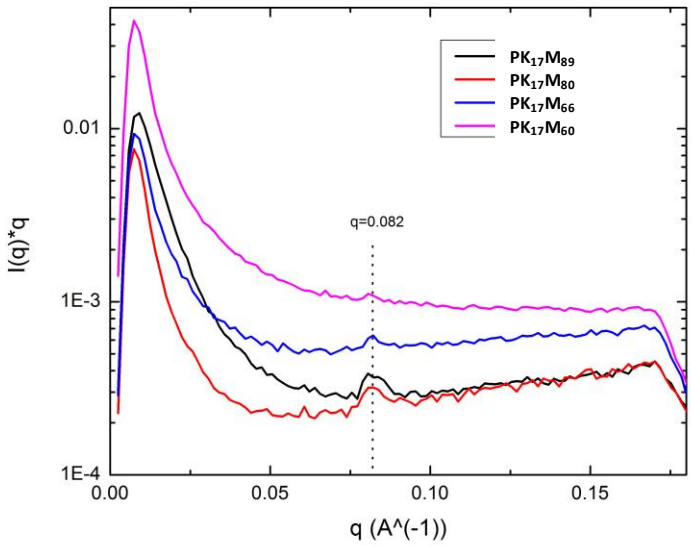

Figure VI.5. SAXS graph of $PK_{17}M_{89}$, $PK_{17}M_{80}$, $PK_{17}M_{66}$, $PK_{17}M_{60}$.

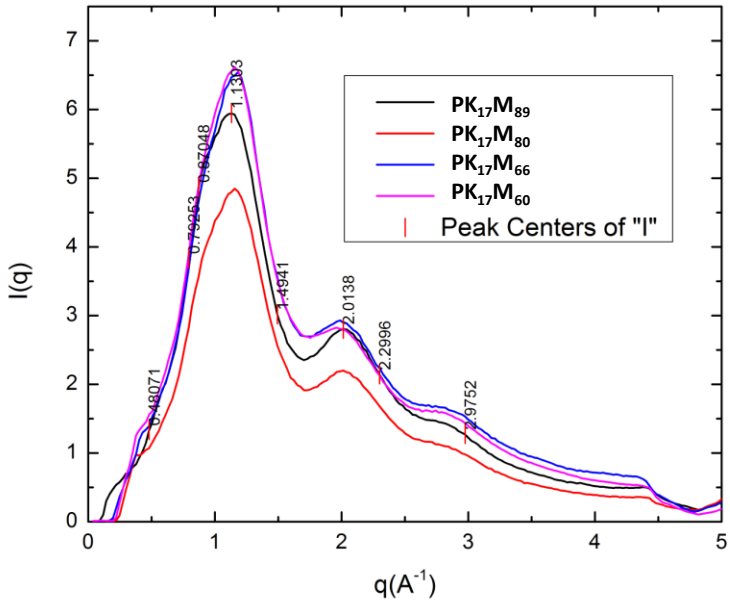

Figure VI.6. WAXS graph of $PK_{17}M_{89}$, $PK_{17}M_{80}$, $PK_{17}M_{66}$, $PK_{17}M_{60}$.

Wide Angle X-ray Scattering (WAXS) was used to evaluate if crystal formation had occurred in the PKM samples. WAXS was performed directly on the samples without a background for 3600 seconds. The peaks obtained in Figure VI.6 were compared to literature values for amorphous PMMA and crystalline PK. As can be seen from Table VI.4, the experimental and literature values have good correlation furthering indicating the probability of crystalline PK and amorphous PMMA. The slight shift in values has been attributed to the literature values coming from homopolymer samples while experimental values are triblock copolymers. Additionally, a TEM image (Figure VI.7) shows the PK crystallites. Notably, the diameter of the crystallites via TEM (d = 7 nm) match those predicted by SAXS (q = 0.082 → d = 7.6 nm).

Table VI.4 Literature and experimental WAXS values for PK and PMMA homopolymers.

Poly(ketone)		Poly(methyl methacrylate)	
Lit. q (A^{-1})[36]	**Exp. q (A^{-1})**	**Lit. q (A^{-1})[37]**	**Exp. q (A^{-1})**
1.3188	1.1308	0.9477	0.87
1.4601	1.4941		
1.9962	2.0138		

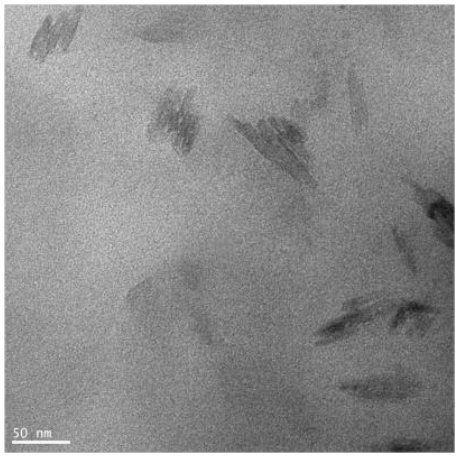

Figure VI.7. TEM image of $PK_{17}M_{88}$ stained with RuO_4 for 5 min.

VI.5. Conclusions and future plans

This work outlined the synthesis of triblock copolymers using polycondensation and atom transfer radical polymerization techniques. Telechelic poly(aryl ether)s were synthesized via polycondensation and were transformed into ATRP macroinitiators. ABA triblock copolymers with a variety of compositions and volume fractions were synthesized to explore differences in morphology. Preliminary results indicated that the samples did not exhibit traditional microphase separation. However, the unique block copolymer architecture and hydrophobic outer blocks suggests these materials may be suitable for use as proton exchange membranes. The future of this work includes sulfonation of the B

block followed by testing as proton exchange membranes, including water uptake, swelling ratio, ion exchange capacity and proton conductivity. Additional morphological studies on the remaining unsulfonated samples, as well as the sulfonated versions of these materials, is currently underway.

VI.7. Acknowledgments

I would like to thank Natalia A. Agudelo for her synthesis of polycondensation materials as well as her help in synthesizing the ABA copolymers during her stay at CMU. Additionally, I would like to thank Prof Lopez and Prof Matyjaszewski for allowing Natalia to visit CMU for 6 months.

VI.8. References

1. Hamrock, S. J.; Yandrasits, M. A. *J. Macromol. Sci., Polym. Rev.* **2006,** *46*, 219-244.
2. Cele, N.; Ray, S. S. *Macromol. Mater. Eng.* **2009,** *294*, 719-738.
3. Bose, S.; Kuila, T.; Nguyen, T. X. H.; Kim, N. H.; Lau, K.-t.; Lee, J. H. *Prog. Polym. Sci.* **2011,** *36*, 813-843.
4. Hickner, M. A.; Ghassemi, H.; Kim, Y. S.; Einsla, B. R.; McGrath, J. E. *Chem. Rev.* **2004,** *104*, 4587-4612.
5. Mauritz, K. A.; Moore, R. B. *Chem. Rev.* **2004,** *104*, 4535-4585.
6. Park, M. J.; Kim, S. Y. *J. Polym. Sci., Part B: Polym. Phys.* **2013,** *51*, 481-493.
7. Wang, F.; Hickner, M.; Kim, Y. S.; Zawodzinski, T. A.; McGrath, J. E. *J. Membr. Sci.* **2002,** *197*, 231-242.

8. Einsla, M. L.; Kim, Y. S.; Hawley, M.; Lee, H. S.; McGrath, J. E. *Chem. Mater.* **2008,** *20,* 5636-5642.

9. Hale, W. F.; Farnham, A. G.; Johnson, R. N.; Clendinn.Ra. *Journal of Polymer Science Part a-1-Polymer Chemistry* **1967,** *5,* 2399-&.

10. Charles Carraher, J. *Polymer Chemistry* 5th ed.; Marcel Dekker, Inc.: New York, 2000.

11. Margolis, J. M.; McGraw-Hill: New York, 2006.

12. Noshay, A.; Robeson, L. M. *Journal of Applied Polymer Science* **1976,** *20,* 1885-1903.

13. Harrison, W. L.; Wang, F.; Mecham, J. B.; Bhanu, V. A.; Hill, M.; Kim, Y. S.; McGrath, J. E. *J. Polym. Sci., Part A: Polym. Chem.* **2003,** *41*, 2264-2276.

14. Bates, F. S. *Annu. Rev. Phys. Chem.* **1990,** *41*, 525-527.

15. Orilall, M. C.; Wiesner, U. *Chem. Soc. Rev.* **2011,** *40*, 520-535.

16. Li, Y.; Roy, A.; Badami, A. S.; Hill, M.; Yang, J.; Dunn, S.; McGrath, J. E. *J Power Sources* **2007,** *172,* 30-38.

17. Bernaerts, K.; Du Prez, F. E. *Prog. Polym. Sci.* **2006,** *31*, 671-722.

18. Wang, J. S.; Matyjaszewski, K. *J. Am. Chem. Soc.* **1995,** *117,* 5614-5615.

19. Matyjaszewski, K.; Xia, J. *Chem. Rev.* **2001,** *101,* 2921-2990.

20. Matyjaszewski, K. *Macromolecules* **2012,** *45*, 4015-4039.

21. Braunecker, W. A.; Matyjaszewski, K. *Prog. Polym. Sci.* **2007,** *32*, 93-146.

22. Kato, M.; Kamigaito, M.; Sawamoto, M.; Higashimura, T. *Macromolecules* **1995,** *28*, 1721-1723.

23. Gaynor, S. G.; Matyjaszewski, K. *Macromolecules* **1997,** *30*, 4241-4245.

24. Zhang, Y.; Chung, I. S.; Huang, J.; Matyjaszewski, K.; Pakula, T. *Macromol. Chem. Phys.* **2005,** *206*, 33-42.

25. Shao, Z.; Sannigrahi, A.; Jannasch, P. *J. Polym. Sci., Part A: Polym. Chem.* **2013,** *51*, 4657-4666.

26. Oh, D. Y.; Lee, J. U.; Jo, W. H. *J. Mater. Chem.* **2012**, 7187-7193.

27. Leibler, L.; Benoit, H. *Polymer* **1981,** *22*, 195-201.

28. Hong, K. M.; Noolandi, J. *Polym. Commun.* **1984,** *25*, 265-268.

29. Burger, C.; Ruland, W.; Semenov, A. N. *Macromolecules* **1990,** *23*, 3339-3346.

30. Sides, W.; Fredrickson, G. H. *J. Chem. Phys.* **2004,** *121*, 4974-4986.

31. Cooke, D. M.; Shi, A.-C. *Macromolecules* **2006,** *39*, 6661-6671.

32. Matsen, M. W. *Eur. Phys. J. E* **2006,** *21*, 199-207.

33. Matsen, M. W. *Phys. Rev. Lett.* **2007,** *99* 1-4.

34. Widin, J. M.; Schmitt, A. K.; Im, K.; Mahanthappa, M. K. *J. Am. Chem. Soc.* **2012,** *134*, 3834-3844.

35. Schmitt, A. L.; Mahanthappa, M. K. *Soft Matter* **2012,** *8*, 2294-2303.

36. Fougnies, C.; Damman, P.; Villers, D.; Dosiere, M.; Koch, M. H. J. *Macromolecules* **1997,** *30*, 1385-1391.

37. Wind, M.; Graf, R.; Renker, S.; Spiess, H. W.; Steffen, W. *J. Chem. Phys.* **2005,** *122*, 014906.

CHAPTER VII

COPOLYMERIC SURFACTANTS WITH CONTROLLED ARCHITECTURE

VII.1. Preface

Polymer surfactants are interesting materials as they possess similar qualities to their small molecule counterparts and may in fact be utilized for identical applications. However, polymeric surfactants also demonstrate unique properties including lower critical micelle concentrations as well as lower diffusion coefficients than traditional surfactants. Amphiphilic block copolymers are the most common choice for use as polymeric surfactants and while they have greatly improved the field of dispersed media, it was the goal of this chapter to study more complex copolymers. This chapter outlines the synthesis and characterization of a library of materials with a range of compositions (gradient, random and block), topologies (linear and star) as well as monomer content (hydrophilic, neutral and hydrophobic) for use as polymeric surfactants in the stabilization of emulsions.

Gradient copolymers have received increasing attention due to their noteworthy characteristics including special interfacial phase behaviors, broadened glass transition temperatures (T_g), and reeling-in micelle effects. Unfortunately, there are limited studies which directly compare gradient and block copolymers as surfactants. The syntheses of block and gradient copolymers were discussed in Chapter I, while Chapter V demonstrated that MWD is an excellent tool to assess the quality within gradient copolymers. In other words, only samples with low MWD values possess a true gradient architecture along the polymer chains. With that information, it was possible to move forward and generate gradient copolymers with confidence of quality based on MWD values.

This work was inspired by a previous group member, Dr. Wenwen Li, whose research demonstrated that changing the topology of polymeric surfactants from linear to star resulted in stable emulsions while utilizing significantly less material. However, what effect would composition of individual arms have on the behavior as surfactants? Likewise, what effect would the overall hydrophilicity or hydrophobicity have on the behavior? It was my goal to answer these questions by designing a library of materials with a range of composition, topology and monomer content for the stabilization of emulsions. I synthesized the 11 linear polymers and the synthesis of stars was done in collaboration with Sangwoo Park. Furthermore, Emily Wallitsch and Prof. Robert Tilton joined the project to characterize the samples as polymer surfactants.

VII.2. Introduction

Within the past two decades, polymeric surfactants have garnered attention as replacements for traditional small molecule surfactants.[1-3] Similar to their small molecule

counterparts, polymeric surfactants are well documented to lie at the interface of dispersed droplets owing to their amphiphilic characteristics and may be utilized for similar applications including dispersants, emulsifiers, wetting agents, and detergents. However, polymeric surfactants exhibit distinctive and fascinating properties which are unavailable to traditional materials. For example, polymeric surfactants have lower critical micelle concentrations, meaning less material is required for micelle formation, as well as lower diffusion coefficients than low molecular weight surfactants.

Amphiphilic block copolymers are the most popular choice for use as polymeric surfactants. One marked advantage of block copolymers over small molecule analogues is wealth of potential architectural features including specific functionalities, stimuli responsive blocks or (non)ionic anchoring blocks.[4] These features provide the ability to tailor interactions between the surfactant and dispersed phase. The introduction of controlled radical polymerizations such as ATRP[5-8] further expanded the structure possibilities as it allows for the synthesis of more complex architectures including molecular bottlebrushes, branched polymers and star polymers.[9-12] While block copolymers are a noteworthy improvement to traditional surfactants, more complex compositions as well as topologies are under consideration for use as polymeric surfactants.

With the advent of CRPs another type of composition emerged, gradient copolymers.[13-17] Unlike block copolymers which instantaneously switch from one block to the other, gradient copolymers have a gradual change in composition along the length of the polymer chain. This distinct composition results in special interfacial phase behaviors, broadened glass transition temperatures (T_g), increased critical micelle concentration and reeling-in micelle effects; rare properties which may be applicable

toward polymer blend compatibilizers, additives for sound and vibration dampening, and stabilizers for emulsions.[15,18-29] In particular, one preliminary study which compares block and gradient copolymers in solution indicates that gradient copolymers behave more hydrophilic than their block copolymer analogues and are more sensitive to changes in monomer composition.[30]

Topology has also been a wide area of study for polymeric surfactants and star polymers are of particular interest as research indicates they are much more efficient stabilizers thereby requiring less material for stable emulsions (c.a. $\leq$ 0.01 wt% of star surfactant).[31-41] Furthermore, it was demonstrated that the composition of the star polymers greatly affects the type of emulsion. For example, a star comprised of only poly(ethylene oxide) PEO arms was shown to generate an O/W emulsion while the inclusion of poly(butyl acrylate) PBA arms into the star yielded a W/O emulsion.[41]

In this work, both linear and non-linear copolymers were tested which are comprised of a variety of compositions and monomer content. 2-Hydroxyethyl acrylate (HEA) and ethylene glycol methyl ether acrylate (MEA) monomers were chosen for their hydrophilic and hydrophobic nature, respectively. From these monomers, nine linear polymers were synthesized based from three compositions (random, block and gradient) as well as three monomer contents (hydrophilic, neutral and hydrophobic). Non linear materials, specifically stars, were formed utilizing the linear materials through the arm-first method by crosslinking with ethylene glycol diacrylate (EGDA) to generate gradient, block and random copolymer stars. Additionally, HEA and MEA homopolymers were synthesized to be used for the formation of mikto arm stars also through the arm-first

method. Table VII.1. summarizes the library of materials outlined for this work; all samples were synthesized and tested as stabilizers for emulsions.

Table VII.1. Library of materials for use as polymeric surfactants.

Composition	Topology	Targeted % CC_{HEA}	Actual % CC_{HEA}[a]
Random	Linear	70 50 30	70 50 30
Random	Star		70 50 30
Block	Linear		74 43 28
Block	Star		74 43 28
Gradient	Linear		72 60 19
Gradient	Star		72 60 19
Mikto	Star		70 50 30

[a] Cumulative composition (C.C.) calculated using equation VII.1 with monomer conversion.

VII.3. Experimental

VII.3.1. Materials

2-Hydroxyethyl acrylate (HEA, 96%, Aldrich) and ethylene glycol methyl ether acrylate (MEA, 98%, Aldrich) were passed through a neutral alumina column prior to use. Ethylene glycol diacrylate (EGDA, 98%, Aldrich) was passed through a basic alumina column prior to use. Cu^0 wire (d = 1mm) was washed with hydrochloric acid and dried before use. Tris(2-pyridylmethyl)amine (TMPA) was synthesized according to previously published procedures.[42] Acetonitrile (MeCN, 99.5%, Aldrich), copper(I) bromide (CuBr, 99.99%, Aldrich), copper(II) bromide ($CuBr_2$, 99.999%, Aldrich), chloroform ($CHCl_3$, 99.9%, Fisher Scientific), *N*,*N*-dimethylformamide (DMF, 99.8%, Aldrich), dimethylsulfoxide (DMSO, 99.9%, Fisher Scientific), 2-ethyl bromoisobutyrate (EBiB,

98%, Aldrich), 1,1,4,7,10,10-hexamethyltriethylenetetramine (HMTETA, 97%, Aldrich), methanol (MeOH, 99.8%, Pharmco Aaper), and *N,N,N',N'',N*''-pentamethyldiethylenetriamine (PMDETA, 99%, Aldrich) were all used as received.

VII.3.2. Synthetic procedures

VII.3.2.1. Synthesis of random copolymers

An example ATRP procedure formulated with $CuBr_2$/PMEDTA catalyst and targeted DP = 80 for each monomer to generate random copolymer $\mathbf{R_{50}}$ is given as follows. A 10 mL Schlenk flask equipped with a stir bar was charged with HEA (2.23 mL,19.44 mmol), MEA (2.5 mL,19.44 mmol), EBiB (0.24 mL of 200 mg/mL solution in DMF, 240 µmol), $CuBr_2$ (0.27 mL of 10 mg/mL solution in acetonitrile, 12 µmol), PMDETA (0.14 mL of 150 mg/mL solution in DMF, 120 µmol), and DMF (4.7 mL). The reaction mixture was degassed by at least three freeze-pump-thaw cycles. With positive pressure of N_2, CuBr (15.6 mg, 110 mmol) was added to the 10 mL Schlenk flask. The flask was evacuated and refilled with nitrogen at least 6 times after which it was placed in a 70 °C oil bath to start the polymerization. Samples were taken periodically to measure conversion *via* GC and number average molecular weights *via* GPC. The polymerization was stopped by exposure to air and the final reaction mixture was flushed through a neutral alumina column with chloroform to remove any residual copper. Excess chloroform was removed and the concentration solution was precipitated into diethyl ether. The polymer sample was dried under vacuum for 12 h to afford a final DP = 80 with $M_{n,GPC}$ = 13,500 and M_w/M_n = 1.24. Specific reaction conditions are available below (note: the subscript numbers refer to the final cumulative composition of HEA) with characterization given in Table VII.2.

R_{70}: [HEA]:[MEA]:[EBiB]:[CuBr]:[$CuBr_2$]:[PMDETA] = 110:50:1:0.45:0.05:0.5. 40% v/v DMF, 10% v/v DMSO, 70 °C. HEA_{52}-*r*-MEA_{23}.

R_{50}: [HEA]:[MEA]:[EBiB]:[CuBr]:[$CuBr_2$]:[PMDETA] = 80:80:1:0.45:0.05:0.5. 40% v/v DMF, 10% v/v DMSO, 70 °C. HEA_{40}-*r*-MEA_{40}.

R_{30}: [HEA]:[MEA]:[EBiB]:[CuBr]:[$CuBr_2$]:[PMDETA] = 50:110:1:0.45:0.05:0.5. 40% v/v DMF, 10% v/v DMSO, 70 °C. HEA_{25}-*r*-MEA_{54}.

VII.3.2.2. Synthesis of block copolymers

The following is an ATRP procedure formulated with $CuBr_2$/HMTETA catalyst to generate HEA macroinitiator **M_{21}**. A 25 mL Schlenk flask equipped with a stir bar was charged with HEA (8 mL, 69.6 mmol), EBiB (0.68 mL of 200 mg/mL solution in DMF, 700 µmol), $CuBr_2$ (15 mg, 70 µmol), HMTETA (95 µL, 350 µmol), and DMF (8 mL). The reaction mixture was degassed by at least three freeze-pump-thaw cycles and filled with nitrogen again. With positive pressure of N_2, CuBr (40 mg, 280 mmol) was added to the flask which was then evacuated and refilled with nitrogen at least 6 times and placed in a 60 °C oil bath to start the polymerization. Samples were taken periodically to measure conversion *via* ^{1}H NMR and number average molecular weights *via* GPC. The polymerization was stopped by exposure to air and the final reaction mixture was dialyzed three times against DMSO and MeOH each to remove any residual copper. The macroinitiator was dried under vacuum for 12 h to afford a final DP = 21 with M_n = 6,600 and M_w/M_n = 1.20. Specific reaction conditions are available below (note: the subscript numbers refer to DP_{HEA}) with characterization given in Table VII.2.

M_{58}: [HEA]:[EBiB]:[CuBr]:[$CuBr_2$]:[HMTETA] = 160:1:0.45:0.05:0.5. 50% v/v DMF, 60 °C. $HEA_{58.}$

M_{37}: [HEA]:[EBiB]:[CuBr]:[$CuBr_2$]:[HMTETA] = 100:1:0.40:0.10:0.5. 50% v/v DMF, 60 °C. $HEA_{37.}$

M_{21}: [HEA]:[EBiB]:[CuBr]:[$CuBr_2$]:[HMTETA] = 100:1:0.40:0.10:0.5. 50% v/v DMF, 60 °C. $HEA_{21.}$

An ATRP chain extension procedure formulated with $CuBr_2$/HMTETA catalyst to generate block copolymer **B_{28}** is given as follows. A 10 mL Schlenk flask equipped with a stir bar was charged with MEA (4.5 mL, 35 mmol), **M_{21}** (291 mg, $M_{n,th}$ = 2,500 117 µmol), $CuBr_2$ (0.26 mL of 10 mg/mL solution in acetonitrile, 12 µmol), HMTETA (16 µL, 58 µmol), DMSO (4 mL) and DMF (0.5 mL). The reaction mixture was degassed by at least three freeze-pump-thaw cycles and filled with nitrogen again. With positive pressure of N_2, CuBr (6.7 mg, 47 µmol) was added to the flask which was then evacuated and refilled with nitrogen at least 6 times and placed in a 60 °C oil bath to start the polymerization. Samples were taken periodically to measure conversion *via* ^{1}H NMR and number average molecular weights *via* GPC. The polymerization was stopped by exposure to air and the final reaction mixture was dialyzed three times against DMSO and MeOH each to remove any residual copper. The macroinitiator was dried under vacuum for 12 h to afford a final DP_{MEA} = 55 with M_n = 33,000 and M_w/M_n = 1.20. Specific reaction conditions are available below (note: the subscript numbers refer to the final cumulative composition of HEA) with characterization given in Table VII.2.

B_{74}: [MEA]:[**M_{58}**]:[CuBr]:[$CuBr_2$]:[HMTETA] = 100:1:0.40:0.10:0.5. 44% v/v DMSO, 6% DMF, 70 °C. HEA_{58}-*b*-MEA_{20}.

B_{43}: [MEA]:[**M_{37}**]:[CuBr]:[$CuBr_2$]:[HMTETA] = 100:1:0.40:0.10:0.5 44% v/v DMSO, 6% DMF, 70 °C. HEA_{37}-*b*-MEA_{48}.

B_{28}: [MEA]:[**M_{21}**]:[CuBr]:[$CuBr_2$]:[HMTETA] = 300:1:0.45:0.05:0.5. 44% v/v DMSO, 6% DMF, 60 °C. HEA_{21}-*b*-MEA_{55}.

VII.3.2.3. Synthesis of gradient copolymers

An example ATRP procedure formulated with $CuBr_2$/PMEDTA catalyst and targeted DP = 80 for each monomer to generate **G_{72}** is given as follows. A 25 mL Schlenk flask equipped with a stir bar was charged with HEA (2.23 mL,19.44 mmol), EBiB (0.24 mL of 200 mg/mL solution in DMF, 240 µmol), $CuBr_2$ (0.14 mL of 10 mg/mL solution in acetonitrile, 6 µmol), PMDETA (70 µL of 150 mg/mL solution in DMF, 60 µmol), and DMF (4.2 mL). A 10 mL Schlenk flask equipped with a stir bar was charged with MEA (2.5 mL, 19.44 mmol), 240 µmol), $CuBr_2$ (0.14 mL of 10 mg/mL solution in acetonitrile, 6 µmol), PMDETA (70 µL of 150 mg/mL solution in DMF, 60 µmol), and DMSO (0.5 mL). The reaction mixtures were degassed by at least three freeze-pump-thaw cycles and filled with nitrogen again. With positive pressure of N_2, CuBr (7.8 mg, 55 mmol) was added to the 25 mL Schlenk flask and CuBr (7.8 mg, 55 mmol) was added to the 10 mL Schlenk flask. Each flask was evacuated and refilled with nitrogen at least 6 times. The 25 mL Schlenk flask was placed in a 70 °C oil bath to start the polymerization, while the contents of the 10 mL Schlenk flask were transferred to an air-tight syringe and immediately fed into the 25 mL Schlenk flask at a rate of 0.375 mL/hr for a total feed time of 8 h with a

kdScientific 100-series syringe pump. Samples were taken periodically to measure conversion *via* GC and number average molecular weights *via* GPC. The polymerization was stopped by exposure to air and the final reaction mixture was flushed through a neutral alumina column with chloroform to remove any residual copper. Excess chloroform was removed and the concentration solution was precipitated into diethyl ether. The polymer sample was dried under vacuum for 12 h to afford a final DP = 73 with $M_{n,GPC}$ = 14,100 and M_w/M_n = 1.24. Specific reaction conditions are available below (note: the subscript numbers refer to the final cumulative composition of HEA) with characterization given in Table VII.2.

G_{72}: [HEA]:[MEA]:[EBiB]:[CuBr]:[$CuBr_2$]:[PMDETA] = 110:50:1:0.45:0.05:0.5. 40% v/v DMF, 10% v/v DMSO, 70 °C. HEA_{53}-*grad*-MEA_{20}.

G_{60}: [HEA]:[MEA]:[EBiB]:[CuBr]:[$CuBr_2$]:[PMDETA] = 80:80:1:0.45:0.05:0.5. 40% v/v DMF, 10% v/v DMSO, 70 °C. HEA_{35}- *grad* -MEA_{27}.

G_{19}: [HEA]:[MEA]:[EBiB]:[CuBr]:[$CuBr_2$]:[PMDETA] = 50:110:1:0.45:0.05:0.5. 40% v/v DMF, 10% v/v DMSO, 70 °C. HEA_{13}- *grad* -MEA_{57}.

VII.3.2.4. Synthesis of homopolymers

The following is an ATRP procedure formulated with $CuBr_2$/HMTETA catalyst to generate a HEA homopolymer (**H_{100}**). A 25 mL Schlenk flask equipped with a stir bar was charged with HEA (8 mL, 69.6 mmol), EBiB (0.42 mL of 200 mg/mL solution in DMF, 440 µmol), $CuBr_2$ (0.49 mL of 10 mg/mL solution in acetonitrile, 20 µmol), HMTETA (69 µL, 220 µmol), and DMF (8 mL). The reaction mixture was degassed by at least three

freeze-pump-thaw cycles and filled with nitrogen again. With positive pressure of N_2, CuBr (28 mg, 200 mmol) was added to the flask which was then evacuated and refilled with nitrogen at least 6 times and placed in a 60 °C oil bath to start the polymerization. Samples were taken periodically to measure conversion *via* ^{1}H NMR and number average molecular weights *via* GPC. The polymerization was stopped by exposure to air and the final reaction mixture was dialyzed three times against DMSO and MeOH each to remove any residual copper. The polymer sample was dried under vacuum for 12 h to afford a final DP = 72 with M_n = 21,700 and M_w/M_n = 1.32. Specific reaction conditions are available below (note: the subscript numbers refer to the final cumulative composition of HEA) with characterization given in Table VII.2.

H_{100}: [HEA]:[EBiB]:[CuBr]:[$CuBr_2$]:[HMTETA] = 160:1:0.45:0.05:0.5. 50% v/v DMF, 60 °C. HEA_{72}.

H_0: [MEA]:[EBiB]:[CuBr]:[$CuBr_2$]:[HMTETA] = 160:1:0.45:0.05:0.5. 50% v/v DMF, 60 °C. MEA_{64}.

VII.3.2.5. Synthesis of star copolymers

An example SARA ATRP procedure formulated with 10 cm of Cu^0 wire and $CuBr_2$/TPMA catalyst to generate **SR_{30}** is given as follows. A 10 mL Schlenk flask was charged with Cu^0 wire (10 cm) and a stir bar, after which, the flask was degassed and backfilled with nitrogen (N_2) six times. A mixture of DMSO (5 mL), **R_{30}** (0.7 mg, 9.46×10^{-5} mol, 18.9 mM in DMSO), and EGDA (147 μL, 9.46×10^{-4} mol) was added to a glass vial and purged with nitrogen for 20 min. Previously deoxygenated $CuBr_2$/TPMA catalyst (0.09 mL of 0.05 M solution in DMF) was added to the flask. Immediately, the reaction mixture was

transferred *via* an airtight syringe to the Schlenk flask, which was placed in a thermostated oil bath at 60 °C. Samples were taken periodically to measure crosslinker conversion *via* ^{1}H NMR and monitor evolution of molecular weights *via* GPC. The polymerization was stopped by exposure to air and the final reaction mixture was dialyzed three times against MeOH each to remove any residual copper. The polymer sample was dried under vacuum for 12 h to afford a final $M_{n,MALLS}$ = 238,800 and N_{arms} = 24. Specific reaction conditions are available below (note: the subscript numbers refer to the final cumulative composition of HEA of the linear polymer. In the case of mikto arm stars, **Smikto**, the subscript number refers to the percentage of **H$_{100}$** incorporated into the polymerization setup) with characterization given in Table VII.3.

SR$_{70}$: [**R$_{70}$**]/[EGDA]/[$CuBr_2$/TPMA]=1/10/0.05, [**R$_{70}$**]= 18.7 mM in DMSO, T=60 °C, Cu wire (10 cm)**.** $M_{n,MALLS}$ = 366,600 *N*arms = 41.

SR$_{50}$: [**R$_{50}$**]/[EGDA]/[$CuBr_2$/TPMA]=1/10/0.05, [**R$_{50}$**]= 17.0 mM in DMSO, T=60 °C, Cu wire (10 cm)**.** $M_{n,MALLS}$ = 244,900 *N*arms = 23.

SR$_{30}$: [**R$_{30}$**]/[EGDA]/[$CuBr_2$/TPMA]=1/10/0.05, [**R$_{30}$**]= 18.9 mM in DMSO, T=60 °C, Cu wire (10 cm)**.** $M_{n,MALLS}$ = 238,800 *N*arms = 24.

SB$_{74}$: [**B$_{74}$**]/[EGDA]/[$CuBr_2$/TPMA]=1/10/0.05, [**B$_{74}$**]= 12.9 mM in DMSO, T=60 °C, Cu wire (10 cm)**.** $M_{n,MALLS}$ = 260,300 *N*arms = 28.

SG$_{72}$: [**G$_{72}$**]/[EGDA]/[$CuBr_2$/TPMA]=1/12/0.05, [**G$_{72}$**]= 14.9 mM in DMSO, T=60 °C, Cu wire (10 cm)**.** $M_{n,MALLS}$ = 222,200 *N*arms = 26.

SG_{60}: [**G_{60}**]/[EGDA]/[$CuBr_2$/TPMA]=1/10/0.05, [**G_{60}**]= 18.1 mM in DMSO, T=60 °C, Cu wire (10 cm)**.** $M_{n,MALLS}$ = 115,400 *N*arms = 17.

SG_{19}: [**G_{19}**]/[EGDA]/[$CuBr_2$/TPMA]=1/10/0.05, [**G_{19}**]= 18.7 mM in DMSO, T=60 °C, Cu wire (10 cm)**.** $M_{n,MALLS}$ = 127,800 *N*arms = 14.

$Smikto_{50}$: [**MI**]/[EGDA]/[$CuBr_2$/TPMA]=1/10/0.05, [MI] = **H_{100}**/**H_0** = 19.8 mM in DMF, [MI] = **H_{100}**/**H_0** = 5/5 by mole, T=50 °C, Cu wire (10 cm)**.** $M_{n,MALLS}$ = 650,200 *N*arms = 77.

$Smikto_{20}$: [**MI**]/[EGDA]/[$CuBr_2$/TPMA]=1/10/0.05, [MI] = **H_{100}**/**H_0** = 19.8 mM in DMF, [MI] = **H_{100}**/**H_0** = 8/2 by mole, T=50 °C, Cu wire (10 cm)**.** $M_{n,MALLS}$ = 544,100 *N*arms = 64.

VII.3.3. Analyses

Monomer conversion was measured either by a Shimadzu GC-17A gas chromatograph following a method of 8 °C/min from 30 – 170 °C or ^{1}H NMR; spectra were recorded in *d*-DMSO as a solvent using Bruker 300 MHz spectrometer. Molecular weight and molecular weight distributions of the formed polymers were measured by gel permeation chromatography (GPC) using Polymer Standards Services (PSS) columns (guard, 10^5, 10^3, and 10^2 Å), with DMF eluent at 35 °C, flow rate 1.00 mL/min, and differential refractive index (RI) detector (Wyatt Technology, Optilab T-rEX). Diphenyl ether was used as the internal standard to correct for any fluctuation of the DMF flow rate. The number-average molecular weights (M_n) and dispersity index (M_w/M_n) were determined with a calibration based on linear poly(methyl methacrylate) standards using

Astra software from Wyatt Technology. The detector employed to measure the absolute molecular weights ($M_{n,MALLS}$) was a multiangle laser light scattering (MALLS) detector (Wyatt Technology, mini-DAWN TREOS). Absolute molecular weights were determined using ASTRA software from Wyatt Technology.

VII.4. Results and discussion

VII.4.1. Linear copolymer synthesis

Three random copolymers were synthesized with hydroxyethyl acrylate (HEA) and methoxyethyl acrylate (MEA), monomers chosen for their hydrophilic and hydrophobic nature, respectively. Table VII.2, entries $\mathbf{R_{70}}$, $\mathbf{R_{50}}$, and $\mathbf{R_{30}}$ detail the polymerizations conducted under normal ATRP conditions, which utilized CuBr/PMDETA catalyst in DMF at 70 °C. The subscript numbers within the entry names refer to the cumulative composition of HEA, which gives insight into the hydrophilic or hydrophobic nature of the polymer. For example, $\mathbf{R_{70}}$ refers to a hydrophilic random copolymer with 70% cumulative composition of HEA, $\mathbf{R_{50}}$ refers to a neutral copolymer while $\mathbf{R_{30}}$ refers to a hydrophobic copolymer with only 30% cumulative composition of HEA.

Table VII.2. Random, block and gradient copolymers and homopolymers with hydrophilic, hydrophobic or neutral compositions.

Entry[a]	Structure[b]	$M_{n,th}$	$M_{n,exp}$ [c]	M_w/M_n [c]	% C.C.$_{HEA}$ [d]
R$_{70}$	HEA$_{52}$-*r*-MEA$_{23}$	8 900	16 700	1.18	70
R$_{50}$	HEA$_{40}$-*r*-MEA$_{40}$	9 800	13 500	1.24	50
R$_{30}$	HEA$_{25}$-*r*-MEA$_{54}$	9 900	14 200	1.20	30
M$_{58}$[e]	HEA$_{58}$	6 700	16 100	1.29	100
M$_{37}$[e]	HEA$_{37}$	4 300	10 700	1.23	100
M$_{21}$[e]	HEA$_{21}$	2 500	6 600	1.20	100
B$_{74}$	HEA$_{58}$-*b*-MEA$_{20}$	9 300	19 600	1.29	74
B$_{43}$	HEA$_{37}$-*b*-MEA$_{48}$	13 100	33 100	1.44	43
B$_{28}$	HEA$_{21}$-*b*-MEA$_{55}$	11 800	33 000	1.20	28
G$_{72}$	HEA$_{53}$-*grad*-MEA$_{20}$	8 400	14 100	1.24	72
G$_{60}$	HEA$_{35}$- *grad* -MEA$_{27}$	6 900	10 800	1.18	60
G$_{19}$	HEA$_{13}$- *grad* -MEA$_{57}$	8 900	11 700	1.20	19
H$_{100}$	HEA$_{72}$	8 400	21 700	1.32	100
H$_0$	MEA$_{64}$	8 300	13 600	1.35	0

[a] R = random copolymer, M = macroinitiator, B = block copolymer, G = gradient copolymer and H = homopolymer; subscript number refers to the cumulative composition of HEA present unless otherwise noted; specific reaction conditions for each sample given in Section VII.3.2. [b] Subscript numbers refer to DP as measured by monomer conversion. [c] Measured by GPC based on linear PMMA standards calibrated with diphenyl ether internal standard. [d] Cumulative composition (C.C.) calculated using equation VII.1 with monomer conversion. [e] subscript numbers refer to DP as measured by monomer conversion.

Previous literature[30] has demonstrated that HEA and MEA monomers have similar reactivity ratios, an expected result as they are both acrylate based. Therefore, when copolymerized in one pot, a random copolymer was spontaneously generated. Equivalent reactivity ratios were confirmed by nearly identical monomer conversion for both monomers as displayed in the kinetic plot within Figure VII.1. Additionally, linear first-order kinetics as well as growth of M_n with monomer conversion indicated well controlled polymerizations. All polymers exhibited narrow molecular weight distributions further indicating a controlled system.

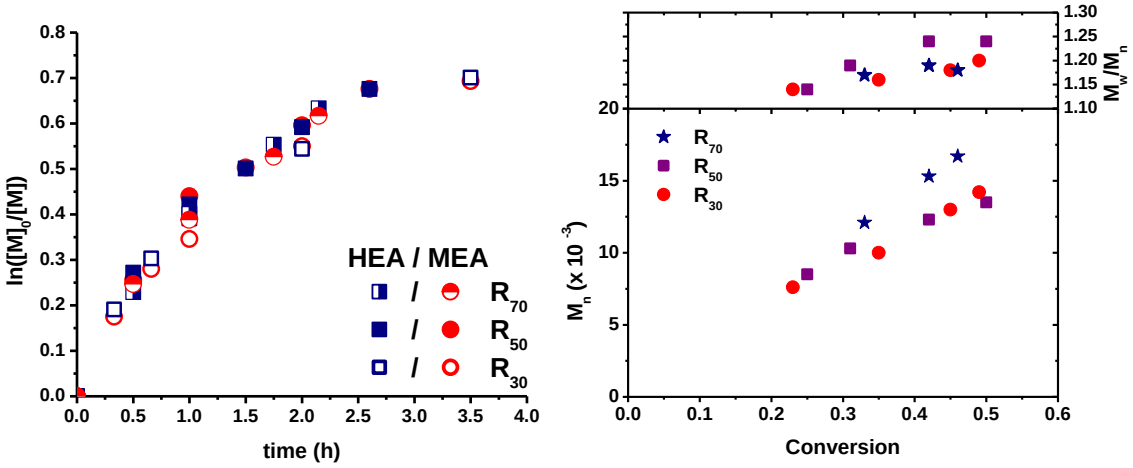

Figure VII.1. First order kinetic plot (left) and evolution of molecular weight and M_w/M_n with monomer conversion (right) of HEA/MEA copolymerizations to generate **R70**, **R50**, and **R30**.

The ratio of monomers incorporated into each reaction system was manipulated to result in copolymers with hydrophilic, neutral and hydrophobic compositions. It is important to note, the total targeted degree of polymerization for all monomers did not change ($DP_{monomer}$ = 160) although the ratio of each monomer did. For example, **R70** targets a hydrophilic polymer with DP_{HEA} = 110 and a DP_{MEA} = 50, while **R30** targets a

hydrophobic polymer with DP_{HEA} = 50 and a DP_{MEA} = 110. Cumulative compositions (CC) of the random copolymers, as plotted in Figure VII.2, were determined from the monomer conversion using equation VII.1, where $(\%\ conv)_1$ and $(\%\ conv)_2$ are the conversion of M_1 (HEA) and M_2 (MEA) at a given time, respectively, and $[M_1]_0$ and $[M_2]_0$ refer to the moles of M_1 or M_2 incorporated into the reaction set up.

$$F_{cum,1} = \frac{(\%conv)_1[M_1]_0}{(\%conv)_1[M_1]_0 + (\%conv)_2[M_2]_0} \quad \text{(VII.1)}$$

The cumulative compositions calculated using equation VII.1 reflected the ratio of monomers integrated during set up. For instance, **R_{50}** employed equimolar amounts of each monomer and the resulting CC_{HEA} = 50% while **R_{70}** and **R_{30}** reflected the skewed ratio of monomers incorporated. Throughout each of the polymerizations, the cumulative compositions remained steady at the initial feed ratio of the two monomers. This also confirms that the reactivity ratios of the monomers are nearly identical and are not affected by monomer conversion.

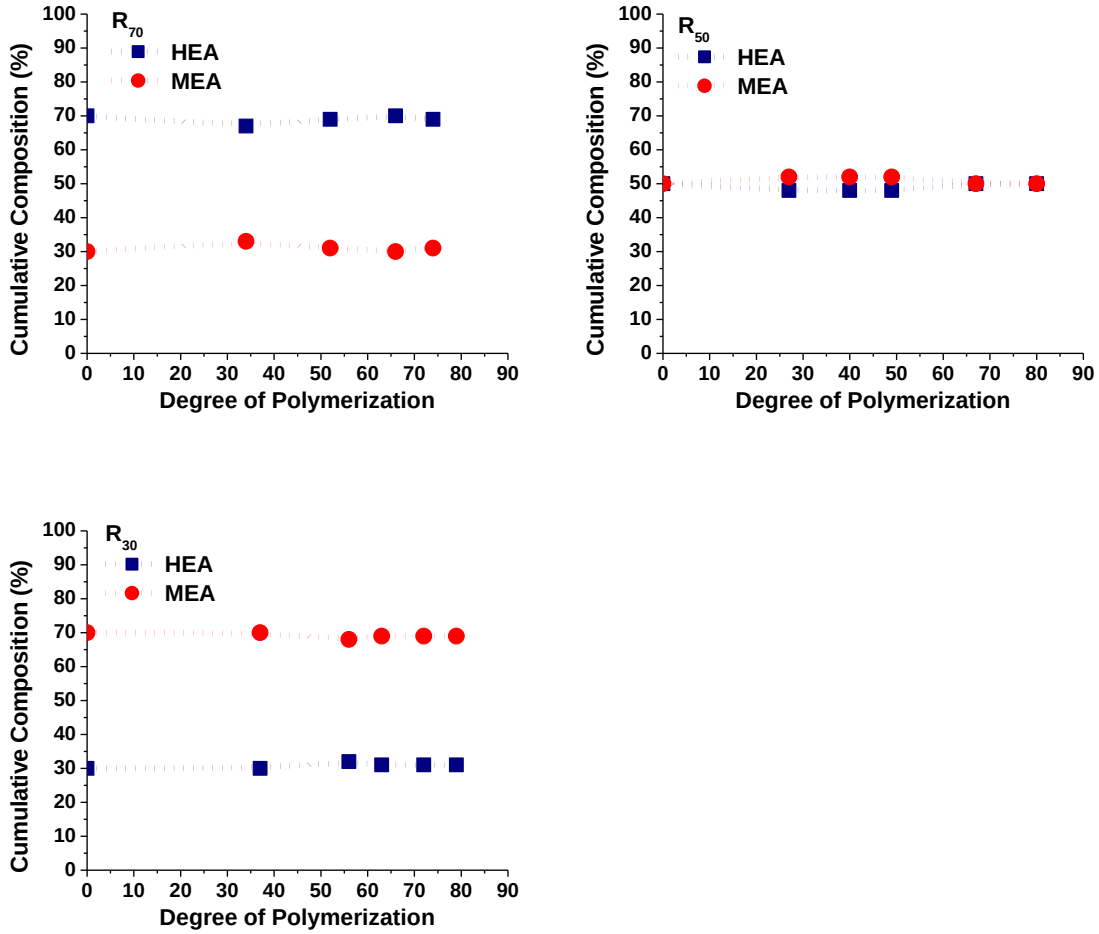

Figure VII.2. Cumulative composition plots for the HEA/MEA copolymerizations of **R70**, **R50**, and **R30**.

As with the random copolymers, block copolymers ranging from hydrophilic to neutral to hydrophobic were desired. Therefore, macroinitiators of different molecular weight were needed. Three homopolymerizations of HEA were conducted under normal ATRP conditions utilizing a CuBr/HMTETA catalyst at 60 °C. The less active ligand, HMTETA, was employed to afford a slower rate of polymerization and increased control to monitor the polymerization. Each successive polymerization was allowed to proceed to higher monomer conversion to result in an increased DP as outlined in Table VII.2, entries

M_{58}, **M_{37}**, and **M_{21}** (note: the subscript numbers refer to the DP_{HEA} as all macroinitiators contain CC_{HEA} = 100%.) In each case, a homopolymer of HEA was achieved with narrow molecular weight distribution as measured by GPC. These polymers were purified by dialysis and were utilized as macroinitiators for chain extension polymerizations to block copolymers.

Chain extension polymerizations of the macroinitiators were conducted under normal ATRP conditions to generate block copolymers **B_{74}**, **B_{43}**, and **B_{28}** (Table VII.2). Once again, the less active CuBr/HMTETA catalyst was utilized with a targeted DP_{MEA} = 300 or 100. The GPC traces displayed in Figure VII.3 displays the original macroinitiators in addition to the block copolymers. The shift in molecular weight for the chain extension from **M_{58}** to **B_{74}** was quite small as only 20 MEA monomer units were added to the HEA macroinitiator, thereby resulting in a hydrophilic block copolymer. For the neutral and hydrophobic block copolymers **B_{43}** and **B_{28}**, the shift in molecular weight was more significant as a total of 48 and 58 MEA monomer units were added to the short HEA macroinitiators, **M_{37}**, and **M_{21}**, respectively. Regardless, a clean shift in the molecular weight for all block copolymers indicated that the macroinitiators possessed high chain end functionality and high initiation efficiency was achieved during the chain extensions.

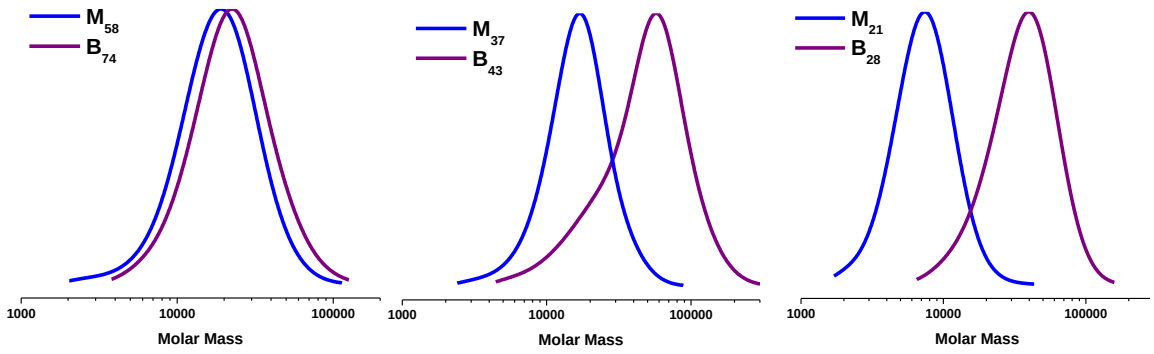

Figure VII.3. GPC trace of macroinitiators **M_{58}**, **M_{37}**, and **M_{21}** and the resulting block copolymers, **B_{74}**, **B_{43}**, and **B_{28}**, generated from chain extension.

As shown with the synthesis of random copolymers, MEA and HEA had nearly identical reactivity ratios therefore, the semi-batch method was utilized to generate gradient copolymers. A solution of M_2 (MEA) was gradually fed into a polymerization of M_1 (HEA) to produce a copolymer with gradient architecture. The length, or time, of $M_{2,MEA}$ feeding determined the polymerization time. In other words, the polymerization was stopped when monomer feeding had concluded. This was to prevent the end of the polymer chain from having a statistical composition from lack of monomer feeding and therefore, to ensure a gradient architecture along the entire length of the chain. To generate hydrophilic, neutral, or hydrophobic monomer content, gradient copolymers of increasing degrees of severity were synthesized. This was accomplished by maintaining the feed time of $M_{2,MEA}$ (t_{feed} = 8h) while altering the ratio of M_1:M_2 to afford the most significant change in composition.

Gradient copolymers, **G_{72}**, **G_{60}**, and **G_{19}**, were synthesized utilizing similar reaction conditions as the random copolymerizations, specifically CuBr/PMDETA catalyst system (Table VII.2). However, in the case of gradient copolymers, the catalyst was divided

between the reaction mixture and the $M_{2,MEA}$ feed solution to prevent a loss in rate of polymerization, R_p, from dilution. The catalyst to monomer ratio was held constant, so for Table VII.2 entry **G72**, 50% of the catalyst was present in both reaction mixture and feed solution, while for entry **G60**, only 30% of the catalyst was present initially in the reaction mixture and the remaining 70% was fed. Finally, in entry **G19** of Table VII.2, only 12.5% of the catalyst was initially present while 87.5% was fed with $M_{2,MEA}$.

Unlike traditional copolymerizations, kinetic plots of semi-batch gradient copolymerizations are not useful. As the reaction mixture and therefore concentration of radicals is constantly changing due to feeding of M_2, the kinetic plots do not contain constructive information. As concluded in Chapter V, MWD is an excellent tool to assess the quality of gradient architecture.[43] Therefore, control of the polymerization and quality of gradient materials was evaluated based on molecular weight distribution from GPC. As given in Table VII.2, each gradient copolymer exhibited a final $M_w/M_n < 1.25$, indicating well controlled polymerizations and high quality gradient copolymers.

Cumulative and instantaneous compositions were also used to characterize the copolymers, most importantly to gain insight on the severity of the gradient architecture (Figure VII.4). These compositions were based on conversions of HEA and MEA relative to internal standards DMF and DMSO, respectively. As displayed in Figure VII.4, the cumulative and instantaneous compositions for the gradient polymerizations exhibit more severe changes along the polymer chain as the ratio of monomers were biased toward MEA. For example, the polymerization with equimolar amounts of monomers, reaches a final CC_{HEA} = 72% (**G72**) while altering the ratio to 20:140 of HEA:MEA allows for a final

cumulative composition of CC_{HEA} = 19% (**G_{19}**). It is important to note these two systems only have a difference of 10 monomer units in the final DPs.

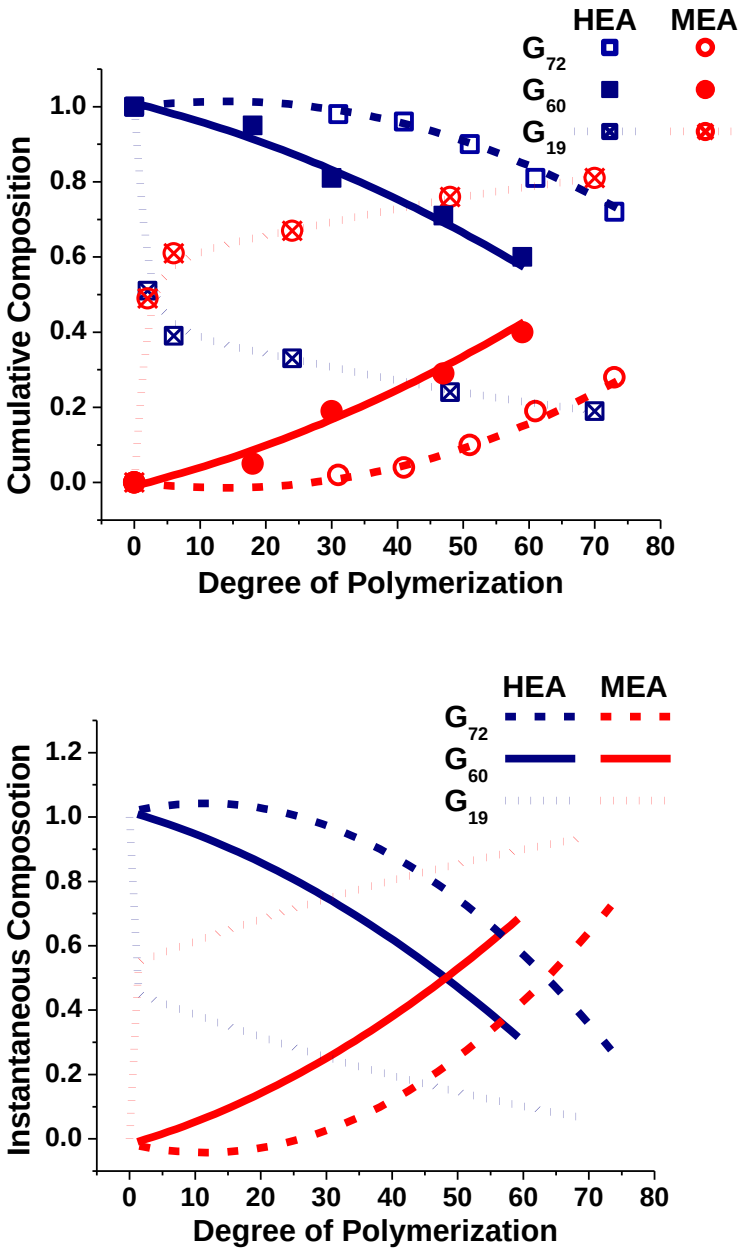

Figure VII.4. Cumulative and instantaneous compositions experimental semi-batch gradient synthesis of **G_{72}**, **G_{60}**, and **G_{19}**.

Finally, two homopolymers, one comprised of HEA (**H_{100}**) and the other of MEA (**H_0**), were prepared as detailed in Table VII.2. The synthesis was carried out under similar conditions to the macroinitiators and block copolymers, utilizing a CuBr/HMTETA catalyst system, resulting in materials with $M_w/M_n \leq 1.35$. The homopolymers will be discussed in the following section as they are utilized for the synthesis of mikto arm stars.

VII.4.2. Star Copolymer Synthesis

The random, block and gradient copolymers discussed in Section VII.4.1 were utilized to generate star polymers by the arm-first method; a procedure which crosslinks pre-formed linear (co)polymers.[41,44-46] Under supplemental activator and reducing agent (SARA) ATRP conditions in the presence of ethylene glycol diacrylate (EGDA) crosslinker, random, block, gradient and mikto arm stars were synthesized. Table VII.3 details the arm structure of each star and characterization of the stars themselves. The entry names refer to the topology of the sample (S = star) as well as the linear polymer from which it was synthesized. For example **SR_{70}** refers to a star polymer of sample **R_{70}**, a random copolymer with $CC_{HEA} = 70$. In the case of mikto arm stars, whose arms are comprised of two types of homopolymers, the subscript number refers to the percentage of **H_{100}** incorporated into the polymerization. Altering the ratio of **H_{100}** and **H_0** homopolymers allowed for the synthesis of hydrophilic (**$Smikto_{70}$**), hydrophobic (**$Smikto_{30}$**), and neutral (**$Smikto_{50}$**), mikto arm stars.

Table VII.3. Synthesis of star polymers

Entry[a]	Arm Structure[b]	$M_{n,th\ arm}$	$M_{n,MALLS}$[c]	N_{arm}[d]
SR$_{70}$	HEA$_{52}$-*r*-MEA$_{23}$	8,900	366,600	41
SR$_{50}$	HEA$_{40}$-*r*-MEA$_{40}$	9,800	244,900	23
SR$_{30}$	HEA$_{25}$-*r*-MEA$_{54}$	9,900	238,800	24
SG$_{72}$	HEA$_{53}$-*grad*-MEA$_{20}$	8,400	222,200	26
SG$_{60}$	HEA$_{35}$- *grad* -MEA$_{27}$	6,900	115,400	17
SG$_{19}$	HEA$_{13}$- *grad* -MEA$_{57}$	8,900	127,800	14
SB$_{74}$	HEA$_{58}$-*b*-MEA$_{20}$	9,300	260,300	28
Smikto$_{50}$[e]	HEA$_{72}$ and MEA$_{64}$	8,400	650,200	77
Smikto$_{30}$[e]	HEA$_{72}$ and MEA$_{64}$	8,400	544,100	64

[a] S = Star, R = random copolymer, B = block copolymer, G = gradient copolymer; subscript number refers to the cumulative composition of HEA present in linear arm structure; specific reaction conditions for each star given in Section VII.3.2. [b] Subscript numbers refer to DP as measured by monomer conversion. [c] Measured by multi-angle laser light scattering (MALLS) GPC. [d] Cumulative composition (C.C.) calculated using equation VII.1 with monomer conversion. [e] subscript number refers to the percentage of **H$_{100}$** incorporated into the star synthesis.

The formation of star copolymers was monitored by ^{1}H NMR as well as GPC. Traditional GPC with a refractive index (RI) detector is unfortunately not capable of providing accurate M_n values for star copolymers as the calibration is based on linear standards. Therefore, the use of GPC with RI detector is simply to observe the shift from linear copolymer to star and not to measure M_n values. As displayed in Figure VII.5, the conversion of EGDA crosslinker occurred quickly and reached a plateau after 10 h reaction

time during the synthesis of **SR$_{30}$**. The GPC traces confirm the lack of polymerization after 10 h reaction time as only a minimal decrease in **R$_{30}$** was observed. It is to be noted that some macroinitiator remained although no more shift toward star copolymers was observed; although the star yield was quite hight (%Y_{star} > 80). This may be due to a lack of chain end functionality after the synthesis of **R$_{30}$** or simply the cores became too congested to incorporate more arms. As the composition of the linear copolymers and stars are identical, it was extremely difficult to separate the linear portions from the stars. The remaining star syntheses proceeded in a similar manner; therefore a summary of the evolution from linear copolymer to star copolymers for the 9 samples is displayed in Figure VII.6.

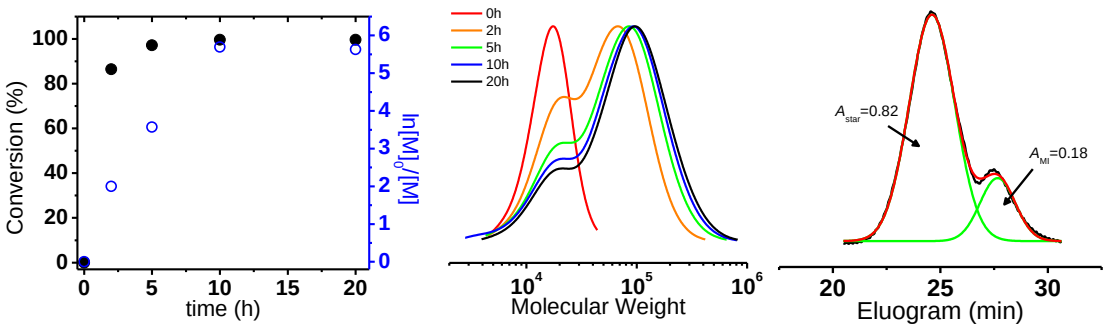

Figure VII.5. Conversion of EGDA (left) and evolution of molecular weight (center) with time during **SR$_{30}$** synthesis. Eluogram displaying a star yield, %Y_{star} = 82.

Employing a MALLS detector it was possible to measure absolute molecular weight. From this value, along with $M_{n,th}$ of the linear copolymers, the number of arms per star was estimated. $M_{n,MALLS}$ and N_{arms} for each star is given in Table VII.3. The majority of the stars exhibited relatively similar arm count, ranging between 20 – 30 arms. Outliers

included the mikto arm stars, **Smikto$_{50}$** and **Smikto$_{30}$**, which incorporated 64 and 77 arms, respectively.

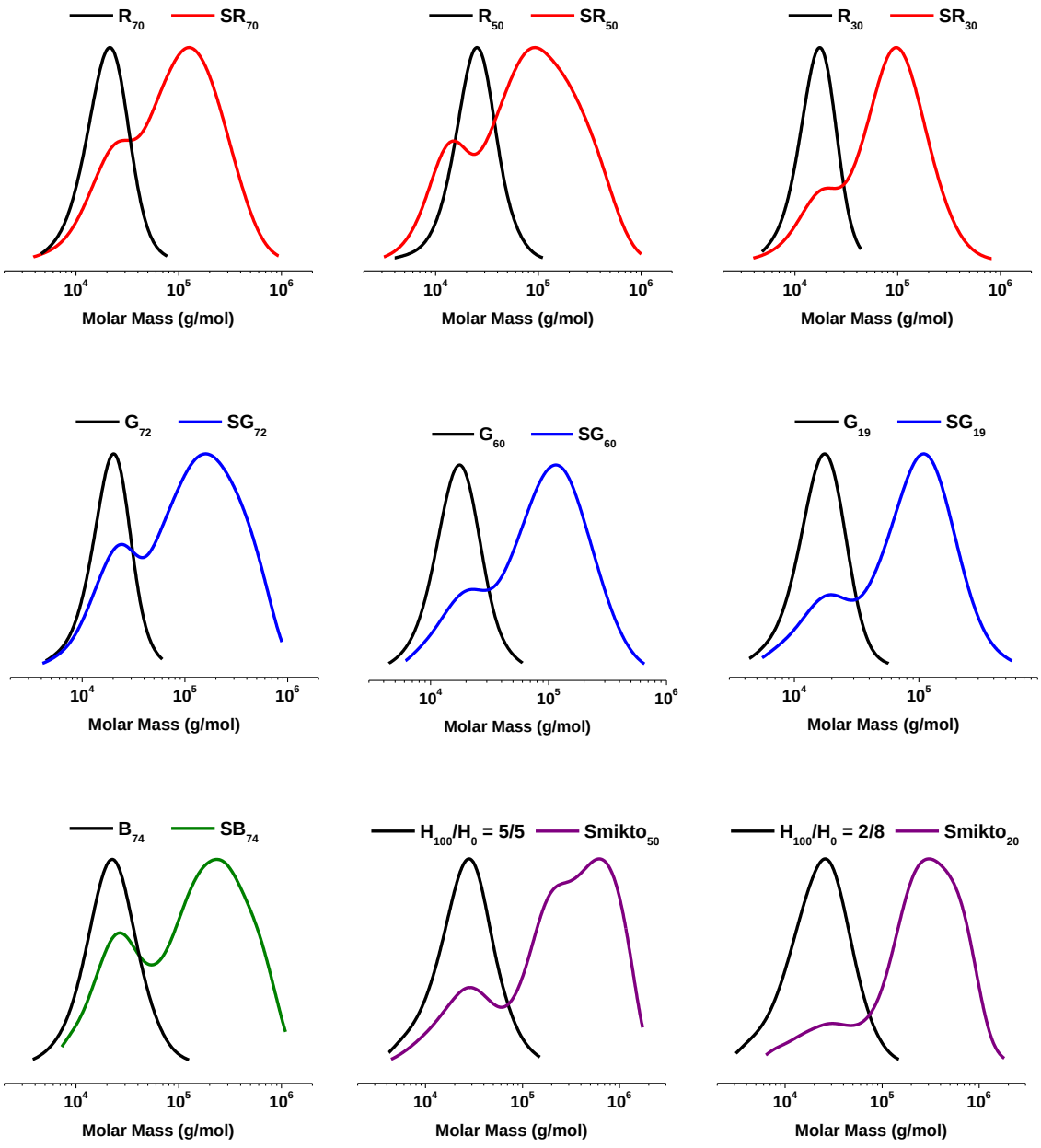

Figure VII.6. GPC traces displaying the evolution of molecular weight from linear polymers to random, block, gradient and mikto arm stars.

VII.5. Conclusions and future plans

A library of random, block and gradient polymers were successfully generated using MEA and HEA monomers to afford samples with compositions ranging from hydrophilic to neutral to hydrophobic. The monomer content of random and gradient copolymers was controlled by altering the HEA:MEA ratio, while relative block length was used to control monomer content of the block copolymers. From these linear materials, star copolymers, including mikto arm stars, were generated to test as surfactants for emulsion systems.

Some difficulty has been encountered during the synthesis of **SB$_{43}$**, **SB$_{28}$**, and **Smikto$_{70}$** as clean star copolymers have not been obtained. Altering the reaction conditions including the concentration of macroinitiator may aid in goal. However, with the current library of materials, it is still possible to acquire trends on the effects of composition, topology and monomer content on the behavior as surfactants. The emulsion studies are currently underway by collaborators Emily Wallistch under the guidance of Prof. Bob Tilton.

VII.6. Acknowledgments

I would like to acknowledge the work of Sangwoo Park on his help and guidance with the synthesis of stars. Additionally, I would like to thank Emily and Prof. Bob Tilton for their contributions to the analysis of my polymers as stabilizers.

VII.7. References

1. Garnier, S.; Laschewsky, A.; Storsberg, J. *Tenside, Surfactants, Deterg.* **2006,** *43*, 88-102.
2. Riess, G. *Prog. Polym. Sci.* **2003,** *28*, 1107-1170.
3. Gohy, J.-F. *Adv. Polym. Sci.* **2005,** *190*, 65-136-.
4. Garnier, S.; Laschewsky, A. *Langmuir* **2006,** *22*, 4044-4053.
5. Wang, J. S.; Matyjaszewski, K. *J. Am. Chem. Soc.* **1995,** *117*, 5614-5615.
6. Tsarevsky, N.; Matyjaszewski, K. *Chem. Rev.* **2007,** *107*, 2270-2299.
7. Braunecker, W. A.; Matyjaszewski, K. *Prog. Polym. Sci.* **2007,** *32*, 93-146.
8. Matyjaszewski, K. *Macromolecules* **2012,** *45*, 4015-4039.
9. Sheiko, S. S.; Sumerlin, B. S.; Matyjaszewski, K. *Prog. Polym. Sci.* **2008,** *33*, 759-785.
10. Lee, H. I.; Pietrasik, J.; Sheiko, S. S.; Matyjaszewski, K. *Prog. Polym. Sci.* **2010,** *35*, 24-44.
11. Gao, H.; Matyjaszewski, K. *Prog. Polym. Sci.* **2009,** *34*, 317-350.
12. Matyjaszewski, K.; Tsarevsky, N. V. *Nat. Chem.* **2009,** *1*, 276-288.
13. Pakula, T.; Matyjaszewski, K. *Macromolecular Theory and Simulations* **1996,** *5*, 987-1006.
14. Kryszewski, M. *Polym. Adv. Technol.* **1997,** *8*, 244-259.
15. Beginn, U. *Colloid Polymer Science* **2008,** *286*, 1465-1474.
16. Zaremski, M. Y.; Kalugin, D. I.; Golubev, V. B. *Polymer Science* **2009,** *51*, 103-122.

17. Matyjaszewski, K.; Ziegler, M. J.; Arehard, S. V.; Greszta, D.; Pakula, T. *Journal of Physical Organic Chemistry* **2000,** *13*, 775-786.

18. Shull, K. R. *Macromolecules* **2002,** *35*, 8631-8639.

19. Okabe, S.; Seno, K.; Kanaoka, S.; Aoshima, S.; Shibayama, M. *Macromolecules* **2006,** *39*, 1592-1597.

20. Mok, M. M.; Pujari, S.; Burghardt, W. R.; Dettmer, C. M.; Nguyen, S. T.; Ellison, C. J.; Torkelson, J. M. *Macromolecules* **2008,** *41*, 5818-5829.

21. Kim, J.; Mok, M. M.; Sandoval, R. W.; Woo, D. J.; Torkelson, J. M. *Macromolecules* **2006,** *39*, 6152-6160.

22. Jakubowski, W.; Juhari, A.; Best, A.; Koynov, K.; Pakula, T.; Matyjaszewski, K. *Polymer* **2008,** *49*, 1567-1578.

23. Sandoval, R. W.; Williams, D. E.; Kim, J.; Roth, C. B.; Torkelson, J. M. *Journal of Polymer Science: Part B: Polymer Physics* **2008,** *46*, 2672-2682.

24. Mok, M. M.; Kim, J.; Wong, C. L. H.; Marrou, S. R.; Woo, D. J.; Dettmer, C. M.; Nguyen, S. T.; Ellison, C. J.; Shull, K. R.; Torkelson, J. M. *Macromolecules* **2009,** *42*, 7863-7876.

25. Qin, S.; Saget, J.; Pyun, J.; Jia, S.; Kowalewski, T.; Matyjaszewski, K. *Macromolecules* **2003,** *36*, 8969-8977.

26. Lee, S. B.; Russell, A. J.; Matyjaszewski, K. *Biomacromolecules* **2003,** *4*, 1386-1393.

27. Buzin, A. I.; Pyda, M.; Costanzo, P.; Matyjaszewski, K.; Wunderlich, B. *Polymer* **2002,** *43*, 5563-5569.

28. Wong, C. L. H.; Kim, J.; Roth, C. B.; Torkelson, J. M. *Macromolecules* **2007,** *40*, 5631-5633.

29. Ribaut, T.; Oberdisse, J.; Annighofer, B.; Fournel, B.; Sarrade, S.; Haller, H.; Lacroix-Desmazes, P. *J. Phys. Chem. B* **2011,** *115*, 836-843.

30. Steinhauer, W.; Hoogenboom, R.; Keul, H.; Moeller, M. *Macromolecules* **2013,** *46*, 1447-1460.

31. Huynhbagia; Jerome, R.; Teyssie, P. *Colloid Polym. Sci.* **1979,** *257*, 1294-1296.

32. Huynhbagia; Jerome, R.; Teyssie, P. *J. Polym. Sci., Part B: Polym. Phys.* **1980,** *18*, 2391.

33. Li, L.; Yang, J.; Zhou, J. *Macromolecules* **2013,** *46*, 2808-2817.

34. Kukula, H.; Schlaad, H.; Tauer, K. *Macromolecules* **2002,** *35*, 2538-2544.

35. Huynhbagia; Jerome, R.; Teyssie, P. *J. Polym. Sci., Part A: Polym. Chem.* **1980,** *18*, 3483-3498.

36. Huynhbagia; Jerome, R.; Teyssie, P. *J. Appl. Polym. Sci.* **1981,** *26*, 343-351.

37. Burguiere, C.; Pascual, S.; Bui, C.; Vairon, J. P.; Charleux, B.; Davis, K. A.; Matyjaszewski, K.; Betremieux, I. *Macromolecules* **2001,** *34*, 4439-4450.

38. Jin, R. H. *J. Mater. Chem.* **2004,** *14*, 320-327.

39. Hadjiyannakou, S. C.; Triftaridou, A. I.; Patrickios, C. S. *Polymer* **2005,** *46*, 2433-2544.

40. Qiu, Q.; Liu, G. Y.; An, Z. S. *Chem. Commun.* **2011,** *47*, 12685-12687.

41. Li, W.; Yu, Y.; Lamson, M.; Silverstein, M. S.; Tilton, R. D.; Matyjaszewski, K. *Macromolecules* **2012,** *45*, 9419-9426.

42. Xia, J. H.; Matyjaszewski, K. *Macromolecules* **1999,** *32*, 2434-2437.

43. Elsen, A. M.; Li, Y.; Li, Q.; Sheiko, S. S.; Matyjaszewski, K. *Macromol. Rapid Commun.* **2014,** *35*, 133-140.

44. Gao, H.; Matyjaszewski, K. *Macromolecules* **2006,** *39*, 3154-3160.

45. Gao, H.; Min, K.; Matyjaszewski, K. *Macromolecules* **2007,** *40*, 7763-7770.

46. Burdynska, J.; Cho, H. Y.; Mueller, L.; Matyjaszewski, K. *Macromolecules* **2010,** *43*, 9227-9229.